universität wien

MASTERARBEIT / MASTER'S THESIS

Titel der Masterarbeit / Title of the Masters's Thesis

„Modelling Venus-like atmospheres in chemical equilibrium“

verfasst von / submitted by

Leander Schlarmann

angestrebter akademischer Grad / in partial fulfilment of the requirements for the degree of

Master of Science (MSc)

Wien, 2022 / Vienna, 2022

Studienkennzahl lt. Studienblatt / degree programme code as it appears on the student record sheet:	A 066 861
Studienrichtung lt. Studienblatt / degree programme as it appears on the student record sheet:	Masterstudium Astronomie
Betreut von / Supervisor:	Univ.-Prof. Dipl.-Phys. Dr. Manuel Güdel

Contents

1 Introduction

Venus is the closest planet to the Earth in the Solar System, not only in distance but also in mass and size (Taylor et al. 2018). Nevertheless, we only have rudimentary knowledge of the deep atmosphere and geology of the planet. Several spacecraft, such as the Soviet *Venera* program and NASA's *Pioneer Venus*, have visited Venus. Probes and landers were able to measure the concentrations of a number of species in the Venusian atmosphere. However, the last mission gathering in-situ atmospheric data, *Vega 2*, completed its task in 1985 (Johnson & de Oliveira 2019).

The atmosphere on Venus consists mostly (96.5%) of carbon dioxide, with about 3.5% of molecular nitrogen. The rest is dominated by sulfur dioxide, argon, and carbon monoxide. Water is present as vapour in the atmosphere and bound in cloud droplets with sulfuric acid (Catling & Kasting 2017). However, the data on the atmospheric composition of Venus is still incomplete and the uncertainties of the measured abundances are often very large (Chassefière et al. 2012). The alleged detection of phosphine in the Venusian atmosphere and its possible biological origin (Greaves et al. 2021; Bains et al. 2021), while controversial, underscores the need to better understand the history of the Venusian atmosphere.

In this master's research project the chemical equilibrium code `FastChem`[1] is used to study the atmospheric chemistry of Venus-like planets. The chemical equilibrium is determined by the minimisation of the Gibbs free energy. Therefore, `FastChem` uses a computationally efficient algorithm, that calculates the composition of the gas phase in chemical equilibrium for a specified temperature, pressure, and element distribution (Stock et al. 2018). Nevertheless, all atmospheres are in disequilibrium to some extent for example due to photochemical processes and volcanic outgassing. The disequilibrium in the lower atmosphere of Venus, however, is expected to be comparatively small, because the high pressure and temperature favour chemical reactions that push the atmosphere close to equilibrium (Krissansen-Totton et al. 2016).

Due to a number of different atmospheric loss mechanisms, different elements escape from the top of an atmosphere at different rates, which can change the chemical composition of the atmosphere over the lifetime of a planet. In this research project, the effects of changes in the carbon-to-oxygen (C/O) and carbon-to-nitrogen (C/N) ratios on the molecule abundance in the atmosphere of Venus-like planets are investigated, to constrain implications of these different escape rates of various elements on the atmospheric evolution. Furthermore, as part of the project, the atmospheric composition of Venus-like planets in thermodynamic equilibrium with different surface minerals are examined, using mineral redox buffers. With surface temperatures of about 735 K and a surface pressure of more than 90 bar, the atmospheric composition can be strongly affected by chemical reactions with solids at the Venusian surface (Sossi et al. 2020).

In this master's thesis, first an overview about our current knowledge of the atmosphere, surface, and evolution of the most Venus-like planet we know today, our planetary neighbour Venus, is given. In chapter 2, we introduce the chemical equilibrium codes `FastChem` and GGchem, used during this project. Chapter 3 focuses on the results obtained for different C/O and C/N ratios, and the atmosphere surface interactions.

[1] `https://github.com/exoclime/FastChem`

1.1 Venus

Venus is our nearest planetary neighbour in the Solar system, orbiting at a distance of about 0.72 astronomical units (AU) from the Sun. Venus is very similar to Earth in terms of size (0.95 $R_\oplus$) and mass (0.816 $M_\oplus$), and is therefore often referred to as Earth's twin- or sister-planet. Furthermore, Venus has a comparable bulk density and surface gravity, implying a similar structure and composition for both planets (Taylor et al. 2018). However, Venus possesses many dissimilarities with Earth such as the lack of any intrinsic magnetic field (Russell et al. 1979a,b), high surface temperature (~735 K) and pressure (~92 bar), as well as a very different atmospheric composition.

Some basic data for the terrestrial planets Venus, Earth, and Mars are presented in Table 1. Compared to Venus and Mars, Earth is unique since it has liquid water on the surface, active plate tectonics, an N_2-dominated atmosphere, and a magnetic dynamo (Lammer et al. 2018). One noticeable difference between Venus and the other terrestrial planets is that Venus has an extremely slow rotation period of 243 days, even longer than its orbital period of about 224 days. Furthermore, Venus rotates in a retrograde direction, meaning that, unlike most planets in the Solar System, Venus rotates in opposite direction than the Sun's rotation. The retrograde rotation can be seen in Table 1 by the obliquity of 177°. Therefore, one solar day on Venus takes 177 Earth days. Moreover, with a mean distance from the Sun of 0.72 AU ($1.082 \cdot 10^8$ km), the Sun illuminates Venus with about twice the intensity than Earth (Basilevsky & Head 2003). Mars only has a mass of 0.107 $M_\oplus$ and radius of 0.53 $R_\oplus$, but has a rotational period and obliquity similar to that of the Earth.

Table 1: Basic data of the planets Venus, Earth and Mars for comparison. Comparative data relative to Earth's mean distance ($1.496 \cdot 10^8$ km), radius (6378 km), mass ($5.97 \cdot 10^{24}$ kg), mean density (5500 kg/m^3), rotational period (23.9345 h) (Taylor et al. 2018).

Astronomical data	Venus	Earth	Mars
Comparative solar distances	0.723	1	1.524
Relative radius	0.95	1	0.53
Relative mass	0.816	1	0.107
Relative density	0.95	1	0.714
Orbital period	0.615	1	1.881
Comparative rotational periods	243	1	1.029
Comparative length of solar day	117	1	1.026
Orbital eccentricity	0.0068	0.0167	0.0934
Obliquity [deg]	177	23.45	23.98
Acceleration of gravity [ms^{-2}]	8.89	9.79	3.79
Solar Constant [kWm^{-2}]	2.62	1.38	0.594

Even though Venus is Earth-sized, the planet is very far from being Earth-like. The Venusian surface environment, with temperatures of about 735 K and a surface pressure of more than 90 bar, is inhospitable for life as we know it. Furthermore, due to the lack of an intrinsic magnetic field, the atmosphere and ionosphere directly interact with the space environment (Brecht et al. 2021). The combination of similarities and dissimilarities with Earth makes Venus a very interesting target to help us to understand the geology and evolution of terrestrial planets.

1.1.1 Missions and Observations

The Venusian environment is characterised by very challenging conditions for spacecraft missions with high surface temperature and pressure and global sulfuric acid clouds. For this reason, relatively few in-situ measurements of the Venusian surface and atmosphere have been made (Johnson & de Oliveira 2019). The first successful Venus flyby mission was the NASA space probe *Mariner 2*, passing Venus in 1962 (Pollack & Sagan 1967). This was soon followed by a series of landings of *Venera* spacecraft developed by the Soviet Union between 1961 and 1984, with the first scientific measurements on the surface by *Venera 5* and *6* in 1969 confirming the high surface temperature and pressure (Avduevsky et al. 1970). *Venera 9* and *10* took the first panorama images of the Venusian surface in 1975 (Keldysh 1977). Furthermore, the *Venera* landers and orbiters were equipped with instruments for studying the the upper Venusian atmosphere and the clouds (Keldysh 1977). In December 1978 the *Pioneer Venus* program of NASA, consisting of an orbiter and multiprobe, successfully encountered Venus (Colin & Hall 1977). The multiprobe contained a bus which carried one large sounder and three smaller probes. The three small probes had identical instruments and were named according to the different parts of the planet they targeted: North (59.3°N, 4.8°), Day (31.3°S, 317°), and Night (28.7°S, 56.7°). The hard landing Day probe functioned on the surface for over 67 minutes (Colin 1980). Furthermore, the large sounder probe measured the chemical composition of the Venusian atmosphere at three altitudes with a gas chromatograph (Oyama et al. 1980). In June 1985, two balloons were released into the atmosphere of Venus by the Soviet *Vega* mission. Each balloon rode the winds just inside the cloud tops at a altitude of about 54 kilometers for several days, making measurements of pressure, temperature, the vertical wind velocity, and the frequency of lightning (Sagdeev et al. 1986). *Vega* was the last mission that performed in-situ compositional data measurements of the deep atmosphere. Figure 1 shows the altitudes of atmospheric measurements from selected missions to Venus, with no claim to completeness.

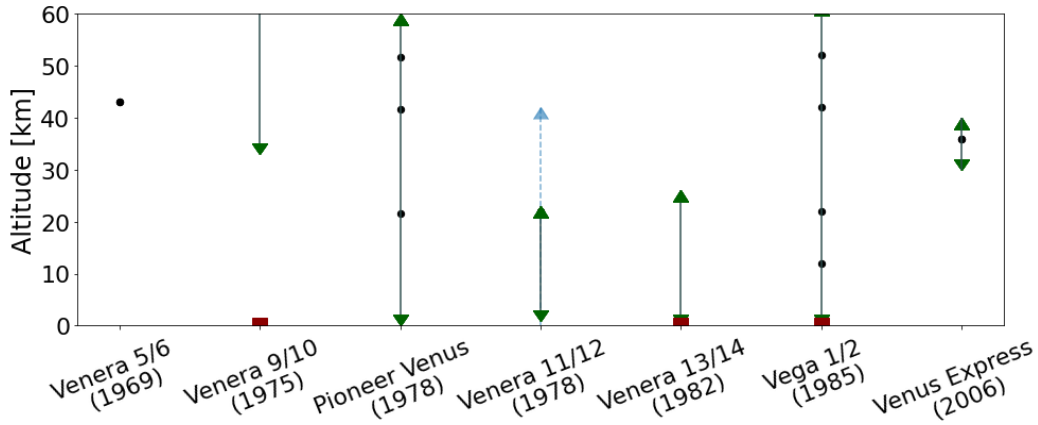

Figure 1: Schematic representation of the altitude of atmospheric measurements for selected Venus missions. Landers that performed geochemistry measurements on the surface are marked with a red square. The inlet leaks of the Pioneer Venus sounder probe's mass spectrometer were blocked by sulfuric acid droplets from approx. 50 to 30 km (Hoffman et al. 1980). For Venera 12 lander the range of the gas chromatograph is indicated as a dotted line. Altitudes with specific measurements found in the literature are marked as black dots.

More recent data were obtained through remote Earth-based, flyby or orbiter observations (Johnson & de Oliveira 2019). The *Venus Express* mission (Svedhem et al. 2007) of the European Space Agency (ESA) arrived at Venus in 2006 and was operational until 2014 (Damiani et al. 2015). The spacecraft was placed in a very elliptical, polar orbit. Thereby, the probe's instruments could study the Venusian atmosphere and surface from various distances.

Table 2: Successful missions to Venus and Spacecraft that returned Venus data (Johnson & de Oliveira 2019).

Name	Country	Type	Launch / Arrival
Mariner 2	USA	Flyby	27.08.1962 / 14.12.1962
Venera 4	USSR	Probe	12.06.1967 / 18.10.1967
Mariner 5	USA	Flyby	14.06.1967 / 19.10.1967
Venera 5	USSR	Probe	05.01.1969 / 16.05.1969
Venera 6	USSR	Probe	10.01.1969 / 17.05.1969
Venera 7	USSR	Lander	17.08.1970 / 15.12.1970
Venera 8	USSR	Lander	27.03.1972 / 22.07.1972
Mariner 10	USA	Flyby	03.11.1973 / 05.02.1974
Venera 9	USSR	Orbiter/Lander	08.06.1975 / 22.10.1975
Venera 10	USSR	Orbiter/Lander	14.06.1975 / 25.10.1975
Pioneer Venus 1	USA	Orbiter	20.05.1978 / 04.12.1978
Pioneer Venus 2	USA	Multiprobe (1 large, 3 small)	08.08.1978 / 09.12.1978
Venera 11	USSR	Flyby/Lander	09.09.1978 / 25.12.1978
Venera 12	USSR	Flyby/Lander	14.09.1978 / 21.12.1978
Venera 13	USSR	Flyby/Lander	30.10.1981 / 01.03.1982
Venera 14	USSR	Flyby/Lander	04.11.1981 / 05.03.1982
Venera 15	USSR	Orbiter	02.06.1983 / 10.10.1983
Venera 16	USSR	Orbiter	07.06.1983 / 14.10.1983
Vega 1	USSR	Flyby/Probe/Lander	15.12.1984 / 11.06.1985
Vega 2	USSR	Flyby/Probe/Lander	21.12.1984 / 15.06.1985
Magellan	USA	Orbiter	04.05.1989 / 10.10.1990
Venus Express	Europe	Orbiter	09.11.2005 / 07.05.2006
Akatsuki	Japan	Orbiter	20.05.2010 / 07.12.2015

In addition, *Venus Express* could travel through different parts of the induced magnetosphere, created by interaction of the solar wind with the ionosphere, to measure the field strength (Zhang et al. 2008). Moreover, the spacecraft included spectroscopic instruments to measure the composition, structure, and dynamics of the Venusian atmosphere (Drossart et al. 2007). The Japanese orbiter *Akatsuki* was launched in 2010 (Nakamura et al. 2011). However, because of a malfunction in the propulsion system the first orbit insertion failed, after which the spacecraft orbited the Sun for 5 years. In 2015, *Akatsuki* once again approached Venus and was successfully placed in a westward equatorial orbit (Nakamura et al. 2016). *Akatsuki* was mainly designed to investigate the Venusian climate. To study the Venusian atmosphere five cameras imaged Venus at different wavelengths to track the distributions of clouds (Lee et al. 2017; Horinouchi et al. 2018). Table 2 provides an overview of successful missions that have visited Venus in the last 60 years.

Remote observations of Venus are mostly limited to the region above the clouds. Some Earth-based facilities, such as the Apache Point Observatory (see Arney et al. 2014), the Canada-France-Hawaii telescope (see Bezard et al. 1990), and the Very Large Array (see Jenkins et al. 2002) have been used to gather data about Venus. In addition, Earth-based observations in the microwave and radar range have lead to very important findings, such as the measurement of the Venusian surface temperature (see Mayer et al. 1958) and rotational period (see Campbell et al. 2019). However, ground-based observations are constrained in phase angle coverage and generally have lower spatial resolution then spacecraft measurements.

The future of Venus investigation is very promising. For example, two missions have been selected to launch in the next decades as part of NASA's Discovery Program. The *DAVINCI+* (Deep Atmosphere Venus Investigation of Noble gases, Chemistry, and Imaging) mission will consist of an orbiter and a deep atmosphere chemistry probe (Garvin et al. 2020). The probe will contain different instruments, measuring the composition of the Venusian atmosphere to understand how it formed and evolved. A mass spectrometer and a tunable laser spectrometer will study the atmospheric composition, including measurements of noble gases and isotope ratios, such as the D/H fraction (D'Incecco et al. 2021). Furthermore, the vertical pressure and temperature structure, including winds, will be investigated and high-resolution emissivity maps will be produced near the surface (Garvin et al. 2020).

VERITAS (Venus Emissivity, Radio Science, InSAR, Topography, and Spectroscopy), the second mission selected by NASA, will map the Venusian surface in high resolution and provide new radar and geochemical data (Smrekar et al. 2020). The spacecraft will carry an X-band interferometric radar, and an emissivity mapper, that will provide maps of the global rock type and search for evidence of recent and active volcanic activity on Venus (Helbert et al. 2020). Moreover, *VERITAS* will provide foundational data sets of high resolution topography and, furthermore, investigate the gravitational field of Venus (Smrekar et al. 2020).

Along with these NASA missions, ESA's *EnVision* was recently selected as a medium-class mission by ESA's Science Programme Committee (Ghail et al. 2018). Main scientific objectives of *EnVision* are to determine the current state of geological activity on Venus, and its relationship with the atmosphere. Therefore, the planet's history, activity and climate will be studied. The payload includes an an S-band synthetic aperture radar, and a subsurface radar sounder. Furthermore, the VenSpec instrument suite is part of the payload, including a nadir pointing, high-resolution infrared spectrometer, an infrared mapper, and a ultraviolet spectrometer (Helbert et al. 2019).

The exploration of Venus will not end with *VERITAS*, *DAVINCI+*, and *EnVision*. Recently, the Chinese Academy of Sciences announced plans for *VOICE* (Venus Volcano Imaging and Climate Explorer), a mission that could launch as early as 2026. The Indian Space Research Organisation (ISRO) is also considering an orbiter mission to Venus. Furthermore, Roskosmos proposed the *Venera-D* mission, that will include a big Vega-type lander, with the possible inclusion of a small spacecraft around the Lagrange points L_1 and L_2 or a subsatellite in high elliptical orbit (Kovalenko et al. 2020). Rocket Lab has also committed to fly a private mission to Venus, including a small direct entry probe, planned to launch in 2023 (French et al. 2022).

In addition to these planned missions, new mission concepts have been proposed to explore the Venusian atmosphere, including balloons, aerobots, rotorcraft, and fixed-wing aircraft (Elston et al. 2021). For example, one interesting proposal is the multi-balloon mission *Venus Dynamics Tracer*, that would include two identical balloons at different altitudes in the Venusian atmosphere for about 20 days together with an orbiter, to investigate the drive of atmospheric motion in the Venus atmosphere (Stenberg et al. 2022). Furthermore, a combination of ground-based observations and future space missions will improve our knowledge of Venus.

1.1.2 Venus Atmosphere

The atmosphere of Venus is much more massive than Earth's atmosphere, with a surface pressure of about 90 bar, while consisting predominantly (~96.5%) of carbon dioxide (CO_2), contributing to the planet's high surface temperatures by being a potent greenhouse gas. In total, the Venusian atmosphere contains approximately twice as much carbon as Earth's atmosphere, hydrosphere and sediments combined (Lécuyer et al. 2000). For Earth, the two largest carbon reservoirs are carbonate rocks and organic matter (Lécuyer et al. 2000). Traditionally, atmospheres are viewed to consist of well enough delimited and defined vertical regions. Based on the Earth's thermal structure, planetary atmospheres are often divided into troposphere, mesosphere, thermosphere, and sometimes exosphere (Brecht et al. 2021). In Figure 2 these atmospheric regions are illustrated for the Venusian atmosphere. A thick cloud layer is completely covering Venus at altitudes between ~45 and ~70 km, with the upper layer mainly consisting of sulphuric acid (Esposito et al. 1983; Markiewicz et al. 2007; Horinouchi et al. 2018).

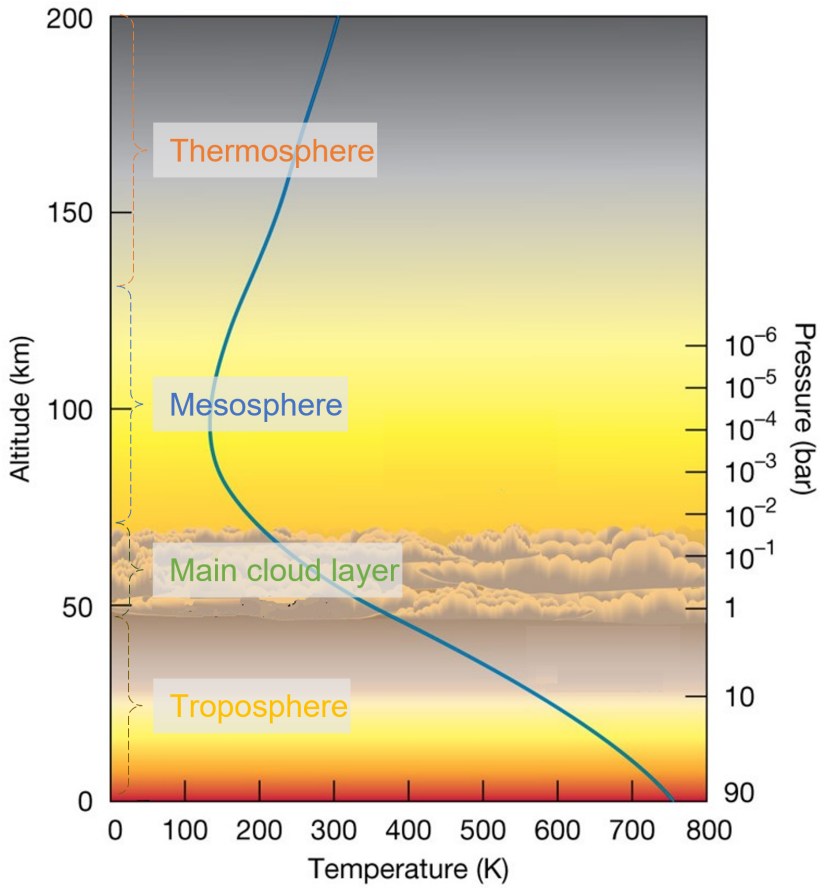

Figure 2: Average thermal profile of the Venusian atmosphere with labels of the estimated locations of the planet's troposphere, mesosphere, and thermosphere, as well as the main cloud layer (adapted from Taylor et al. 2018; Kane et al. 2019).

The atmosphere of Venus circulates westward around the planet with a period of 4 days at an altitude of 50–60 km. However, the planet itself rotates westward as well, but more slowly with a period of 243 days. This phenomena of the zonal atmospheric flow being faster than the planets solid body rotation, is called atmospheric superrotation (Schubert et al. 2007). It has been proposed that thermal tides in the thick Venusian atmosphere could maybe have led to the present rotation rate (Dobrovolskis & Ingersoll 1980; Horinouchi et al. 2020).

Table 3 shows the present abundance of the main atmospheric species of Venus, Earth, and Mars. The atmosphere on Venus consists mostly (96.5%) of carbon dioxide, with about 3.5% of nitrogen. Furthermore sulfur dioxide (150 ppm), carbon monoxide (40 ppm), argon (70 ppm) and other noble gases are present in the Venusian atmosphere. Both sulfur dioxide (SO_2) and water vapour (H_2O) are known to be depleted in the cloud layer of Venus. The concentration of sulfuric acid (H_2SO_4) in the Venusian clouds has been estimated at 75% to 96% (Schulze-Makuch 2021). Mars, similar to Venus, has a CO_2-rich atmosphere with minor N_2 (Sossi et al. 2020). Earth's atmosphere is dominated by molecular nitrogen (N_2), with about 21% molecular oxygen (O_2) (Catling et al. 2018).

Table 3: Composition of the atmospheres of Venus and Earth and Mars (Taylor et al. 2018; Catling et al. 2018; Patel et al. 2002). The concentration of water vapour (H_2O) in the Earth's atmosphere varies significantly between 0.1 ppm and 4% depending strongly on the temperature (Catling et al. 2018). Therefore, the abundances of H_2O and HDO, which vary for the atmosphere of Earth and Mars, are marked with a tilde (~).

Species	Formula	Venus	Earth	Mars
Carbon dioxide	CO_2	96.5 %	0.03 %	95.32 %
Nitrogen	N_2	3.5 %	77 %	2.7 %
Sulfur dioxide	SO_2	150 ppm	0.2 ppb	<0.3 ppb
Argon	Ar	70 ppm	0.93 %	1.6 %
Water vapour	H_2O	30 ppm	~1 %	~0.03 %
Carbon monoxide	CO	40 ppm	0.12 ppm	0.07 %
Neon	Ne	5 ppm	18 ppm	2.5 ppm
Carbonyl sulfide	CS	4 ppm	0.5 ppb	trace
Heavy water	HDO	3 ppm	~1 ppm	~0.8 ppm
Hydrogen chloride	HCl	0.5 ppm	trace	<0.2 ppb
Hydrogen fluoride	HF	0.005 ppm	trace	trace
Molecular oxygen	O_2	trace	21 %	0.173%

Recently, the detection of phosphine (PH_3) in the atmosphere of Venus was reported by Greaves et al. (2021) at ~20 ± 10 ppb, based on spectroscopy of the J=1-0 transition using the Atacama Large Millimeter/submillimeter Array (ALMA) and the James Clerk Maxwell Telescope (JCMT). Phosphine is a reduced, reactive gaseous phosphorus species, which is not expected to be present in the oxidised, hydrogen-poor Venusian atmosphere. Bains et al. (2021) investigated possible photochemical, geochemical, meteorological, and other non-equilibrium processes as sources for PH_3, and even looked at biological processes. They found that life cannot be ruled out as a source of phosphine on Venus, but cannot be favored over unknown photochemistry or unknown atmospheric chemistry either. The claimed detection of PH_3, however, has been contested by several subsequent, independent analyses of the ALMA and JCMT data (Snellen et al. 2020; Villanueva et al. 2021; Thompson 2021). Furthermore, searches for infrared signatures of PH_3 using ground-based observations (Encrenaz et al. 2020, $PH_3 < 5$ ppbv) and from spacecraft data (Trompet et al. 2021, $PH_3 < 0.2$ ppbv) have resulted in non-detections of phosphine. Lincowski et al. (2021) claimed that nominal mesospheric SO_2 would be a more plausible explanation for the JCMT and ALMA data than PH_3. Outgassing has also been suggested to be a possible source of PH_3, as a product of the ejection of volcanic phosphides into the clouds (Truong & Lunine 2021). However, this scenario was found to be unlikely, as it would require a highly unexpected set of conditions, such as Venus entering a global resurfacing epoch (Bains et al. 2022). Nonetheless, the scientific dispute of the phosphine detection in the Venusian atmosphere shows that our current understanding of Venus atmospheric chemistry has to improve.

1.1.3 Surface

Venus has very diverse surface features, including mountain ranges, craters, and chaotic terrain (Basilevsky & Head 2003). Between 1972 and 1985, five *Venera* landers (*Venera 8, 9, 10, 13, 14*) and two *Vega* landers (*Vega 1, 2*) performed geochemistry measurements of the Venusian surface at different locations. Major element analyses were only performed on *Venera 13* & *14*, and *Vega 2*. The measurements of the four other landers only included the elements potassium (K), uranium (U), and thorium (Th). The low precision of the measurements compared to terrestrial and Martian rock analysis standards makes their interpretation beyond broad generalities difficult (Treiman 2007). Gamma spectrometric analysis at the landing site of *Venera 8* showed that the surface material has a relatively high content of K (4%), U (2.2 ppm), and Th (6.5 ppm), which led to the interpretation that the material was either alkaline basalt or a intermediate subalkaline rock (Basilevsky 1997).

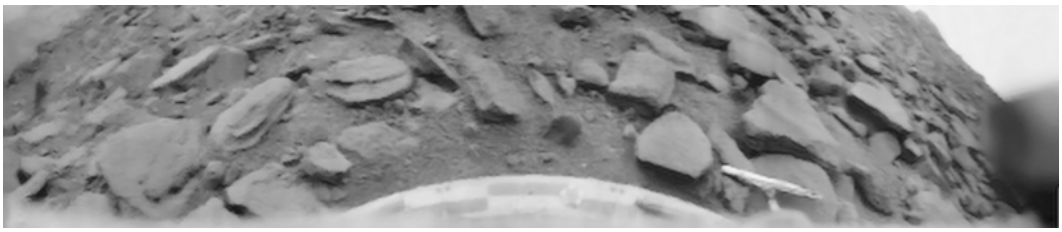

(a) *Venera 9*

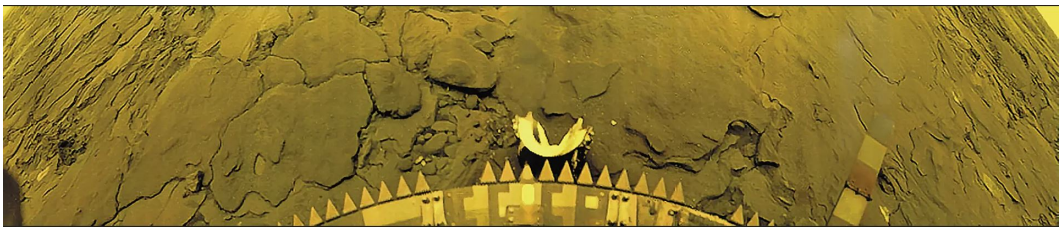

(b) *Venera 14*

Figure 3: The Venus surface as seen from the Soviet *Venera 9* (Top) and *Venera 14* (bottom) landers. Credit: USSR Academy of Sciences/Brown University/Ted Stryk.

Close-up images of the Venusian surface were taken by panoramic cameras on board of *Venera 9, 10, 13* and *14*. The pictures of the *Venera* landers, as seen in Figure 3, showed lava plains with some smooth surface and some amount of regolith and rocks. The panoramic picture from the *Venera 9* lander in Figure 3(a) shows a mostly flat surface with a large number of rocks (Keldysh 1977). At the *Venera 14* landing site, shown in Figure 3(b), a fine, dark soil can be seen, with flat rocks all the way to the horizon. This picture indicates the presence of rock formations undergoing geomorphic degradation (Florensky et al. 1983). The *Venera 13* and *14* probes determined the chemical composition of the Venusian rocks at landing sites, using a special drilling device and an X-ray fluorescence spectrometer (Surkov et al. 1982). The chemical composition of the rock at the *Venera 14* landing site was found to be similar to that of tholeiitic basalts of the oceanic crust of the Earth (Surkov et al. 1983). At the *Venera 13* landing site, the surface material was found to have a bulk composition similar to alkaline basalt (Basilevsky 1997). In Table 4 the chemical composition of rock at the *Vega 2* landing site analysed using X-ray fluorescence is shown. The analysed rock shows great similarity to basic rocks of the Earth's crust (Surkov et al. 1986).

Table 4: *Vega 2* measurements of the oxide mass fractions (%) of Venusian surface rock (Rimmer et al. 2021; Surkov et al. 1986).

SiO_2	Al_2O_3	MgO	FeO	CaO	SO_3	TiO_2	MnO	Na_2O	K_2O
45.6±3.2	16±1.8	11.5±3.7	7.7±1.1	7.5±0.7	4.7±1.5	0.2±0.1	0.14±0.12	2	0.1±0.08

From the in-situ measurements by *Venera* and *Vega* probes, the crust of Venus is expected to be largely composed of basalt. Many geologic features on Venus suggest that the mantle of Venus is broadly similar to that of Earth in composition (Taylor et al. 2018). However, the chemical compositions of the planet's crustal materials are still poorly known. With only seven landing sites visited by probes, there are many interesting and diverse terrain types that remain unsampled (Treiman 2007). Theoretical modelling and experiments can help to better understand the mineralogy of the Venus surface. Orbital remote sensing of the geochemistry is difficult because of the thick Venusian atmosphere, which is relatively opaque (Gilmore et al. 2017). In the future, landers with contact instruments, balloons or even sample return missions, such as the planned Mars Sample Return (MSR), will be crucial to better constrain the geochemistry of the Venusian surface (Landis et al. 2011).

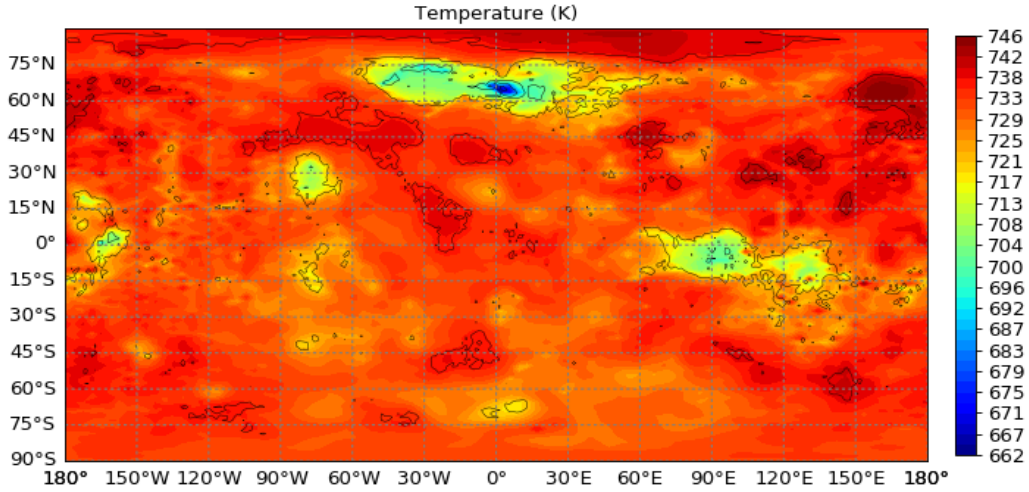

(a) Surface temperature

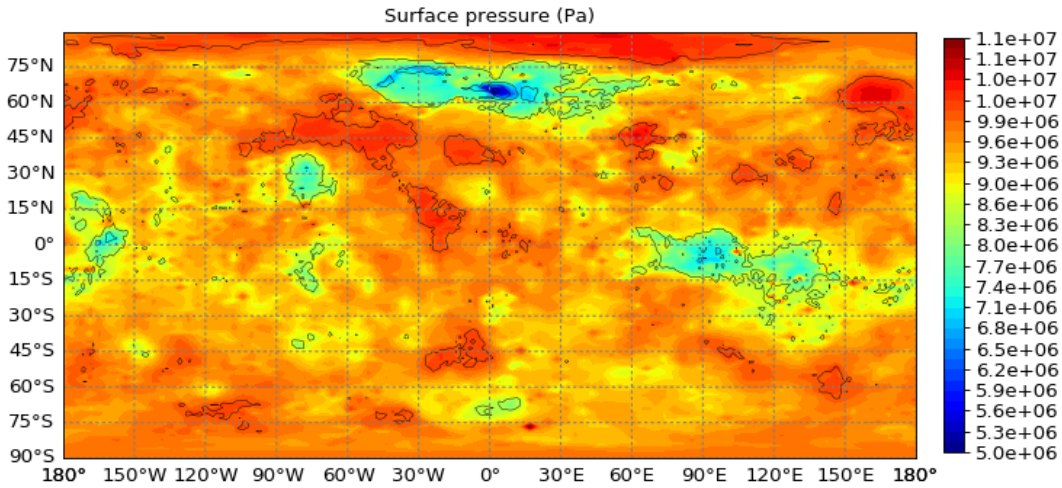

(b) Surface pressure

Figure 4: The Venus surface temperature (top) and pressure (bottom) simulated using the Venus Climate Database (VCD) (Lebonnois et al. 2021).

Using the Venus Climate Database (VCD)[2], that is based on the outputs of a Venus Global Climate Model (GCM) developed by Lebonnois et al. (2021), a map of different Venusian meteorological variables can be created. Figure 4 shows the variations of the temperature and pressure on the Venusian surface. Most of the Venusian surface consists of volcanic plains and rises (Treiman 2007). The two continent-sized highland plateaus Ishtar Terra (45° N to 75° N; 60° W to 75° E) in the northern hemisphere and Aphrodite Terra (10° N to 20° S; 60° E to 150° E) near the equator are the most prominent features in Figure 4. The Maxwell Montes (65° N; 1.5° E), the highest mountain range on Venus rising about 11 km above mean planetary radius (Head et al. 1984), can also be clearly seen as a dark blue region in Figure 4. This is the case because these higher altitude regions have relatively lower temperatures and pressures than regions at low altitude.

The Venusian surface shows clear signs of volcanism. An analysis of Magellan data by Head et al. (1992), covering over 90% of the Venusian surface, revealed hundreds of large shield volcanoes. Furthermore, the impact cratering record on Venus is unique in comparison to Earth and Mars. Impacts are thought to occur throughout the history of the solar system. Therefore, surfaces with fewer craters are considered younger. In a global high-resolution analysis of Magellan data, a global population of only about a thousand impact craters was found by Schaber et al. (1992) with a highly uniform spatial distribution. This suggests a young average age of the Venusian surface that could be explained by a global resurfacing event (Kreslavsky et al. 2015). Strom et al. (1994) suggested that such a catastrophic event may have occurred about 300 My ago, probably lasting tens of millions of years or ending more abruptly (< 10 My), followed by a dramatic reduction of volcanism and tectonism. Other terrestrial bodies have non-uniform and spatially non-random crater distributions, due to different ages and intensities of resurfacing events (Schaber et al. 1992).

1.1.4 Evolution

The history of the formation and evolution of Venus is still poorly understood. In contrast to Venus, Mars has extensively been studied with in-situ rover missions and through the analysis of Martian SNC meteorites, named after the three representative members Shergottites, Nakhlites, and Chassignites. Because of this, there are sill many questions on the evolution of Venus (Chassefière et al. 2012). Planetary atmospheres are either primary or secondary in nature. Primary atmospheres can be accreted directly from the protoplanetary disk, or outgassed during the initial formation. For rocky planets these primary atmospheres can undergo significant changes due to geological, physical, and chemical processes, such as hydrodynamic escape or volcanic outgassing. Through these processes, the atmospheric composition can change to a secondary atmosphere (Liggins et al. 2021). Earth may have evolved from an H_2- to a CO_2-, and finally to an N_2-dominated atmosphere, while Venus and Mars ended with CO_2 atmospheres (Lammer et al. 2018). Understanding and characterising the evolution of Venus will help to study terrestrial planets and their divergent evolution.

Venus likely received similar amounts of volatiles from the protoplanetary disk as Earth, although there is no consensus, particularly concerning the origin of water in the terrestrial planets (see Drake 2005; O'Brien et al. 2018). However, the atmosphere of Venus contains about twice as much carbon and nitrogen than the atmosphere, hydrosphere and sediments of Earth (Lécuyer et al. 2000). The deuterium-to-hydrogen (D/H) ratio of water in the Venusian atmosphere, which is a key diagnostic to determining where in the Solar System an object originated, is larger by a factor of 150 than that on Earth's hydrosphere (Chassefière et al.

[2] http://www-venus.lmd.jussieu.fr/

2012). This suggests that Venus once had much more water than today, maybe even had an ocean that could have been lost due to a combination of atmospheric hydrogen escape and crustal hydration (Lécuyer et al. 2000). However, Grinspoon & Lewis (1988) argued that the water abundance on Venus may be near a state in which the hydrogen loss to space is in balance with the replenishment of water from comets and outgassing of juvenile water. In this case, an increased past water inventory of Venus would not be required to explain the high D/H ratio (Kulikov et al. 2006).

As demonstrated, the past climate evolution of Venus is still uncertain, despite decades of study. Another subject of ongoing debate, related to the suggestion that Venus once had a liquid water oceans, is whether Venus ever was habitable. Krissansen-Totton et al. (2021) applied a fully coupled geochemical evolution model called PACMAN (Planetary Atmosphere, Crust, and MANtle)[3] to study Venus's atmospheric-interior-climate evolution from the post accretion magma ocean to the present. They concluded that both a habitable Venusian past and one where Venus never possessed liquid surface water are consistent with modern constrains. Moreover, their model allows for the scenario that the surface of Venus could have been temperate for 0.04 to 3.5 Gyr with a global ocean depth of up to a few hundred meters. Krissansen-Totton et al. (2021) emphasize the need for in-situ observations to better constrain past atmospheric evolution. Furthermore, Chassefière et al. (2012) stated that a precise measurements of the isotopic ratios of noble gases and other species are needed to help answering fundamental questions regarding the evolution of Venus.

Way et al. (2016) simulated several hypothetical Venus climates with ROCKE-3D (Resolving Orbital and Climate Keys of Earth and Extraterrestrial Environments with Dynamics), a global climate model (GCM). Their simulations showed that Venus could have had liquid water on its surface for approximately two billion years, between 2.9 Gya (billion years ago) until at least 0.715 Gya. Furthermore, they found that rotation rate and topography play crucial roles to understand the climatic history of Venus. For example, a slow rotation of Venus could lead to the formation of subsolar clouds, which would reflect the incident solar flux effectively and stabilize a potential oceans. In any case, all traces of an ocean would have disappeared, because of the possible resurfacing of the Venusian surface.

Turbet et al. (2021) also investigated the possible formation of surface liquid water on the surface of Early Venus. However, they criticised that most other studies have focused only on finding the conditions necessary to delay complete evaporation on Venus, while the presence of a liquid water ocean is often presumed. In their study, simulations were performed with a 3D global climate model (GCM), that also included clouds and atmospheric dynamics. This is important to investigate whether the water initially present in the atmosphere is able to condense on the surface. Their results showed that on early Venus water clouds have a strong net warming effect, preventing surface water condensation even at modest insolation. Therefore, in contrast to the results of Way et al. (2016), oceans may never have formed on the Venusian surface.

[3] https://github.com/joshuakt/Venus-evolution

1.2 Venus as a Laboratory for Exoplanets

As discussed in chapter 1.1.4, the surface temperature of early Venus might have been compatible with the presence of water oceans. Therefore, studying Venus could help us to understand how a planet that may have had liquid water on its surface became uninhabitable (Kane et al. 2019). One of the most fundamental questions in planetary science is the origin and evolution of life. As exoplanet detection methods are becoming more sensitive, we will be able to characterise the atmospheres of more terrestrial planets. In this research project, the composition of Venus-like atmospheres is simulated, using chemical equilibrium calculations. Even though this is a simplified model, the results can still help us to understand the possible composition of a variety of different Venus-like exoplanets.

In the foreseeable future, we will not be able to obtain in-situ data for exoplanet surface environments (Kane et al. 2019). At present, it is even difficult to obtain such data for our planetary neighbour Venus, as described in chapter 1.1.3. Furthermore, we still have problems to understand fundamental properties of objects within the solar system. For example, the interior structure and bulk composition of Venus are still unsure (Treiman 2007). In future we will have to characterise the surface environments of exoplanets indirectly from parameters we can measure, such as the planetary size and mass and the atmospheric composition. Therefore, the oxygen fugacity, defined as the partial pressure of oxygen within a system (Li et al. 2019; Frost & Lindsley 1991), could be a helpful tool to obtain information on the surface composition. Minerals on the surface could stabilise the atmospheric composition with mineral redox buffers, mineral assemblages that can buffer the redox state and oxygen fugacity of the atmosphere at a certain temperature and pressure (Holm & Andersson 2005; Frost & Lindsley 1991). In this research project, we will investigate the possible interaction between the surface and the atmosphere for Venus-like planets in chapter 3.4.

There are many questions about Venus's past that still have to be answered. For example, it is uncertain if Venus had a habitable period, as described in chapter 1.1.4. Furthermore, some properties of the Venus' deep atmosphere are still uncertain, as the thermal structure below the cloud layer at high latitudes remains unknown and no in-situ measurements have been made at latitudes above 60° (Ando et al. 2020). Current and future missions, such as the Transiting Exoplanet Survey Satellite (TESS) and JWST, will yield many new potential Venus- and Earth analogue planets (Ostberg & Kane 2019). However, the transit method to detect exoplanets is biased towards planets that are close to the host star. Therefore, especially around smaller M-dwarfs, the atmospheres of potential analogues to Venus might be easier to characterise than Earth analogues (Kane et al. 2019).

Kane et al. (2014) defined the "Venus Zone" (VZ) in which a planet is most likely a Venus analogue. This zone is similar to the habitable zone (HZ) that is defined as the region around a star where a planet with an Earth-like atmosphere can maintain liquid water on its surface (Kasting et al. 1993; Kopparapu et al. 2013, 2014). The outer boundary of the VZ is analogue to the inner boundary of the HZ defined by the runaway greenhouse effect, where the received flux would cause surface water on a terrestrial planet to be completely evaporated. The inner boundary of the VZ is located at a distance where a planet would receive ~25 times the Earth incident flux. This corresponds to a distance, where Venus would start to experience severe atmospheric loss, based on work by Catling & Zahnle (2009). The defined VZ will help to identify potential Venus analogues with future missions focused on the detection of exoplanets, such as JWST, PLATO, and NASA's mission concept LUVOIR (Large Ultraviolet Optical Infrared Surveyor).

2 Methods

2.1 Atmospheres in Chemical Equilibrium

One approach to modeling atmospheres is to assume chemical equilibrium (CE), an approximation but sometimes a very useful one. The thermodynamic state of a system can be described by a number of state variables. If the chemical system is closed at a constant temperature and pressure, chemical equilibrium is achieved when the Gibbs free energy of the system is minimised. Changes in the Gibbs free energy ΔG can be defined with Eq. 1, where ΔH and ΔS refer to the enthalpy and entropy changes of the system, respectively, under constant temperature T.

$$\Delta G = \Delta H - T\Delta S \tag{1}$$

Thermochemical equilibrium calculations can predict steady-state abundances of chemical species in the gas and solid phase. These reactions are highly dependent on temperature and pressure. Therefore, it can be estimated which species form in the gas phase, which compounds form condensates, and in what proportions (Perryman 2018). The determination of the chemical equilibrium offers a fast approximation to determine the composition of atmospheres. In this research project, Venus-like atmospheres in chemical equilibrium are investigated with the codes `FastChem` and GGchem. However, all atmospheres are out of chemical equilibrium to at least some extent because they receive a free energy from sunlight and the release of volcanic gases. Furthermore, atmospheric dynamics drive the chemical composition in atmospheres away from equilibrium (Tsai et al. 2018). Gases that are in chemical equilibrium in one part of the atmosphere may not be in equilibrium in another, as temperature and pressure can vary in different atmospheric layers. However, these layers can still exchange atmospheric species due to atmospheric turbulence.

Krissansen-Totton et al. (2016) calculated the thermodynamic chemical disequilibrium for atmospheres of different planets and moons in the Solar System. Therefore, they quantified the chemical disequilibrium in atmospheres by calculating the difference between the Gibbs free energy of the observed atmospheric species and that of the same atmosphere after all its constituents had reacted to chemical equilibrium. Furthermore, they quantified the atmosphere-ocean disequilibrium using multiphase Gibbs energy minimisation. For the Venusian atmosphere, they found a comparatively small disequilibrium, with the largest contributor being the coexistence of carbon dioxide (CO_2) and elemental sulfur (S), which is predicted to be depleted in equilibrium by the reaction shown in Eq. 2. However, the disequilibrium is maintained by photodissociation of sulfur dioxide (SO_2) and carbonyl sulfide (COS) in the upper atmosphere (Yung & DeMore 1998).

$$2\,CO_2 + S \rightleftharpoons SO_2 + 2\,CO \tag{2}$$

In Figure 5, the available Gibbs free energy they calculated for different solar system planets and Saturn's moon Titan is shown. In comparison to Venus, the disequilibrium in the Martian atmosphere is relatively large, which is also mainly due to photochemistry, whereas the disequilibrium in the atmosphere of Earth is maintained by the productive surface biosphere. As one can see in Figure 5, the atmospheres of gas giants, such as Jupiter, are very close to equilibrium, as photochemically produced species are mixed into the high temperature interior, where they reform their equilibrium species (Krissansen-Totton et al. 2016).

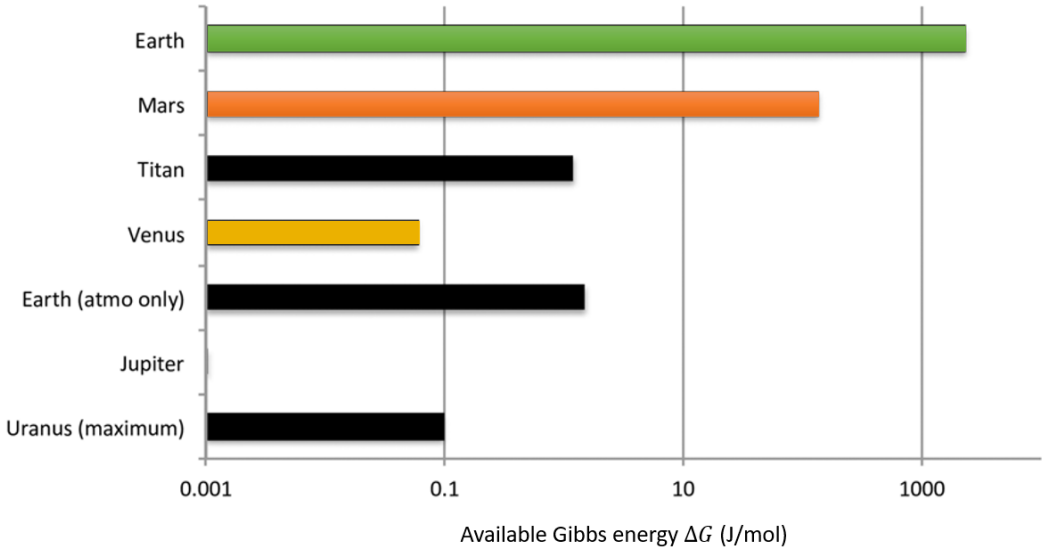

Figure 5: Available Gibbs free energy for planets in the solar system and Saturn's moon Titan (adapted from Krissansen-Totton et al. 2016). Please note the small disequilibrium in the Venusian atmosphere in comparison to Earth and Mars. For Uranus, where the observational knowledge of the atmosphere is limited, the maximum disequilibrium is shown.

Chemical disequilibrium of planetary atmospheres, such as the coexistence of the two long-term incompatible species oxygen and methane, was proposed as a possible biosignature, that could indicate the presence of life on an exoplanet (Seager & Bains 2015). After the first detections of exoplanets around the millisecond pulsar PSR B1257+12 by Wolszczan & Frail (1992), and the Sun-like main-sequence star 51 Pegasi by Mayor & Queloz (1995), more than 5000 exoplanet detections have been confirmed to date[4]. Observing the transits of exoplanets in multiple wavelengths enables the characterisation of their atmospheres. The ExoAtmospheres Database[5] lists such exoplanet atmospheric detections. Due to observational limitations the study of exoplanet atmospheres has mostly been focused on gas giants (e.g. Snellen et al. 2010). Hot Jupiters (e.g., HD 189733b, WASP-43b), warm Neptunes (e.g., GJ 436b, HAT-P-11b), and warm sub-Neptunes (e.g., GJ 1214b) are being studied extensively with the Hubble Space Telescope (HST), Spitzer, and other facilities.

[4] http://exoplanet.eu/
[5] http://research.iac.es/proyecto/exoatmospheres/

2.2 FastChem

2.2.1 Introduction to the code

FastChem[6] is an open-source chemical equilibrium code dealing with the gas-phase chemistry of different elements and including ions (Stock et al. 2018). In Figure 6 a graphical illustration of functionality of FastChem is shown. The model requires three input files. One file for the abundances of all elements that are used in the model. Other requirements are a temperature-pressure structure and thermochemical data for all molecules and ions, including their stoichiometric information and a parametrisation for their mass action constants. Then, the chemical equilibrium composition is numerically calculated by minimising the Gibbs free energy (Stock et al. 2022). The FastChem output includes two files with details on the chemistry and diagnostic. The chemistry output includes number densities or mixing ratios of all defined species. Furthermore, the gas pressure & temperature, total element density, gas number density, and mean molecular weight is given in the chemistry output file.

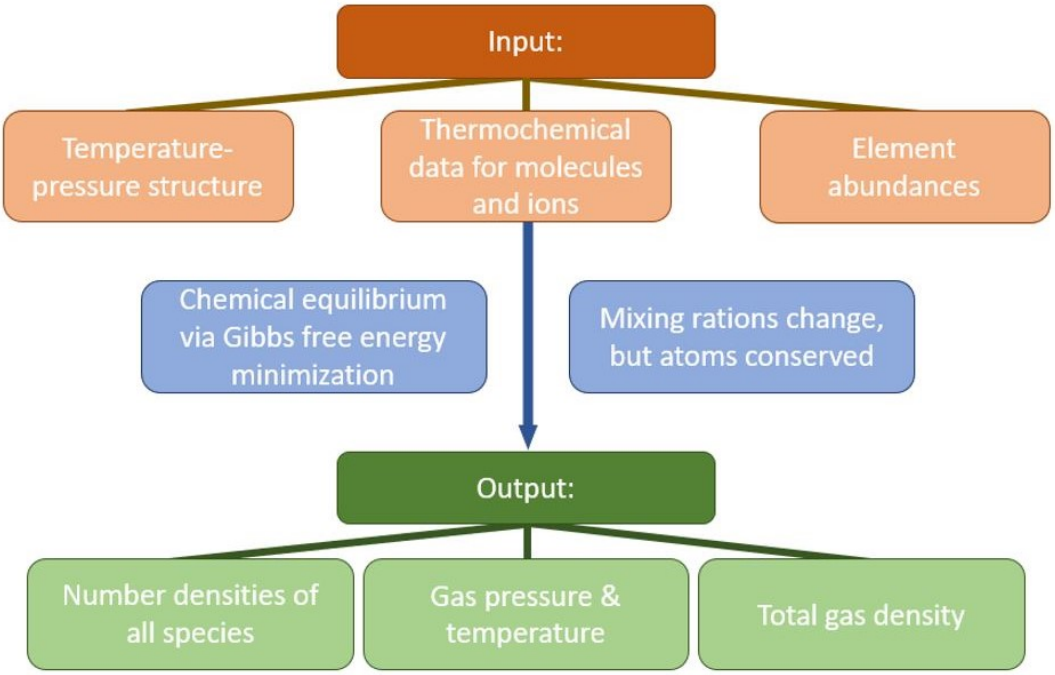

Figure 6: Graphical description of FastChem

The program code of FastChem is written in object-oriented C++. Moreover, the FastChem repository contains an additional open source code that makes it possible to call the code from within Python scripts, using the PyBind11 library. Prerequisites for the use of FastChem are a C++ compiler and CMake. The program can mainly be compiled and run on Linux and MacOS. In this project a virtual Linux environment was used to run FastChem on Windows, using Oracle VirtualBox.

[6] https://github.com/exoclime/FastChem

2.2.2 Algorithm

In this section the algorithm of `FastChem` is shortly described. For a more details see Stock et al. (2018, 2022). First, a set of all species in the gas phase $\mathcal{S} = \{S_1, ..., S_{|\mathcal{S}|}\}$, for which thermodynamic data is given in the model input, is selected, with $\mathcal{E} = \{E_1, ..., E_{|\mathcal{E}|}\} \subset \mathcal{S}$ being the set of all chemical elements considered in the model. Furthermore, in this description $\mathcal{S}_0$ refers to the set of all species and $\mathcal{E}_0 \subset \mathcal{S}_0$ to the set of all elements of the model including the electron. To determine the chemical equilibrium composition for a given total gas pressure p and temperature T, dissociation equilibrium is assumed. Therefore, the dissociation reaction (Eq. 3) is considered for each species:

$$S_i \rightleftharpoons \nu_{i,0}E_0 + \nu_{i,1}E_1 + ... + \nu_{i,j}E_j + ... = \sum_{j\in\mathcal{E}_0} \nu_{i,j}E_j \tag{3}$$

The coefficients $\nu_{i,j}$ are the stoichiometric coefficients of element j in molecule i. If an element is not involved in the formation of a molecular species, $\nu_{i,j} = 0$ (Gail & Sedlmayr 2014). The number densities n_i are then determined in dissociative equilibrium using the law of mass action, where K_i denotes the mass action constant.

$$n_i = K_i \sum_{j\in\mathcal{E}_0} n_j^{\nu_{i,j}} \quad \forall i \in \mathcal{S}\backslash\mathcal{E} \tag{4}$$

In combination with the element and charge conservation equations, $\epsilon_j n_{\langle H\rangle}$ can be determined, with ϵ_j being the relative elemental abundance with respect to hydrogen, and $n_{\langle H\rangle}$ being the sum of all hydrogen nuclei per unit volume.

$$\epsilon_j n_{\langle H\rangle} = n_j + \sum_{i\in\mathcal{S}\backslash\mathcal{E}} \nu_{ij} n_i \tag{5}$$

For the `FastChem` algorithm, instead of solving Eq. 3 and Eq. 4 simultaneously, the equation system is decomposed into a set of equations, each of them in one variable n_j, which reduces the number of variables from $|\mathcal{S}_0|$ to $|\mathcal{E}_0|$. Therefore, $n_{j,min}$ is employed as a correction term.

$$\epsilon_j n_{\langle H\rangle} = n_j + \sum_{k=1}^{N_j} k\, n_j^k \sum_{\substack{i\in\mathcal{S}\backslash\mathcal{E} \\ \nu_{ij}=k \\ \epsilon_i=\epsilon_k}} K_i \prod_{\substack{l\in\mathcal{E}_0 \\ l\neq j}} n_l^{\nu_{il}} + n_{j,min} \quad \text{with } n_{j,min} = \sum_{\substack{i\in\mathcal{S}\backslash\mathcal{E} \\ \epsilon_i<\epsilon_j}} \nu_{ij} n_i \qquad j \in \mathcal{E} \tag{6}$$

This essentially reduces to the problem of finding the root of the polynomial $P_j(n_j)$, with the coefficients A_{jk}, that are evaluated by employing Horner's rule.

$$P_j(n_j) := \sum_{k=0}^{N_j} A_{jk} n_j^k \tag{7}$$

First, the initial values for the electron density $n_0^{(0)}$ and the correction terms $n_{j,min}^{(0)}$ are set and the logarithm of the dimensionless mass action constants K_i are calculated with Eq. 8 for the considered species at a given temperature T, using coefficients calculated from various thermochemical tables (e.g., Chase 1998) specified in the species data file.

$$\log K_i = a_1/\mathrm{T} + a_2 \ln \mathrm{T} + a_3 + a_4 \mathrm{T} + a_5 \mathrm{T}^2 \tag{8}$$

Then, the number densities are calculated for all atomic species n_j ($j \in \mathcal{E}$) via Eq. 6 in descending order, starting with the most abundant element. The results are used to calculate the number densities of the molecular species n_i ($i \in \mathcal{S}\backslash\mathcal{E}$) via the law of mass action, shown in Eq. 5. Finally, $n_{j,min}$ is updated and the electron density n_0 is calculated.

2.2.3 Input parameters

`FastChem` requires multiple input data files. The element composition has to be specified in the form indicated by Eq. (9), where the convention of stellar atmospheric theory ($\varepsilon_H = 12$) is used. This astronomical scale for logarithmic abundances is defined for hydrogen to be $\log \varepsilon_H = 12$. With this condition, the abundance of other elements can be converted using $\log \varepsilon_X = \log(N_X/N_H) + 12$, where N_X and N_H are the number densities of elements X and H, respectively.

$$x_j = 10^{\varepsilon_j - 12.0} = N_j/N_H \tag{9}$$

Using the main molecular composition of the Venusian atmosphere, collected from various sources, the elemental abundance can be calculated. Elements not present in the input data file are ignored. In Table 5 the initial molecule abundances from measurements in the Venusian atmosphere and element abundances calculated from these are shown. Note that `FastChem` uses the Hill notation for all species. Therefore, the number of carbon atoms of the molecule is initiated first, then the number of hydrogen atoms, and last the number of all other elements in alphabetical order of the chemical symbols.

Table 5: Molecular composition of the Venusian atmosphere and the calculated fractional element abundances and using the convention of stellar atmospheric theory, normalised so that $x_H = 12$ on a decadic logarithmic scale. The element abundances are given as mixing ratios and in solar photospheric element abundances according to Asplund et al. (2009).

Molecule abundance			Element abundance		
CO_2	0.964678				
N_2	0.034988		O	0.650900	16.50371
Ar	7.00E-05		C	0.325397	16.20261
Ne	5.00E-06		N	0.023603	15.06316
H_2O	3.00E-05		Ar	2.36E-05	12.06331
SO_2	1.50E-04	$\Longrightarrow$	Ne	1.69E-06	10.91718
CSO	4.00E-06		H	2.04E-05	12
CO	4.50E-05		S	5.19E-05	12.40573
HCl	5.00E-07		Cl	1.69E-07	9.917179
HF	5.00E-09		F	1.69E-09	7.917179
He	9.00E-06		He	3.04E-06	11.17245
(O_2)	2.00E-05				

The references for the molecular abundances used in the calculations are given for all species in more detail in the following section:

Carbon dioxide & nitrogen:
For both CO_2 and N_2 the typically quoted values of 96.5% and 3.5% recommended by Von Zahn et al. (1983) were used for the calculations. Since minor species are also included in the calculations, the initial CO_2 and N_2 decreases slightly for the calculations, so the total molecule abundance adds up to 1. This can be justified, since the uncertainty of both values is about 0.8%. In-situ measurements from *Pioneer Venus* of N_2 varied from 4.60 ± 0.14% (3σ) N_2 at 51.6 km to 3.41 ± 0.01% (3σ) at 21.6 km altitude. Similarly, for CO_2 the *Pioneer Venus* measurements varied between 96.4 ± 1.0% (3σ) at 21.6 km to 95.4 ± 2.5% (1σ) at 51.6 km (Oyama et al. 1980).

Water vapour:
For H_2O, the commonly cited value of 30 ± 15 ppmv for altitudes between 0 and 45 km was used (Taylor et al. 1997). This is consistent with Earth based infrared (IR) observations (e.g., Pollack et al. 1993; De Bergh et al. 1995), and *Venus Express* measurements of 31 ± 2 ppmv (1σ) at 30-40 km (Marcq et al. 2008).

Sulfur dioxide:
For SO_2 the 150 ppm observed by the *Venera 12* UV spectrometer at an altitude of 22 km was used (Von Zahn et al. 1983). A gas chromatograph on *Venera 12* measured 130 ± 60 ppm (Gelman et al. 1979). The adopted value is also consistent with remote data from IR spectra measured with the VIRTIS-H instrument of *Venus Express*, that resulted in 130 ± 50 ppmv (1σ) at 35 km (Marcq et al. 2008). For the lower atmosphere, where no other data is available, Bertaux et al. (1996) reported 20-25 ppm at 12 km, measured with the *Vega 1 & 2* UV spectrometer.

Carbon monoxide:
The calculations were done with a CO mole fraction of 45 ppm, observed with Earth based telescopes for 42 km (Bezard et al. 1990). At 12 km the gas chromatograph of Venera 11/12 measured 17 ± 1 ppmv in situ (Gelman et al. 1979). Furthermore, *Pioneer Venus* measured 19.9 ± 3.12 ppm (3σ) at 21.6 km (Oyama et al. 1980).

Carbonyl sulfide:
For CSO a value of 4 ppm was used. This is consistent with Earth-based measurements by Pollack et al. (1993) (4.4 ± 1 ppm) and *Venus Express* measurements of 2.5 – 4 ± 1 ppmv (1σ) with VIRTIS-H (Marcq et al. 2008).

Hydrogen cloride & hydrogen flouride:
The HCl (0.5 ppm) and HF (5 ppb) used were mainly derived from Earth-based observations. Bézard (1994) presented 0.5 ± 0.15 ppmv for HCl at 15-30 km and 5 ± 2 ppbv for HF at 30 – 40 km measured with near-infrared spectroscopy of the night side. *Venus Express* data include 0.17 ± 0.03 ppm (1σ) for HCl at 70 – 75 km and 0.001 - 0.003 ppb for HF at 75-85 km, measured with the Solar Occultation in the InfraRed (SOIR) spectrometer on board the *Venus Express* spacecraft at different orbits (Bertaux et al. 2007).

Oxygen:
Molecular oxygen (O_2) was measured in the Venusian atmosphere by *Pioneer Venus* between 43.6 ± 2.9 ppm and 16.0 ± 0.9 ppm at 51.6 km and 41.7 km altitude (Oyama et al. 1980). *Venera 12* estimated an upper limit of 20 ppm for altitudes below 42 km, that was used for the calculations (Gelman et al. 1979).

Noble gases:
Adopted values for the noble gases argon (Ar; 70 ± 25 ppm) and neon (Ne; 7 ± 3 ppm), are mean values from *Pioneer Venus* and *Venera 11/12* measurements recommended by Von Zahn et al. (1983) for altitudes < 100 km. These are a combination of reported values. For He (9 ± 6 ppm) an extrapolation for the middle to lower atmosphere by Krasnopolsky & Gladstone (2005) was used. The addition of non-reactive noble gases to the system should have no effect on the chemical equilibrium calculations.

Minor species that were observed in the Venusian atmosphere in trace amounts, but not included in the input for the calculations are: Kr, Xe, H_2, HDO, H_2S, H_2SO_4 and CH_4.

Besides the elemental abundances of the atmosphere and a list of all considered species, `FastChem` requires temperature-pressure data. The temperature-pressure profile of Venus, shown in Figure 7, from the Venus International Reference Atmosphere (VIRA, Moroz & Zasova 1997) was used for the calculations in this project. The profile goes from the surface (92 bar, 735 K) to an altitude of about 68 km (0.01 bar, 216 K), which includes the troposphere and main cloud layer regions in Figure 2. A steeper decrease in pressure can be seen starting from about 250 K. This represents the radiative-convective boundary, which is around 0.2 bars. Above this value radiation is the primary mechanism of heat transport in the atmosphere. The exact values of the 24 data points for temperature and pressure, that are indicated in Figure 2, are given in Table 6.

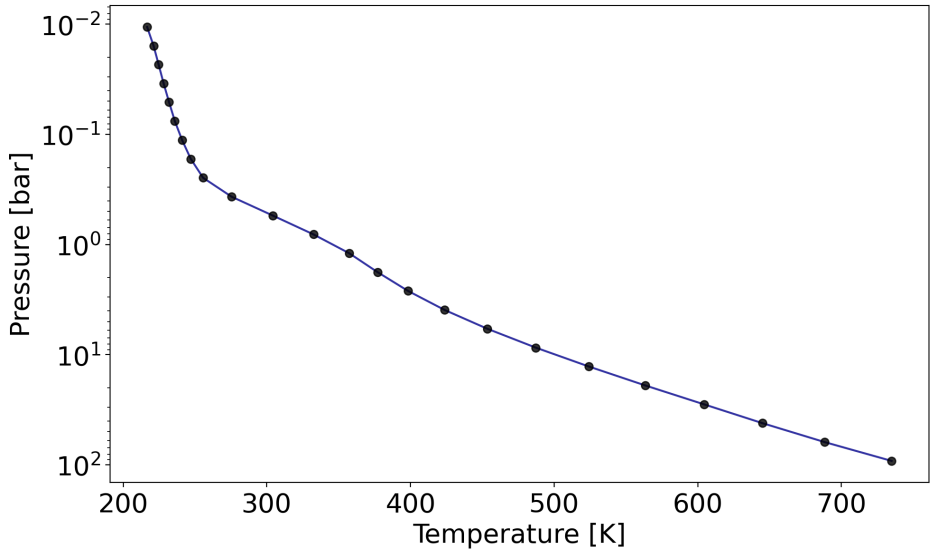

Figure 7: Temperature-pressure profile used for the calculations. The profile includes 24 data points from the Venus International Reference Atmosphere (VIRA, Moroz & Zasova 1997) between the surface (~92 bar) and an altitude of 68 km (~0.01 bar).

Table 6 shows the temperature and pressure values for the 24 data points used in the calculations and the corresponding altitudes. Please note the high temperature (735 K) and pressure (92.1 bar) at the surface of Venus.

Table 6: Data of the temperature pressure profile used for the calculations.

Altitude [km]	Pressure [bar]	Temperature [K]	Altitude [km]	Pressure [bar]	Temperature [K]
0	9.21E+01	735.0	46.886	8.09E-01	332.5
5.473	6.21E+01	688.3	49.370	5.45E-01	304.1
10.607	4.18E+01	645.0	51.634	3.68E-01	275.5
15.426	2.82E+01	604.3	53.709	2.48E-01	255.7
19.941	1.90E+01	563.4	55.676	1.67E-01	247.1
24.145	1.28E+01	524.2	57.586	1.13E-01	241.1
28.066	8.63E+00	487.3	59.453	7.58E-02	236.0
31.715	5.82E+00	453.6	61.286	5.11E-02	232.0
35.122	3.92E+00	423.7	63.089	3.45E-02	228.2
38.317	2.64E+00	398.4	64.865	2.32E-02	224.7
41.336	1.78E+00	377.1	66.615	1.57E-02	221.2
44.199	1.20E+00	357.4	68.333	1.06E-02	216.7

For the computation of the chemical equilibrium, the algorithm requires a list of all chemical elements, molecules, and/or ions, that should be included in the calculations. Ions can be cations and anions of atoms and molecules. This list must include the coefficients to calculate the natural logarithm of the dimensionless mass action constant K_i with Eq. (8).

The set of all species used in the calculation during this project is listed in Table 7. This list corresponds to all species included in `FastChem`, containing O, C, N, Ar, S, H, He, Ne, Cl, and F, without considering species that contain other elements. In total, this includes 243 species. There are many chlorides and fluorides included as molecules, which should not be relevant for simulating the Venusian atmosphere, since only hydrogen chloride (HCl) and hydrogen fluoride (HF) have been detected so far. Nonetheless, it could be interesting to investigate the behaviour of these species in chemical equilibrium.

Table 7: List of all species included in the calculations.

Element	Molecules, Ions
O	HO, HO_2, H_2O, H_2O_2, O_2, O_3, HO^+, HO^-, H_3O^+, O^+, O^-, O_2^+, O_2^-
C	CCl, CClFO,CClN, CClO, CF, CFN, CFO, CH, CHCl, CHF, CHFO, CHN_1, CHN_2, CHNO, CHO, CH_2, CH_2Cl_2, CH_2ClF,CH_2F_2, CH_2O, CH_3, CH_3Cl, CH_3F, CH_4, CH_4O_2, CO, CO_2, C_2, C_2H, C_2HCl, C_2HF, C_2H_2, $C_2H_2O_2$, $C_2H_2O_4$, $C_2H_3ClO_2$,C_2H_4, C_2H_4O, $C_2H_4O_3$, $C_2H_6O_2$, C_2O, C_3, C_3H, C_3N_2O, C_3O_2, C_4, $C_4H_6O_4$, C_4N_2, C_5, C^+, C^-, CF^+, CF_2^+, CF_3^+, CH^+, CH^-, CHO^+, CN^+, CN^-, CO_2^-, C_2^-
N	CN, CNO, CN_2 (CNN), CN_2 (NCN), NO_2, NO_3, N_2, N_2O, N_2O_3, N_2O_4, N_2O_5, N_3, N^+, N^-, NO^+, NO_2^-, N_2^+, N_2^-, N_2O^+, C_2N, C_2NO, C_2N_2
Ar	Ar^+
S	COS, CS, CS_2, HS, H_2SO_4, H_2S, NS, OS, S_2O, SO_2, SO_3, S_2, S_3, S_4, S_5, S_6, S_7, S_8, HS^-, S^+, S^-
H	HN, HNO, HNO_2 (cis), HNO_2 (trans), HNO_3, H_2, H_2N, H_2N_2, H_2O, H_2O_2, H_3N, H_4N_2, H_2^+, H_2^-, H^+, H^-
He	He^+
Ne	Ne^+
Cl	$ClFO_2S$,$ClFO_3$, ClF_3, ClF_5, ClF_5S, ClH, $CHClF_2$,$CHCl_2F$,ClHO, ClNO, $ClNO_2$, ClO, ClO_2, ClO_3, ClS, ClS_2, Cl_2, Cl_2O (ClOCl), Cl_2O (ClClO), Cl_2O_2 (ClO_2Cl), Cl_2O_2 (ClOClO), Cl_2O_2S, Cl_2S, CCl_3, CCl_2, CCl_2O, CCl_3F, CCl_4, $CHCl_3$, ClF, C_2Cl_2, C_2Cl_4, C_2Cl_6, Cl^+, ClS^+, Cl^-, Cl_2S^+
F	FH, FHO, FHO_3S, FN, FNO, FNO_2, FNO_3, FO, FO_2 (OFO), FO_2 (FOO), FS, F_2, F_2H_2, F_2N, F_2N_2 (cis), F_2N_2 (trans), F_2O, F_2OS, F_2O_2, F_2O_2S, F_2S, F_2S_2 (1), F_2S_2 (2), F_3H_3, F_3N, F_3NO, F_3S, F_4H_4, F_4N_2, F_4S, F_5H_5, F_5S, F_6H_6, F_6S, F_7H_7, $F0S_2$, $CClF_3$, CCl_2F_2, CF_2, CF_2O, CF_3, CF_4, CF_4O, CF_8S, CHF_3, C_2F_2, C_2F_3N, C_2F_4, C_2F_6, F^+, F^-, FS^+, FS^-, F_2S^+, F_2S^-, F_3S^+, F_3S^-, F_4S^+, F_4S^-, F_5S^+, F_5S^-, F_6S^-

The list of species in Table 7 includes two dichlorine dioxides: chloryl chloride (ClO_2Cl) & chlorine chlorite (ClOClO). Similarly, for CN_2 and Cl_2O, and FO_2 there are different isomers with the same chemical formula included as an input. For F_2S_2 the isomers difluorodisulfane (F_2S_2 (1)) and thiothionyl fluoride (F_2S_2 (2)) are included. Furthermore, the species F_2N_2 and HNO_2 are incorporated as cis- and trans-isomers, where the compounds have a different configurations. Most of these species are not expected to strongly influence the composition of the Venusian atmosphere. The thermochemical data for the species listed in Table 7 is mostly based on the National Institute of Standards and Technology (NIST)-JANAF thermochemical tables from Chase (1998).

2.2.4 Convergence

We encounter a stoichiometric equilibrium problem at a C/O ratio near 0.5 when trying to simulate the Venusian atmospheres with `FastChem`, using the input parameters described in chapter 2.2.3. This is relevant for this work, as the C/O ratio of the Venusian atmosphere is 0.499918, calculated from the element abundances in Table 3. In the beginning, `FastChem` reached the maximum amount of chemistry iteration (100.000) for calculations with C/O ratios between 0.49987 and 0.50020, when using the default accuracy. As one can see in Figure 8, in this region the abundances of some species changes abruptly between different atmospheric layers. Moreover, very small changes in the C/O ratio seem to have a substantial effect on the molecular abundance in the modelled atmosphere.

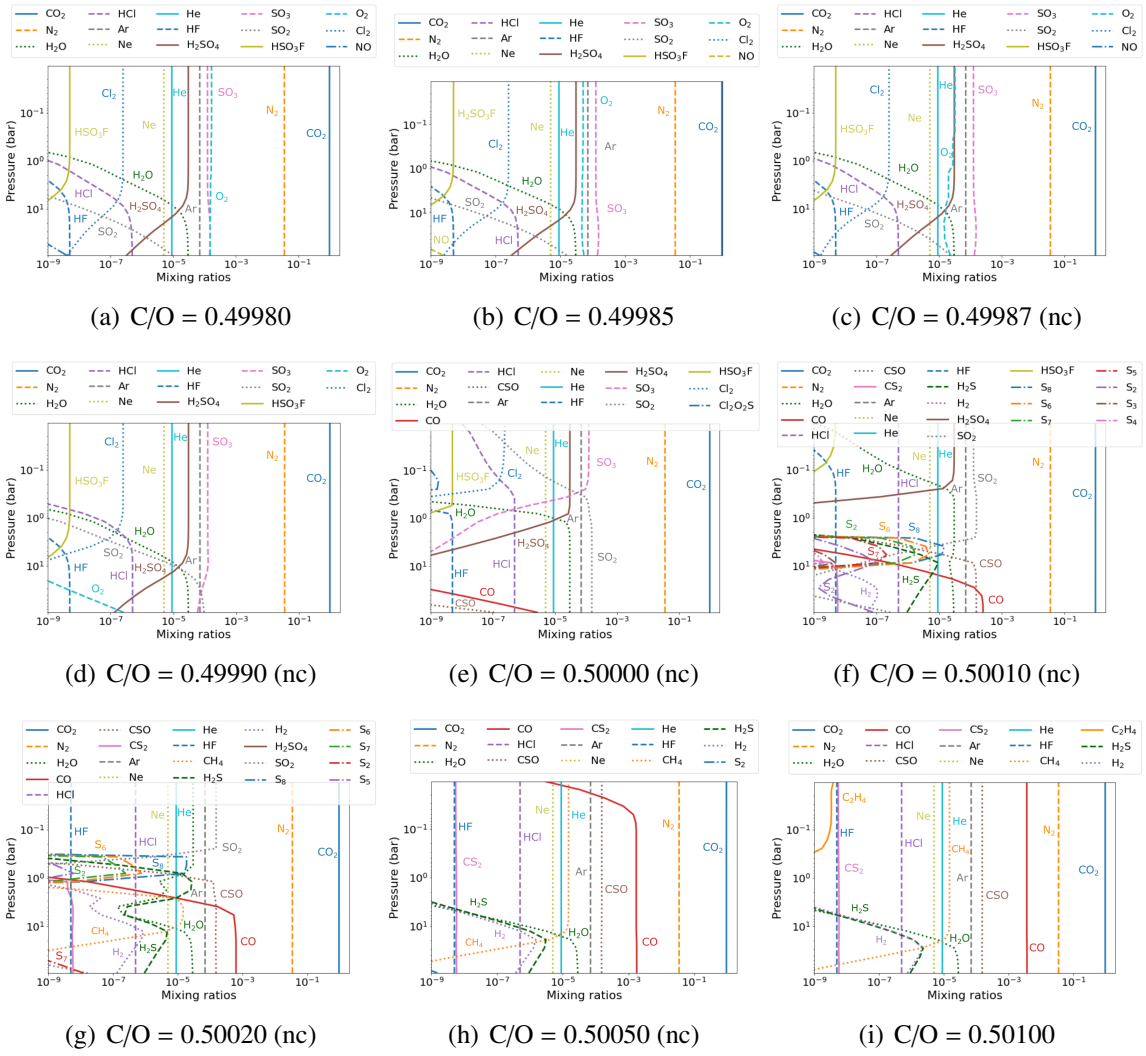

(a) C/O = 0.49980 (b) C/O = 0.49985 (c) C/O = 0.49987 (nc)

(d) C/O = 0.49990 (nc) (e) C/O = 0.50000 (nc) (f) C/O = 0.50010 (nc)

(g) C/O = 0.50020 (nc) (h) C/O = 0.50050 (nc) (i) C/O = 0.50100

Figure 8: Convergence problem at C/O ratios around 0.5. When no convergence was reached when running the model, the plot is marked with (nc) in the caption.

Fortunately, this encountered chemistry convergence problem can be solved by decreasing the desired numerical accuracy or increasing the maximum number of iteration steps. Therefore, the accuracy of a chemistry iteration (*chem_acc*) and the maximum number of chemistry iterations (*chem_it*) can be changed as input variables. An higher chemical accuracy of the simulation requires more chemistry iterations and consequently more computation time. Therefore, it is important to find the minimum chemical precision needed to answer the questions to be addressed, representing the best compromise between accuracy and computational cost. To locate this "sweet spot", test calculations of different chemical accuracy

were performed, to determine the number of iteration steps needed for the model to converge, respectively. In Figure 9, the mean and maximum number of iteration steps of the 24 pressure and temperature points, required to achieve certain chemistry accuracies between $5 \cdot 10^{-2}$ (low accuracy) and $5 \cdot 10^{-5}$ (high accuracy) are plotted logarithmically.

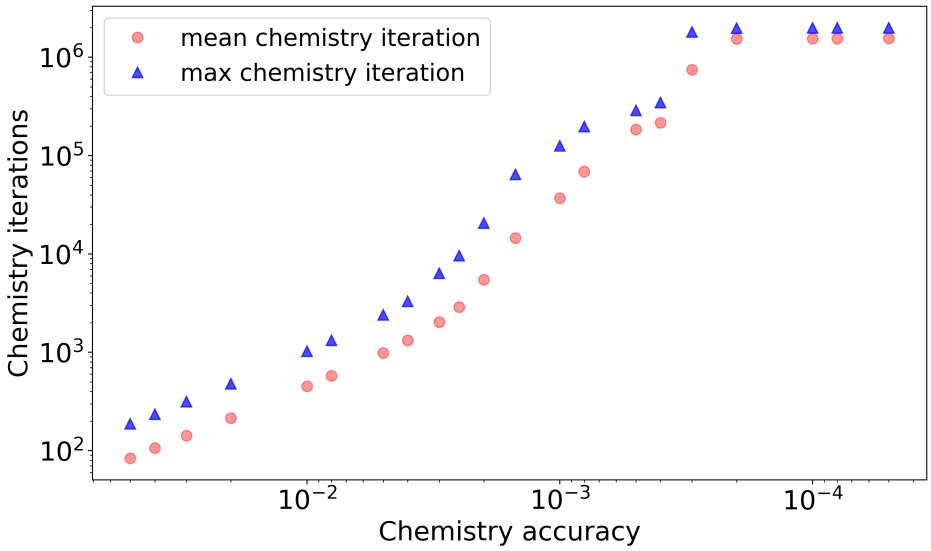

Figure 9: Optimisation of the chemical accuracy. The mean and maximum number of iteration steps of the 24 T-p data points required to achieve different chemical accuracies are plotted. Please note that the chemistry accuracy is increasing from left to right.

As one can see in Figure 9, the mean and maximum number of required iteration steps increases in a power-law fashion, which also translates to the computational time. While a model run with an accuracy of $5 \cdot 10^{-2}$ takes only a few 10 seconds, running the model with $5 \cdot 10^{-5}$ can take hours, depending on the computational power. The chemistry of these models changes significantly, as shown in Figure 10 where the atmospheric composition for models with accuracy $8 \cdot 10^{-3}$ and 10^{-4} is illustrated. Furthermore, there is a recognisable plateau in Figure 9 for high accuracy, between 10^{-4} and $5 \cdot 10^{-5}$, which indicates that here the chemistry of the models does no longer change.

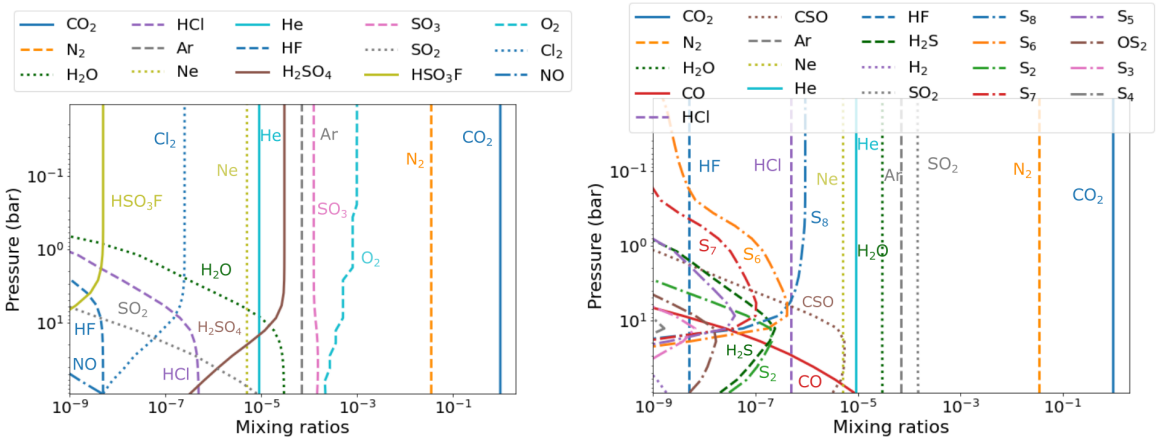

(a) *chem_acc* = $8 \cdot 10^{-3}$

(b) *chem_acc* = 10^{-4}

Figure 10: Atmospheric composition of the Venusian atmosphere (C/O = 0.499918) for models with high (right) and low (left) accuracy.

While in the low accuracy model (Figure 10(a)) many oxygenated species, such as H_2SO_4,

SO_2, SO_3, HSO_3F, and O_2 are present, the high accuracy model (Figure 10(b)) includes more reduced species, such as CO, CSO, H_2S, H_2, or even allotropes of sulfur. In Figure 11 the change of the chemistry for models with accuracies between 10^{-2} and $5 \cdot 10^{-5}$ is shown. One interesting aspect is, that for low accuracy models the computationally most costly layers are located in the lower atmosphere (T = 92.1; p = 735), while for higher accuracy they are at lower temperatures and pressures.

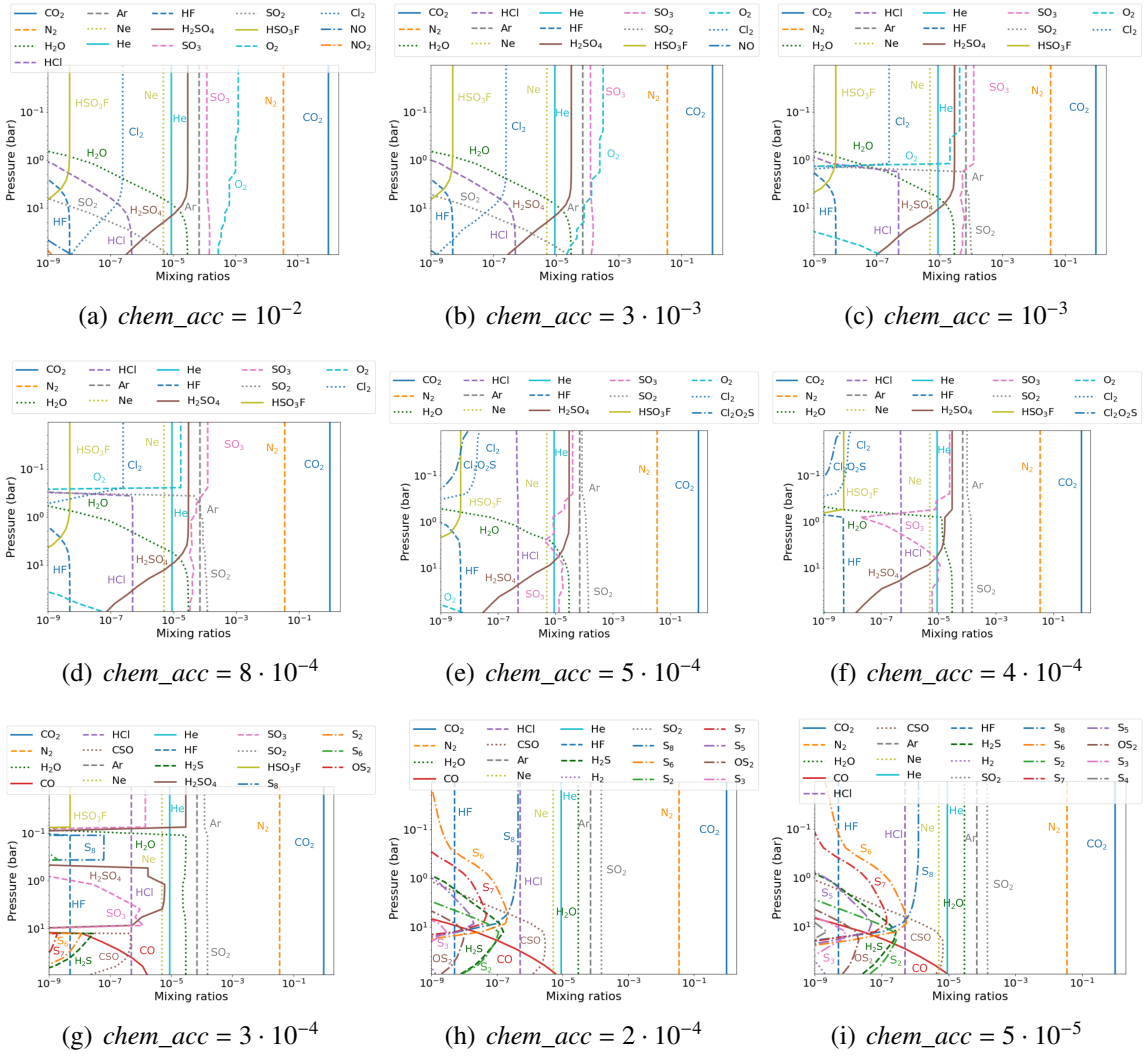

(a) *chem_acc* = 10^{-2} (b) *chem_acc* = $3 \cdot 10^{-3}$ (c) *chem_acc* = 10^{-3}

(d) *chem_acc* = $8 \cdot 10^{-4}$ (e) *chem_acc* = $5 \cdot 10^{-4}$ (f) *chem_acc* = $4 \cdot 10^{-4}$

(g) *chem_acc* = $3 \cdot 10^{-4}$ (h) *chem_acc* = $2 \cdot 10^{-4}$ (i) *chem_acc* = $5 \cdot 10^{-5}$

Figure 11: Element abundance for different `FastChem` accuracy.

Another indicator, how well a certain model reproduces the Venusian atmosphere, is to compare the mixing ratios the species with the Venusian molecular abundances used as an input from Table 3. Since the objective of this project is to simulate the atmospheres of Venus-like planets in chemical equilibrium, the atmospheres do not have to perfectly resemble the "real" Venus. Nonetheless, it is a good measure for the accuracy of the chemical equilibrium calculations. The chemical composition of models with an accuracy higher than 10^{-4}, or in other words *chem_acc* set to a value below 10^{-4}, is close to the molecular and elemental composition used as an input. However, the molecular composition of models with an accuracy smaller than 10^{-4} is quite dissimilar from the input composition. The difference for oxidised species, such as SO_2 and H_2O gets significantly larger, while OCS and CO vanish completely and O_2 rises. Furthermore, the mixing ratios of HCl and HF alter and other chlorine and fluorine species, such as Cl_2 and HSO_3F become abundant. For this project, an optimised accuracy of $5 \cdot 10^{-5}$ is used to simulate the atmospheres of Venus-like planets in chemical equilibrium.

2.3 GGchem

`FastChem` does not include condensates in the model. However, the existence of clouds in the Venusian atmosphere is evident from Earth-based observations, for example polarimetric observations by Hansen & Hovenier (1974). Therefore, the fast thermochemical equilibrium code GGchem[7], which includes equilibrium condensation down to 100K (Woitke et al. 2018), was used to investigate the influence of condensates on the chemical composition on Venus-like planets. Similar to `FastChem`, the code is also based on the principle of minimising the total Gibbs free energy to calculate the chemical equilibrium. However, the code can do this for molecules in the gas phase and, in addition to that, calculate the phase equilibrium for condensates. The supersaturation ratio of a condensate S_j can be calculated from the vapour pressure p_j^{vap} of the bulk condensate.

$$S_j = \frac{p_j}{p_j^{vap}(T)} \tag{10}$$

In phase equilibrium there are two outcomes considered for the supersaturation ratio S_j :

$$S_j \begin{cases} < 1 \text{ condensate is unstable and not present} \\ = 1 \text{ condensate is stable and present} \end{cases} \tag{11}$$

There are two kinds of condensation that can occur in a planetary atmosphere. Either, condensation directly from the gas phase, which lowers the gas phase abundances of elements, or a transition from one condensate to another with no changes in the gas phase (Herbort et al. 2022). Depletion of elements by condensation can also be simulated with GGchem, by using the "remove condensates" option. Then thermally stable condensates are removed from the model, until saturation is achieved (Herbort et al. 2022). The required input data of GGchem is similar to `FastChem`. First, the elements included in the calculations have to be defined. Their abundances can be either chosen the pre-installed options "Solar" (from Asplund et al. 2009), "EarthCrust", "Ocean", and "Meteorites", or customised. Then, the molecular equilibrium constants, K_p(T), are calculated for the defined species in the temperature-pressure range using data from the NIST-JANAF thermochemical tables (Chase 1998) and the geophysical database SUPCRTBL (Zimmer et al. 2016).

To compare to the `FastChem` model results for Venus, only including gas-phase species, with the GGchem results, also including condensates, the same input parameters described in chapter 2.2.3 are used for the model. The output file of GGchem contains all computed molecular, atom and ion particle densities. Furthermore, the supersaturation ratios and the concentration of condensates, in units per hydrogen nucleus, is given in the output file. From this file, the total gas phase particle density $n_{\text{tot;gas}}$ can be calculated by the sum of the particle densities of all present gas phase species. Furthermore, the sum over all present condensates gives $n_{\text{tot;cond}}$. This can be used to derive the total particle density $n_{\text{tot}} = n_{\text{tot;gas}} + n_{\text{tot;cond}}$. Gas phase mixing ratios are defined as $n_x/n_{\text{tot;gas}}$ in this thesis.

[7] https://github.com/pw31/GGchem

3 Results

3.1 Venusian Atmosphere in Chemical Equilibrium

We first investigated how well the measured Venusian atmosphere could be reproduced by chemical equilibrium (CE) calculations. To simulate the Venusian atmosphere, the code is run with the atmospheric temperature-pressure (T-p) profile from Table 6, with 24 pressure and temperature points, and the element abundances from Table 3. Furthermore, a species datafile containing all species listed in Table 7 is taken as an input. In Figure 12 the simulated Venusian atmosphere in chemical equilibrium is shown together with the temperature-pressure profile. The output is similar to the observed atmospheric composition of Venus, only at mixing ratios smaller than 10^{-6} many reduced sulfur species are present, for example the allotropes of sulfur S_8, S_6, S_2, S_7, S_5, S_3, and S_4, as well as hydrogen sulfide (H_2S).

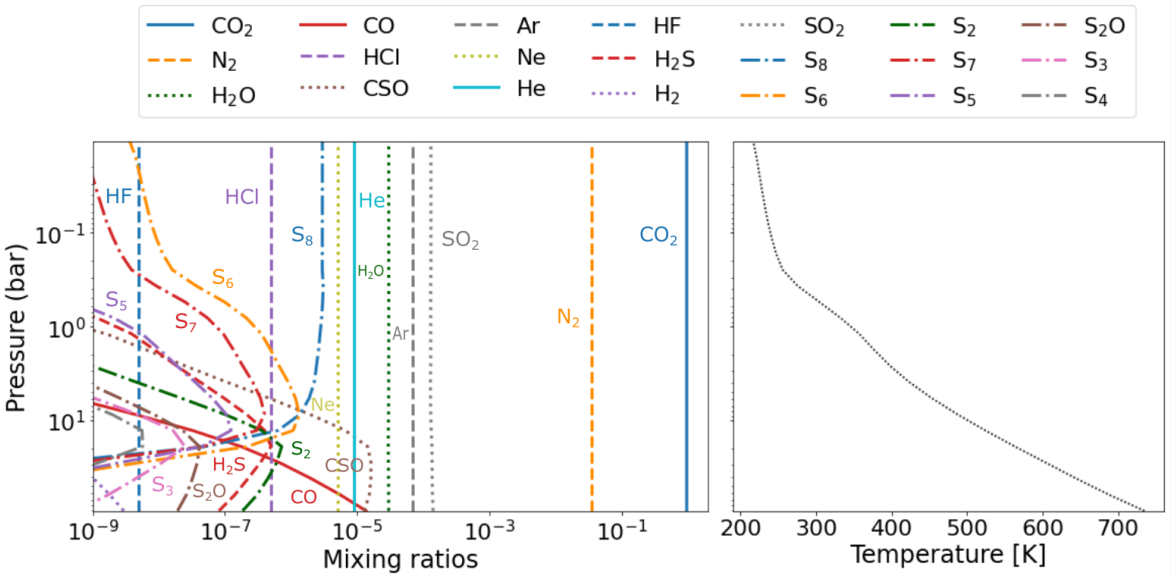

Figure 12: Mixing ratios of the simulated Venusian atmosphere with T-p structure. The abundance of species with mixing ratios above 10^{-9} is shown between the surface (92.1 bar) and an altitude of 68 km (0.01 bar).

In Table 8 the model output is compared to the molecular composition of the Venusian atmosphere. Therefore, the mean and maximum abundance of all species with abundances over 10^{-7} are calculated over the 24 temperature and pressure data points. Furthermore, the difference between the maximum mixing ratio of the `FastChem` output and the Venusian input is calculated and given in percentage terms. Please note that there can be very minor differences in the molecular abundance of noble gases (Argon, Helium, Neon), which would in theory not be expected. This is caused by the change of the total number of molecules, when atoms are bound in larger species (e.g., CO_2) in contrast to species containing fewer atoms (e.g., CO). Therefore, abundance changes in the mixing ratio that are smaller than the ones observed for noble gases can be neglected. For N_2, HCl, HF, and H_2O there are no or very minor differences between the input and output element abundances. The mean abundance for SO_2, CO and CSO is smaller in the model and seems to be absorbed by CO_2 together with O_2, that vanished completely in the model. This is not unexpected, since the observations of molecular oxygen (O_2) by *Pioneer Venus* between 43.6 ppm and 16.0 ppm (Oyama et al. 1980) were measured at 51.6 km and 41.7 km altitude and questioned by Von Zahn et al. (1983). The calculations were repeated without the additional source of oxygen from O_2, but resulted in similar abundances. Furthermore, some sulfur species, such as S_8, S_6, H_2S, S_2, and S_7 can be found in the atmosphere, that were not defined as input species.

Table 8: Comparison of the molecular composition of the Venusian atmosphere with the model outputs of FastChem and GGchem. The percentage difference $Diff_{IF}$ and $Diff_{IG}$ between the maximum abundance from the models outputs and observations of the Venusian atmosphere (Input) is indicated. Furthermore, the difference between the maximum abundance of both model outputs $Diff_{FG}$ is shown. S_2[s] denotes condensed sulfur dioxide in the solid phase, which can be found in the output of GGchem.

Species	Input	FastChem Output		$Diff_{IF}$	GGchem Output		$Diff_{IG}$	$Diff_{FG}$
		Mean	Max	%	Mean	Max	%	%
CO_2	9.65E-01	9.65E-01	9.65E-01	-0.03	9.65E-01	9.65E-01	-0.03	0.00
N_2	3.50E-02	3.50E-02	3.50E-02	-0.03	3.50E-02	3.50E-02	-0.03	0.00
SO_2	1.50E-04	1.46E-04	1.50E-04	0.17	1.42E-04	1.48E-04	-1.07	-1.23
Ar	7.00E-05	7.00E-05	7.00E-05	0.00	7.00E-05	7.00E-05	0.00	0.00
H_2O	3.00E-05	3.00E-05	3.00E-05	0.00	2.99E-05	3.00E-05	0.00	0.00
CO	4.50E-05	6.09E-07	8.79E-06	-80.5	7.06E-16	1.03E-05	-77.1	17.1
He	9.00E-06	9.00E-06	9.00E-06	0.00	9.00E-06	9.00E-06	0.00	0.00
Ne	5.00E-06	5.00E-06	5.00E-06	0.00	5.00E-06	5.00E-06	0.00	0.00
CSO	4.00E-06	1.37E-06	6.05E-06	51.3	2.30E-12	8.27E-06	106.7	36.7
HCl	5.00E-07	5.00E-07	5.00E-07	0.00	5.00E-07	5.00E-07	0.00	0.00
HF	5.00E-09	5.00E-09	5.00E-09	0.00	5.00E-09	5.00E-09	0.00	0.00
O_2	2.00E-05	–	–	–	–	–	–	–
S_8	–	7.02E-07	1.07E-06	–	1.65E-15	1.27E-06	–	–
S_6	–	9.87E-08	4.67E-07	–	2.07E-14	7.11E-07	–	–
H_2S	–	4.28E-08	2.55E-07	–	1.45E-11	3.10E-07	–	–
S_2	–	3.93E-08	2.35E-07	–	1.47E-14	3.32E-07	–	–
S_7	–	2.38E-08	1.17E-07	–	3.88E-16	1.90E-07	–	–
S_2[s]	–	–	–	–	8.77E-195	4.65E-06	–	–

3.1.1 Comparison with GGchem

In Figure 13 the result of the Venus model calculated with GGchem, including condensates, is shown. The model output looks similar to the results obtained with FastChem. In the gas-phase, the same species are present in the GGchem model as in the FastChem output (Figure 12). A noticeable difference in the two models can be found in the sulfur species, that are only abundant up to pressures of approximately 1 bar in the GGchem model. The cause of this depletion of sulfur in the upper atmosphere is the condensation to S_2[s] at this level, that can be seen in Figure 13.

In Table 8 the abundance of species with a mixing ratios above 10^{-7} in the GGchem output is compared to the input and the FastChem results. The calculations with GGchem included 237 species, 10 elements, and 16 condensed species. Of the included condensed species only S_2[s] reached a supersaturation ratio of 1, meaning that it occurs as a condensate. The GGchem calculations were performed with the option "remove condensates". This means that, starting from the bottom layer, in each atmospheric layer all thermally stable condensates are removed, depleting the atmosphere above in the effected elements. Therefore, the layers with a pressure below approximately 1 bar, where the S_2[s] condensate is present, are depleted from the sulfur species H_2S, CSO as well as the allotropes of sulfur (S_8, S_7,...). This can also be recognised in Table 8, as the mean abundance of these species drops significantly, while the maximum abundance stays the same. However, apart from the occurrence of the condensate S_2[s], further differences between the outputs of FastChem and GGchem include the abundance of SO_2, CO and CSO. The GGchem model output has less SO_2 than

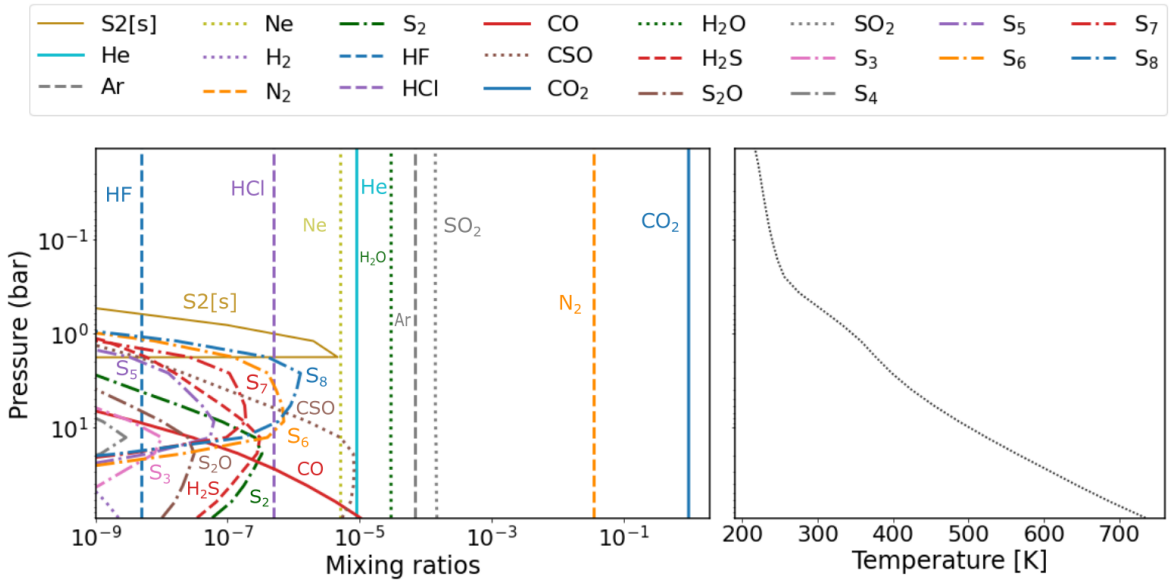

Figure 13: Mixing ratios of the simulated Venusian atmosphere using GGchem.

FastChem, but the maximum abundance of CO and CSO is higher. Both models are depleted from oxygen O_2 with respect to observations, which is expected as the uncertainty of O_2 measured on Venus is high. Nonetheless, the GGchem results increase the validity of the FastChem model of Venus in chemical equilibrium. Including condensates in the calculations does not totally change atmospheric composition in the equilibrium calculations. One very interesting aspect of the GGchem results is that the S_2[s] condensate appears at a pressure regime of approximately 1 bar, where the cloud layer of Venus is expected. The dominant species of the Venusian clouds is expected to be sulfuric acid, that should form from the abundant H_2O and SO_2. Physical and chemical analyses of the clouds by *Vega 2* using an X-ray fluorescent radiometer detected variable abundances of sulfur (S), chlorine (Cl), and phosphorus (P), indicating the presence of H_2SO_4, other sulfur aerosols (S_8), phosphoric acid (H_3PO_4), and aluminium chloride ($AlCl_3$) (Krasnopolsky 1989, 2006). However, Lewis & Fegley Jr (1982) ruled out aluminum chlorides as Venus cloud condensates, because of the low volatility of $AlCl_3$ (Fegley Jr & Treiman 1992). Iron chloride ($FeCl_3$) was also suggested to be present in the Venusian clouds (Krasnopolsky 2017). Some of these condensates cannot be reproduced with our GGchem model, since we do not include aluminium, iron, and phosphorus in the model input. Nevertheless, the presence of the S_2[s] condensate in the GGchem model indicates the presence of the cloud layer, that is not included in the FastChem results.

3.2 C/O ratio variation

The carbon-to-oxygen (C/O) ratio is the ratio between the elemental abundances of carbon and oxygen in all species of a planetary atmosphere. All known atmospheres of Solar-System planets and moons are mainly composed of hydrogen, carbon, oxygen, and nitrogen (Herbort et al. 2020). Therefore, the ratio of these elements plays a crucial role in what species will form at certain temperature and pressure regimes. There are many important and abundant molecules containing C and O, such as O_2, CO_2, CO, CH_4, and H_2O that can influence the climate of a planet. It has long been known that the C/O ratio governs the overall chemistry of an atmosphere (oxidising vs. reducing) and that a fundamental change in chemistry occurs around C/O=1 (e.g., Lewis & Prinn 1980). Furthermore, the C/O ratio can have a substantial influence on spectroscopic signatures of a planetary atmosphere by influencing both the temperature structure and the chemistry of a planet (Madhusudhan 2012). Therefore, the C/O ratio could also be an important parameter for characterising the atmospheres of exoplanets, especially for Hot Jupiters, and could even provide information about the primordial origins and subsequent evolution of the planets (Madhusudhan et al. 2011).
In this part of the project, compositional changes for the atmospheres of Venus-like planets with different C/O ratios are monitored using `FastChem`. Therefore, the optimised Venusian atmosphere from chapter 3.1 with the temperature-pressure profile from Table 6 and a initial C/O ratio of approximately 0.5 is used. While varying the C/O ratio, the abundances of all other elements (N, Ar, Ne, H, S, Cl, F, He) are kept constant. In Figure 14, the modelled atmospheres of planets with C/O ratios of 0.25, 0.75, 1.0, and 1.5 are shown.

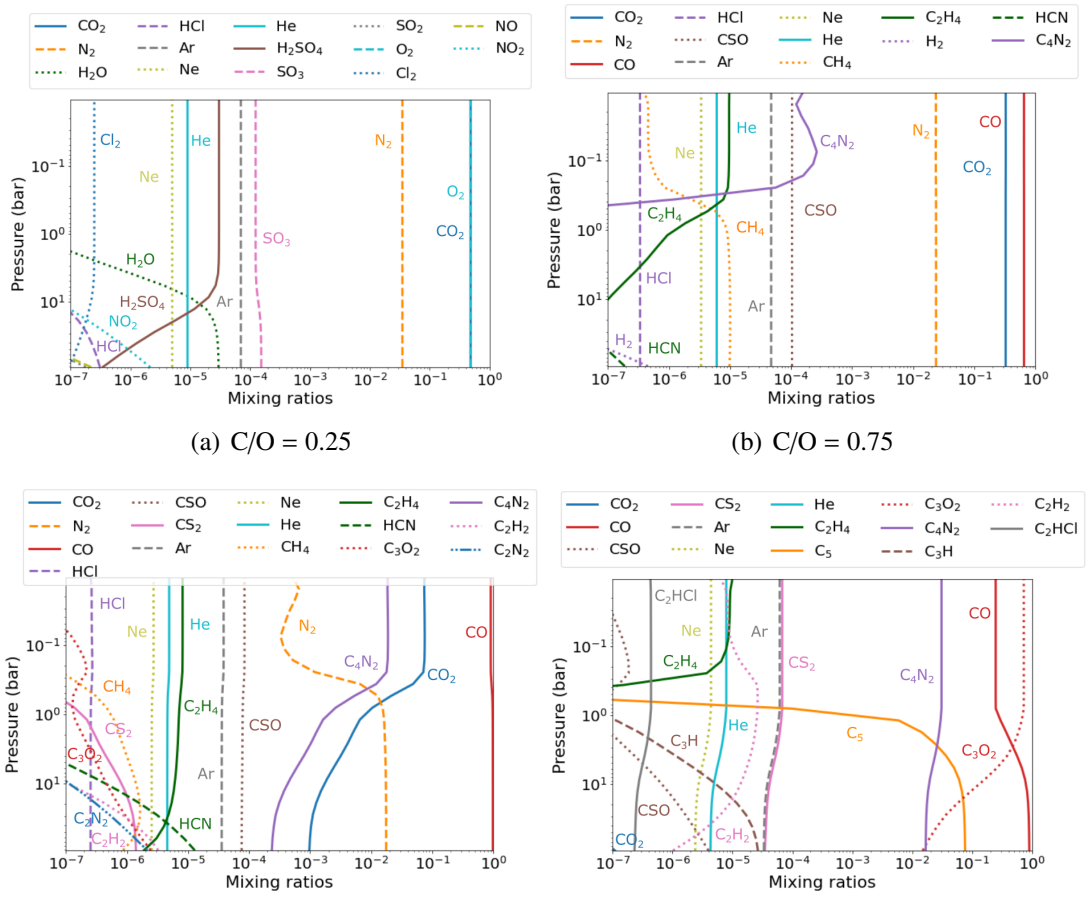

(a) C/O = 0.25 (b) C/O = 0.75

(c) C/O = 1.0 (d) C/O = 1.5

Figure 14: Mixing ratios of Venus-like atmospheres with C/O ratios between 0.25 and 1.5. Please note the significant chemistry changes for dominant species CO_2, O_2, CO, and C_3O_2.

There are strong chemistry changes observable between the different C/O ratios shown in Figure 14. While the oxidised species CO_2 and O_2 are most abundant at an C/O ratio of 0.25 (Fig. 14(a)), carbon monoxide (CO) becomes the most abundant species at a C/O ratio of 0.75 (Fig. 14(b)). At a C/O ratio of 1.5, carbon suboxide (C_3O_2) becomes the most abundant species in the upper atmosphere, while in the lower atmosphere elemental carbon C_5 appears. Moreover, the dominant nitrogen species changes from molecular nitrogen (N_2) to carbon subnitride (C_4N_2) starting at C/O of unity, while chloride transitions from its molecular form (Cl_2) at C/O of 0.25, to hydrogen chloride (HCl) at C/O of 0.75, and even the carbonated species chloroethyne (C_2HCl) at C/O of 1.5. Presumably, the hydrogen (H) in the chlorine species is coming from the small amount of H_2O in the atmosphere, which becomes unstable as C/O increases. At a C/O ratio of 0.25, sulfur is bound in sulfur trioxide (SO_3) and sulphuric acid (H_2SO_4), while for C/O ratios of 0.75 and 1 carbonyl sulfide (CSO) and at C/O ratios of 1.5 carbon disulfide (CS_2) are the dominant sulfur species. In Figure 14(d), the change of CO, consisting of one carbon atom and one oxygen atom, to C_3O_2, containing three carbon atoms and two oxygen atoms, also has an effect on the *relative* mixing ratios of species that would normally stay constant, such as the noble gases argon (Ar), neon (Ne), and helium (He). These chemically inert species are being diluted by C-O species, as the molecular abundance of the C-O species depends on how many C and O atoms are in each molecule. Large carbon species bind more carbon and oxygen atoms, that together contribute to about 97.6% of all elements in the Venusian atmosphere. Therefore, changes in these species can be recognised in the far less abundant noble gases, even though their elemental abundance stays the same. In Table 9 the mean mixing ratios of all relevant species are shown for the investigated C/O ratios in Figure 14. The described changes in abundance of different species can be seen in Table 9. For a C/O ratio of 0.25 (1/4) the CO_2 and O_2 abundance are the same, which is expected from the ratio.

Table 9: Comparison of the molecular composition of the eight most abundant species, not including the noble gases Ar, Ne, and He, for C/O ratios of 0.25, 0.75, 1.0, and 1.5. Nitrogen species are marked in blue, sulfur species in orange, and chlorine species in purple. For the species the mean mixing ratios over the 24 temperature pressure data points is given.

C/O	1.	2.	3.	4.	5.	6.	7.	8.
0.25	CO_2	O_2	N_2	SO_3	H_2SO_4	H_2O	Cl_2	NO_2
	4.83E-01	4.82E-01	3.50E-02	1.31E-04	2.30E-05	7.25E-06	2.23E-07	2.02E-07
0.75	CO	CO_2	N_2	CSO	C_4N_2	CH_4	C_2H_4	HCl
	6.50E-01	3.26E-01	2.35E-02	1.04E-04	6.46E-05	5.80E-06	4.30E-06	3.37E-07
1.0	CO	CO_2	N_2	C_4N_2	CSO	C_2H_4	HCN	CH_4
	9.49E-01	3.25E-02	1.03E-02	8.11E-03	8.01E-05	6.71E-06	1.37E-06	6.48E-07
1.5	C_3O_2	CO	C_5	C_4N_2	CS_2	C_2H_2	C_3H	C_2H_4
	4.78E-01	4.69E-01	2.62E-02	2.59E-02	5.66E-05	1.37E-05	4.90E-06	3.04E-06

For this thesis, the most relevant C/O ratios are located near the Venusian ratio of 0.5. Around this ratio, the chemistry of the atmosphere changes completely. The expected species to form at C/O = 0.5 is carbon dioxide (CO_2). However, when the C/O ratio changes sightly from 0.5, either carbon or oxygen becomes available, which can react with less abundant elements to form either more reduced or more oxygenated species. In Figure 15 the two different cases for atmospheric composition below and above a C/O ratio of 0.5 are shown. Therefore, the C/O ratios of 0.49985 and 0.50015 were chosen. For these cases, the behaviour of species that have a maximum mixing ratio of 10^{-9} in the observed temperature-pressure regime are investigated. This also includes fluoride species, that are not shown for the C/O ratios between 0.25 and 1.0 in Figure 14.

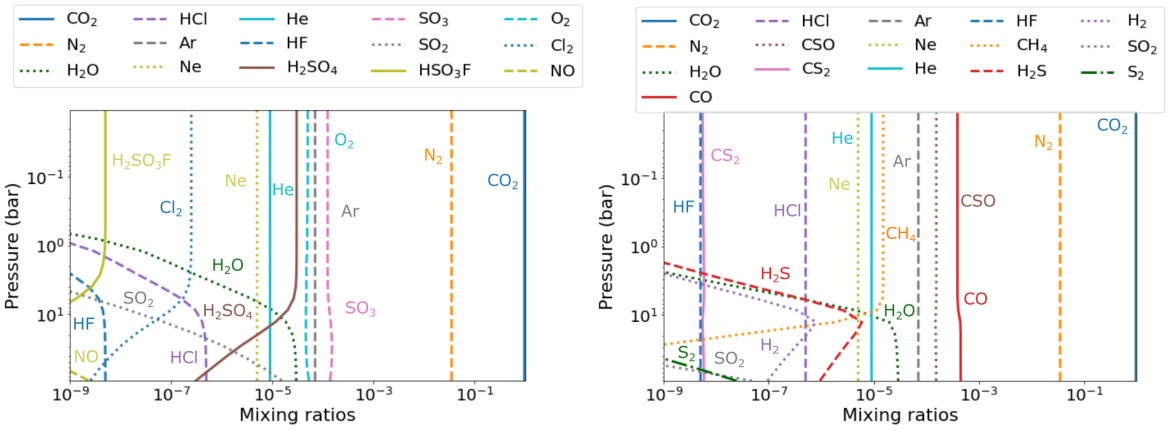

(a) Case 1: C/O = 0.49985

(b) Case 2: C/O = 0.50015

Figure 15: Atmospheric composition for C/O < 0.5 and C/O > 0.5

Case 1: C/O < 0.5

In the first case, with a C/O ratio of 0.49985, not all oxygen in the atmosphere can be bound to form CO_2, which leads to the occurrence of molecules containing more oxygen. Therefore, sulfur trioxide (SO_3), sulfurous acid (H_2SO_4), and fluorosulfuric acid (HSO_3F) are abundant. On the contrary, carbon monoxide (CO) does not reach mixing ratios above 10^{-9}. The abundance of most molecules, such as CO_2, N_2, O_2, is stable over the whole pressure regime, but the abundance of some species changes with higher pressure. While water (H_2O) and sulfur dioxide (SO_2) are mainly present at high temperatures and pressures in the lower atmosphere, the upper atmosphere is dominated by sulfurous acid (H_2SO_4) and sulfur trioxide (SO_3). This relation can be described with the following chemical equations:

$$H_2SO_4 \rightleftharpoons H_2O + SO_3 \tag{12}$$

$$2\,SO_3 \rightleftharpoons 2\,SO_2 + O_2 \tag{13}$$

For chloride and fluoride species, hydrogen chloride (HCl) and hydrogen fluoride (HF) are the dominant species at the low atmosphere, in the upper atmosphere, starting at a pressure of approximately 1 bar, molecular chloride (Cl_2) and fluorosulfuric acid (HSO_3F) take over, as described by the following reactions based on all potentially involved species:

$$2\,HCl \rightleftharpoons Cl_2 + H_2 \tag{14}$$

$$HF + SO_3 \rightleftharpoons HSO_3F \tag{15}$$

Case 2: C/O > 0.5

In the second case, at a C/O ratio of 0.50015, carbon containing molecules, such as carbon monoxide (CO), carbonyl sulfide (COS), methane (CH_4), carbon disulfide (CS_2), or ethylene (C_2H_4) are abundant. In contrast to the first case, carbon monoxide (CO) becomes the third most abundant molecule in the atmosphere. Furthermore, no sulfuric or fluorosulfuric acid can be found. Most molecules seem to be very stable over the whole pressure regime, only the abundance of methane (CH_4) and water (H_2O) together with molecular hydrogen H_2 and H_2S seem to be pressure and temperature dependent. At the lower atmosphere carbon monoxide (CO) becomes slightly more abundant, which enables H_2O formation, wheras the free hydrogen is bound in H_2 and H_2S. In the upper atmosphere, hydrogen is mainly bound in methane CH_4. The following reaction (Eq. 16) is based on the abundance changes of H_2O and CH_4, that can be observed in Figure 15, including potentially involved species.

$$CH_4 + {}^3/_2\,O_2 \rightleftharpoons CO + 2\,H_2O \tag{16}$$

3.2.1 Comparison with GGchem

In Figure 16 the results of the GGchem models for the two described cases are shown, using carbon-to-oxygen ratios of 0.49985 and 0.50015. There was a convergence problem for GGchem at C/O ratios above 0.5, when using the "remove condensates" option, where atmosphere layers above a condensate are depleted of effected elements. Therefore, for the second case each layer is investigated independently. Here a bigger difference from the Venusian model is visible when comparing the GGchem results to the `FastChem` results.

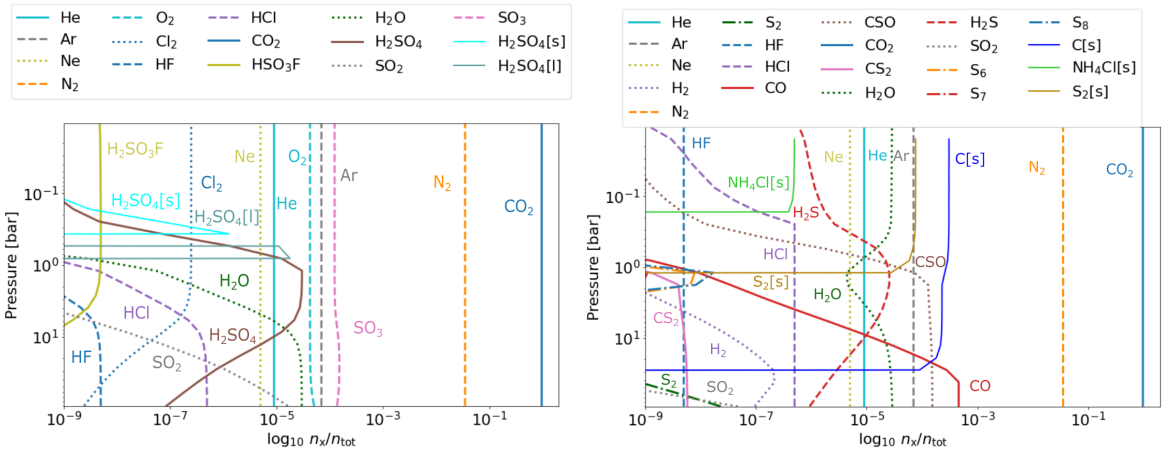

(a) Case 1: C/O = 0.49985 (GGchem)

(b) Case 2: C/O = 0.50015 (GGchem)

Figure 16: Mixing ratios of Venus-like atmospheres with C/O ratios above and below 0.5.

For the first case, sulfuric acid (H_2SO_4) can be found as liquid [l] and solid [s] condensate above a pressure of 1 bar, as seen in Fig. 16(a). Starting from this altitude, the gas phase sulfuric acid gets depleted. The transition from liquid to solid H_2SO_4 seems quite rough in the plot, which is just a remnant of the amount of pressure data points in the region. In reality, the transition between liquid and solid condensate would be smoother. There are no other noticeable changes between the `FastChem` and GGchem models, except for the absence of nitrogen oxide (NO) in the GGchem model. In Table 10 the maximum and mean abundance of each species over the 24 temperature pressure data points for the `FastChem` and GGchem models are shown. One can see that for the first case the GGchem output includes more SO_2 and SO_3, but less oxygen (O_2) than `FastChem`.

The second case deviates more from the `FastChem` results. In the GGchem output, three condensates are present in the atmosphere: C[s] (graphite), S_2[s] (sulfur) and NH_4Cl[s] (ammonium chloride). The presence of these condensates influences the abundance and carbon monoxide (CO), carbonyl sulfide (CSO), and hydrogen chloride (HCl). Furthermore, no methane (CH_4) can be found in the GGchem model, while water (H_2O) and hydrogen sulfide (H_2S) behave in an opposite way. At the lower and upper atmosphere water is more abundant, while at cloud level, where further the sulfur allotropes S_8 and S_6 emerge, hydrogen sulfide takes over. Furthermore, the maximum of the molecular hydrogen abundance drops. In Table 10 the percentage changes in maximum abundance between the `FastChem` and GGchem model can be seen for all species.

Table 10: Comparison of the molecular composition of the Venusian atmosphere with the model outputs of FastChem and GGchem.

Case 1: C/O=0.49985						Case 2: C/O = 0.50015					
	FastChem		GGchem				FastChem		GGchem		
	Mean	Max	Mean	Max	Diff. [%]		Mean	Max	Mean	Max	Diff. [%]
CO_2	9.65E-01	9.65E-01	9.65E-01	9.65E-01	0.00	CO_2	9.64E-01	9.64E-01	9.64E-01	9.65E-01	0.02
N_2	3.50E-02	3.50E-02	3.50E-02	3.50E-02	0.00	N_2	3.50E-02	3.50E-02	3.50E-02	3.50E-02	0.01
SO_3	1.30E-04	1.51E-04	1.31E-04	1.52E-04	1.10	CO	4.03E-04	4.48E-04	7.39E-10	4.58E-04	2.22
Ar	7.00E-05	7.00E-05	7.00E-05	7.00E-05	0.00	CSO	1.53E-04	1.54E-04	9.33E-07	1.53E-04	-0.66
O_2	4.87E-05	5.31E-05	4.33E-05	5.10E-05	-4.05	Ar	7.00E-05	7.00E-05	7.00E-05	7.00E-05	0.01
H_2SO_4	2.30E-05	3.03E-05	9.73E-08	3.02E-05	-0.19	CH_4	1.11E-05	1.50E-05	–	–	-100
He	9.00E-06	9.00E-06	9.00E-06	9.00E-06	0.00	He	9.00E-06	9.00E-06	9.00E-06	9.00E-06	0.01
H_2O	7.22E-06	2.97E-05	9.53E-12	2.99E-05	0.75	H_2O	6.75E-06	2.90E-05	1.90E-05	2.90E-05	0.01
Ne	5.00E-06	5.00E-06	5.00E-06	5.00E-06	0.00	Ne	5.00E-06	5.00E-06	5.00E-06	5.00E-06	0.01
SO_2	1.11E-06	1.55E-05	3.43E-13	1.64E-05	5.79	H_2S	8.58E-07	5.92E-06	3.73E-06	2.56E-05	333
Cl_2	1.80E-07	2.50E-07	9.73E-08	2.50E-07	0.00	HCl	5.00E-07	5.00E-07	1.36E-07	5.00E-07	0.01
HCl	1.40E-07	4.95E-07	1.71E-11	4.95E-07	0.03	H_2	1.05E-07	7.86E-07	3.43E-10	2.18E-07	-72
HSO_3F	3.26E-09	5.00E-09	1.23E-09	5.00E-09	-0.02	CS_2	5.65E-09	5.82E-09	2.10E-13	5.82E-09	-0.05
HF	1.74E-09	4.99E-09	2.61E-12	4.99E-09	-0.02	HF	5.00E-09	5.00E-09	5.00E-09	5.00E-09	0.01
NO	1.48E-10	2.34E-09	–	–	-100	SO_2	2.09E-09	4.75E-08	5.02E-17	4.74E-08	-0.27
H_2SO_4[s]	–	–	5.89E-182	1.29E-06	100	S_2	1.25E-09	2.44E-08	2.20E-15	2.33E-08	-4.25
H_2SO_4[l]	–	–	5.36E-280	1.79E-05	100	S_8:	–	–	8.32E-19	1.70E-08	100
						S_6:	–	–	6.96E-17	7.87E-09	100
						S_7:	–	–	5.06E-19	1.11E-09	100
						C[s]	–	–	6.72E-42	3.06E-04	100
						NH_4Cl[s]	–	–	1.20E-205	4.98E-07	100
						S_2[s]	–	–	2.04E-142	7.66E-05	100

For completeness, in Figure 17 the result of the GGchem model for C/O = 0.49985 when not using the "remove condensates" option is shown. One can see that the abundances of species in the gas phase stay the same. The main difference to Figure 16(a) is that the solid H_2SO_4[s] condensate does not deplete in the upper atmosphere. Therefore, the differences in the abundances of gas phase species should also not be too large for the GGchem model at C/O = 0.50015 in Figure 16(b), when using the not converging "remove condensates" option.

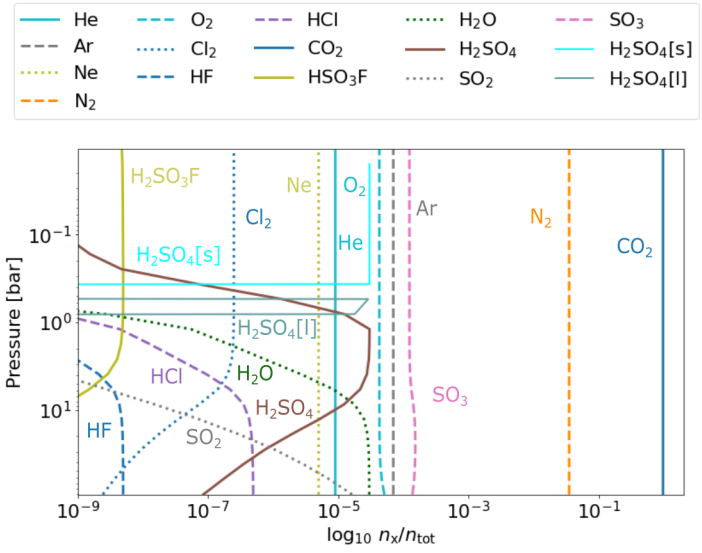

Figure 17: Mixing ratios of GGchem atmosphere model for a C/O ratio of 0.49985 without using the "remove condensates" option. Please note that the abundance of the solid sulfuric acid condensate (H_2SO_4[s]) stays at a constant level in the upper atmosphere.

3.2.2 Extreme cases

Some extreme cases of the C/O ratio have also been studied using `FastChem`, for example, atmospheres entirely depleted of carbon (C) and/or oxygen (O). As carbon and oxygen are the third and fourth most abundant element in the universe (see e.g., Asplund et al. 2009; Grevesse et al. 2007), it is very unlikely that such atmospheres exist. One possible scenario would be steam (H_2O) atmospheres with some additional volatiles, but no carbon, added. Another would be an atmosphere entirely derived from volatilised organics, with lots of C but not O. Nevertheless, these cases could maybe be interesting for some exoplanet atmospheres. For example, the redox atmospheres of giant planets and Titan, Saturn's largest moon, are dominated by hydrogen-bearing species (Catling & Kasting 2017). Titan's atmosphere is predominantly composed of molecular nitrogen, methane, molecular hydrogen (Kunde et al. 1981). For the study of extraterrestrial atmospheres, we have to be open minded and also investigate unexpected cases.

Without including carbon and oxygen as in the atmosphere, N_2, that is not very reactive, becomes the most abundant species in the atmosphere, as shown in Figure 18. With a mean abundance of 99.6%, the atmosphere completely dominated by N_2. Chlorine (Cl) and fluorine (F) are bound in hydrogen chloride (HCl) and hydrogen fluoride (HF). For sulfur species, octasulfur (S_8) dominates in the upper atmosphere, at lower pressure. In the lower atmosphere, sulfur is bound more in disulfur (S_2), hexasulfur (S_6), heptasulfur (S_7), pentasulfur (S_5), trisulfur (S_3), and tetrasulfur (S_4). Furthermore, the mixing ratio of molecular hydrogen (H_2) changes quite rapidly between the surface and a pressure of 1 bar. Therefore, the molecular hydrogen is probably bound in hydrogen sulfide (H_2S) at lower pressures in the upper atmosphere.

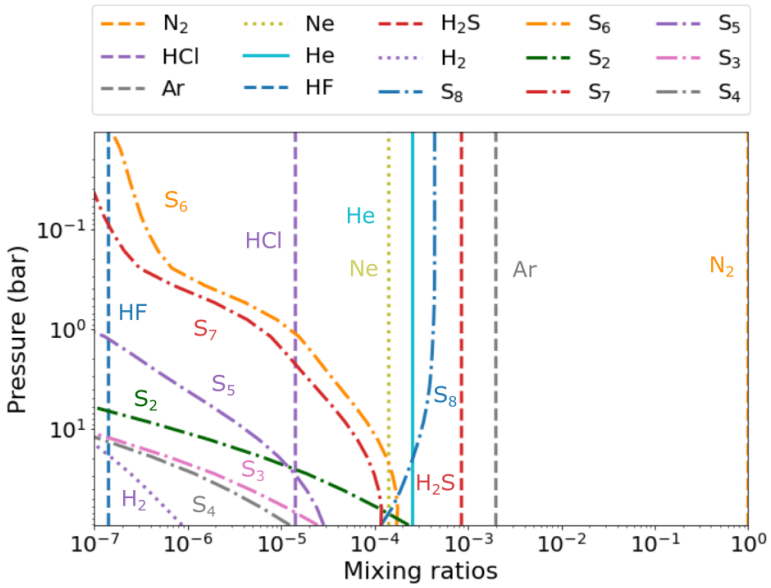

Figure 18: Mixing ratios of an atmosphere with no carbon and oxygen

An atmosphere with a C/O ratio of 0, meaning that 97.6% of the input elements are oxygen, is shown in Figure 19(a). Therefore, the atmosphere is dominated by O_2 (96.48%). The remaining oxygen is mainly bound in SO_3 ($\sim 10^{-4}$), H_2SO_4 (upper atmosphere), H_2O (lower atmosphere, $\sim 10^{-5}$), and even NO_2 and NO. Furthermore, the abundances of H_2O and H_2SO_4, as well as the abundances of HCl and Cl_2 seem to be dependent on temperature and pressure. This behaviour is described by Eq. 12 and Eq. 14 for the case of C/O < 0.5 near the simulated Venusian atmosphere. Similar to this extreme case, Earth's atmosphere is

also dominated by molecular nitrogen and oxygen, and a lot of carbon is bound in carbonate rocks. With relatively high sulfur trioxide (SO_3) and sulfuric acid (H_2SO_4) abundances, there could be possibly be very acidic rain in such an atmosphere.

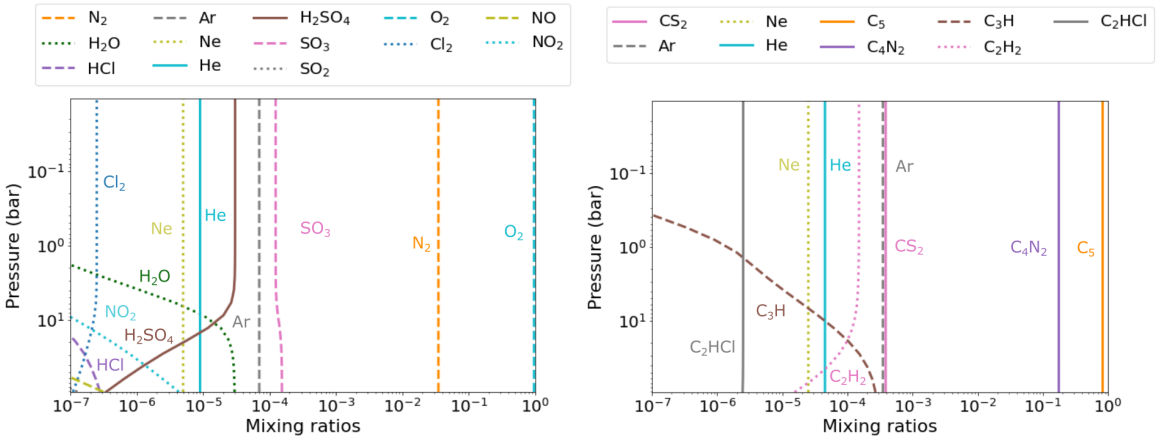

(a) C/O = 0.0 (b) O/C = 0.0

Figure 19: Mixing ratios of atmospheres with no carbon (a) or no oxygen (b).

In Figure 19(b) the O/C ratio is set to zero, meaning that there is no oxygen in the atmosphere. On the contrary, 97.6% of the chemical element composition used as an input for the model is carbon. Consequently, the most abundant species is C_5 (82.4%), which is the largest molecule only containing carbon included in the `FastChem` model. Therefore, it cannot be ruled out that larger carbon species, such as fullerenes C_{60}, C_{70}, or large carbon rings could form under this extreme carbon over-abundance. These large carbon molecules have been detected in the interstellar medium (ISM) together with ionised buckminsterfullerene C_{60}^+ (see e.g., Cami et al. 2010; Schlarmann et al. 2021). With this supersaturation of carbon, graphite condensation would likely occur, which is not included in the `FastChem` model. However, the gravitational settling of the condensates would presumably lead to a depletion of gaseous carbon, maintaining the gas-phase C/O ratio near 1, if graphite clouds would occur in the atmosphere of such an exoplanet (Moses et al. 2013). Except for noble gases all species in this extreme atmosphere are carbonised. Sulfur is bound as CS_2 ($3.8 \cdot 10^{-4}$). Even nitrogen, that is normally found as the unreactive N_2, forms dicyano-acetylene (C_4N_2), that has been detected as ice in Titan's stratosphere (Samuelson et al. 1997). Furthermore, the abundance of acetylene C_2H_2 or C_3H seems to depend on the pressure and temperature, as described with the reaction in Eq. 17.

$$2\,C_3H + 2\,H_2 \rightleftharpoons 3\,C_2H_2 \tag{17}$$

3.2.3 Atmosphere types

To get a better overview of the atmospheric changes at different C/O ratios, the mixing ratios of different species are plotted against the C/O ratio for specific temperature and pressure regimes at the surface (T = 735 K, p = 90 bars), cloud layer (T = 357 K, p = 1.2 bar) and top layer (T =217 K, p = 0.01 bar). These three regions should be representative for the other nearby regions. In Figure 20 the abundance of gas species with an abundance greater than 10^{-7} are shown for C/O ratios between 0 and 2. The solar $(C/O)_{\odot}$ ratio has a value of approximately 0.54 (calculated from Grevesse et al. 2007), but higher values have been observed for exoplanets. For example Madhusudhan et al. (2011) reported a C/O > 1 for the atmosphere of the transiting hot-Jupiter WASP-12b. Bond et al. (2010) found that for C/O values close to or above 0.8 in proto-planetary disks, planets can incorporate carbon as a significant planet-building material. This could in theory lead to the formation of terrestrial "carbon planets", consisting of carbides (e.g., SiC, TiC) and graphite instead of silicates.

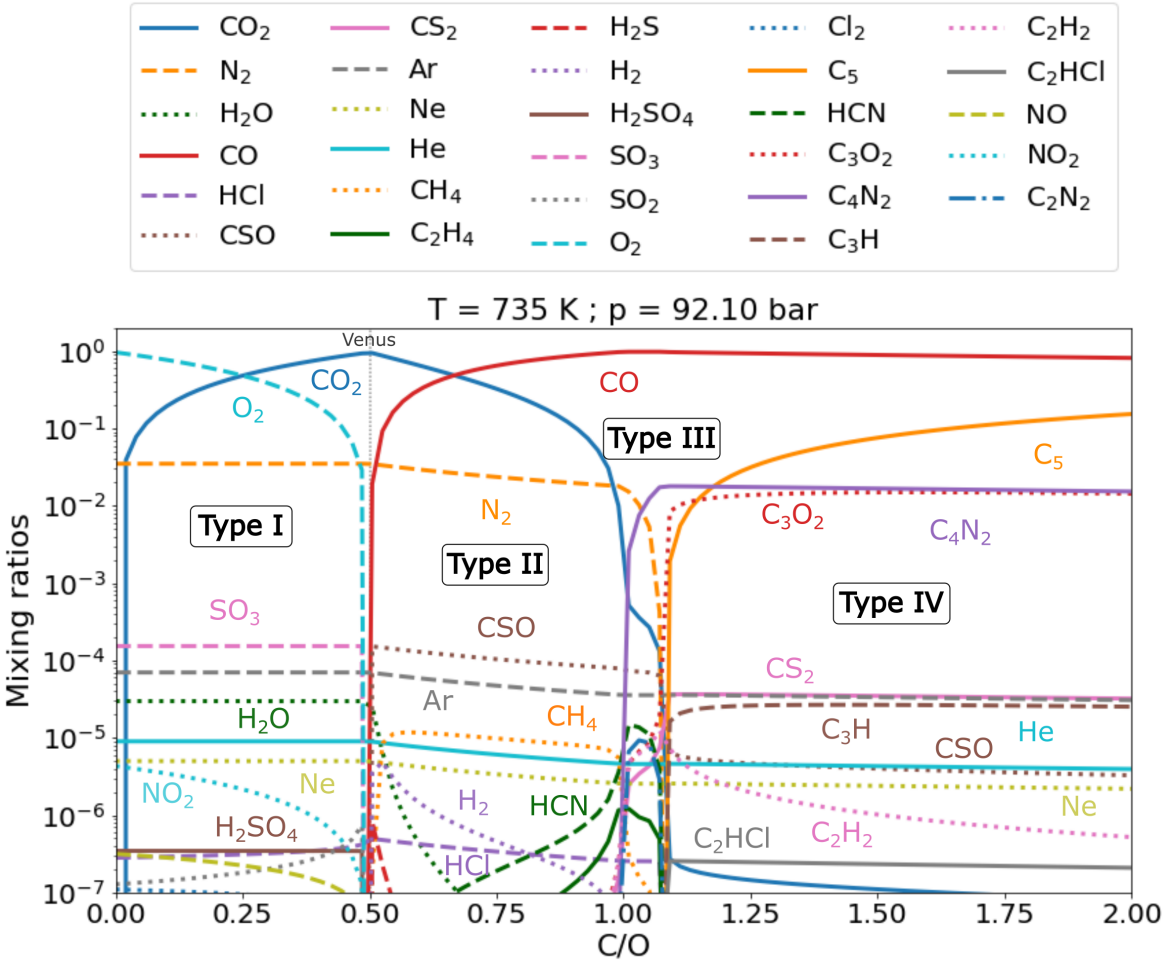

Figure 20: Mixing ratios under temperature and pressure conditions on the Venusian surface under different C/O ratios from 0 to 2. The C/O ratio of the Venusian atmosphere is indicated as a very faint dotted line. Please note the strong chemistry changes for the different atmospheric types. The C/O ratio is reflected in the most abundant carbon and oxygen species as well as in less abundant molecules.

The atmospheric chemistry in Figure 20 changes significantly with the C/O ratio. As expected the most abundant carbon/oxygen species for low C/O ratios is molecular oxygen (O_2), then around the Venusian C/O ratio of 0.5 carbon dioxide (CO_2) dominates the atmosphere, until carbon monoxide (CO) takes over for high C/O ratios. Important chemistry transitions occur at C/O = 0.5 and around C/O = 1. The Venusian atmosphere, with an C/O ratio of approximately 0.499918, is located exactly at one of these transitions. At a C/O ratio of 1, the atmospheric composition changes from being oxygen-rich to carbon-rich.

Woitke et al. (2021) proposed a classification of exoplanet atmospheres at low temperatures (T < 600 K) based on the element abundances of hydrogen, carbon, oxygen, and nitrogen. The temperature on the Venusian surface exceeds their upper boundary, still a similar approach can be attempted for the results from our Venus-like planets, that also include sulfur and chlorine. Furthermore, much of the Venusian atmosphere of our model lies below 600K, starting at an altitude of approximately 16 km, as can be seen from the temperature pressure structure. The abundance of fluorine species falls under the mixing ratio cut-off value of 10^{-7}. Nonetheless, they are also considered in the simulation. In Figure 20 four different atmospheric types can be identified for different C/O ratios:

Type I: (0 < C/O < 0.5) Oxygenated species, such as O_2, CO_2, SO_3, and H_2SO_4 dominate this atmosphere type. Furthermore nitrogen is primarily bound in N_2, but also occurs as NO and NO_2. Chlorine is mostly bound in HCl, but at C/O < 0.15, the Cl_2 abundance slightly exceeds the cut-off value of 10^{-7}.

Type II: (0.5 < C/O < 0.95) Carbon atoms that are not locked up in CO or CO_2 are primarily found in the form of CSO, CH_4, and HCN, a prebiotic precursor molecule, in this region. While the N_2 and CH_4 abundance decreases towards a C/O ratio of 1, HCN and C_2H_4 rise significantly. The water (H_2O) abundance sinks strongly between C/O values of 0.5 to 0.7. H_2 appears at C/O = 0.5 with an abundance of 10^{-5} and then increases again.

Type III: (0.95 < C/O < 1.075) In this narrow region, CO is the main carbon species. While the CO_2 abundance changes rapidly on the edges of the region, it stays relatively constant at a mixing ratio of approximately $3 \cdot 10^{-4}$. While the N_2 abundance decreases with C/O, the C_4N_2 abundance rises, and C_4N_2 becomes the most abundant nitrogen species from C/O = 1.04. Nitrogen can also be found in the form of C_2N_2 at abundances up to 10^{-5}. Furthermore, the HCN, C_3O_2, and C_2H_2 level rises in comparison to Type II atmosphere, while the CH_4 abundance decreases until it vanishes.

Type IV: (1.075 < C/O) C_5 and C_3O_2 rise strongly and are the dominating carbon species of the atmosphere together with CO. Moreover, nitrogen and sulfur are mainly bound in C_4N_2 and CS_2, with contribution of CSO. Hydrogen and chlorine species are also abundant as the carbonated species C_3H, C_2H_2, and C_2HCl.

For the cloud layer at a temperature of 357 K and pressure of 1.2 bar, shown in Figure 21, the four atmosphere types described before can still be recognised, even though the boundaries are more blurry. This is about the level where observations using emission from the planet (detected by secondary eclipse method in the infrared) will sense. While for the surface layer 29 species had a mixing ratio above 10^{-7}, for the cloud layer there are only 21 species that fulfil this condition. The CH_4 abundance already starts to strongly decrease at C/O~0.9, which indicates that the boundary between Type II and Type III is slightly shifted for the upper atmosphere.

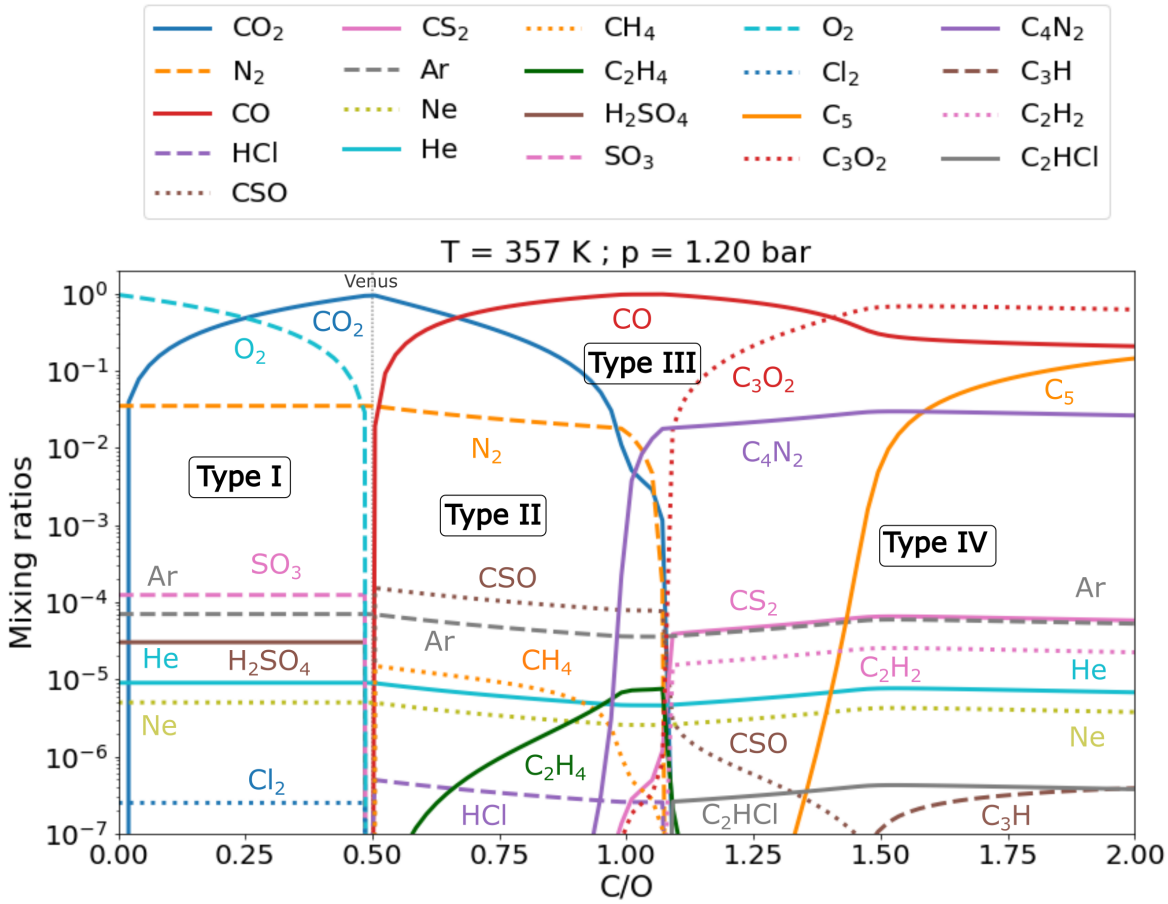

Figure 21: Mixing ratios under temperature and pressure conditions on the Venusian cloud layer under different C/O ratios from 0 to 2. The Venusian C/O ratio is indicated with a faint dotted line. Please note that fewer species exceed a mixing ratio of 10^{-7} compared to the surface layer. Most noticeable is the absence of H_2O, NO_2, H_2, and HCN in comparison to the surface conditions.

Type I: (0 < C/O < 0.5) Most notably, there is no water H_2O and H_2 at the temperature and pressure regime of the cloud layer, but the H_2SO_4 abundance increases compared to the surface layer. Nitrogen only appears as N_2, while NO_2 and NO vanish in comparison to the surface layer.

Type II: (0.5 < C/O < 0.95) There is no H_2 and HCN present at the cloud level. The CH_4 abundance decrease starts earlier than in the surface layer, while C_2H_4 reaches a higher abundance.

Type III: (0.95 < C/O < 1.075) The region where the Type III atmosphere is located broadens a bit. The CO_2 and C_2H_4 abundance rises in comparison to the surface layer, while the CS_2 and C_3O_2 abundance decreases. For nitrogen species, the rise of C_4N_2 starts earlier at C/O of ~0.95, while C_2N_2 vanishes. The C_3O_2 and CS_2 abundance decreases in this region, and C_2H_2 totally vanishes from this region.

Type IV: (1.075 < C/O) C_3O_2 becomes the most abundant carbon species, while the CO abundance decreases. The CSO abundance declines and vanishes at C/O ≈ 1.5, where C_3H starts to arise. C_2H_2 becomes more abundant than at surface level, while the C_5 abundance starts to increase later at C/O ≈ 1.3.

At the top layer of our model (T = 217 K, p = 0.01 bar), that for exoplanets could be sensed using transit spectroscopy (e.g., with JWST), there are some changes in the atmospheric composition at different C/O ratios in comparison with the surface and cloud layer. The region where C_2H_4 becomes most abundant gets broader and stretches from C/O ratios from 0.5 to 1.6, while the CH_4 abundance gets smaller. Therefore, it seems like the Type II and Type III atmosphere are nearly merging.

Type I: (0 < C/O < 0.5) This atmosphere type looks exactly the same as in the cloud layer.

Type II: (0.5 < C/O < 0.95) The CH_4 decrease happens not that abruptly, but continuously. On the contrary, C_2H_4 grows much faster and stays at a plateau, even until C/O ≈ 1.6.

Type III: (0.95 < C/O < 1.075) A prompt change between CO_2 and C_3O_2 (and CS_2) can be observed at C/O ≈ 1.075, while the N_2 and HCl decline is expanded. The C_2H_4 abundance stays constant, while there is no CH_4 present.

Type IV: (1.075 < C/O) C_3O_2 and C_5 are the most abundant carbon species for C/O > 1.6, where an abrupt change in the CO and C_5 abundance takes place. The abundance of C_2H_2, and C_2HCl starts to rise later than in the cloud layer, while C_3H falls under 10^{-7}.

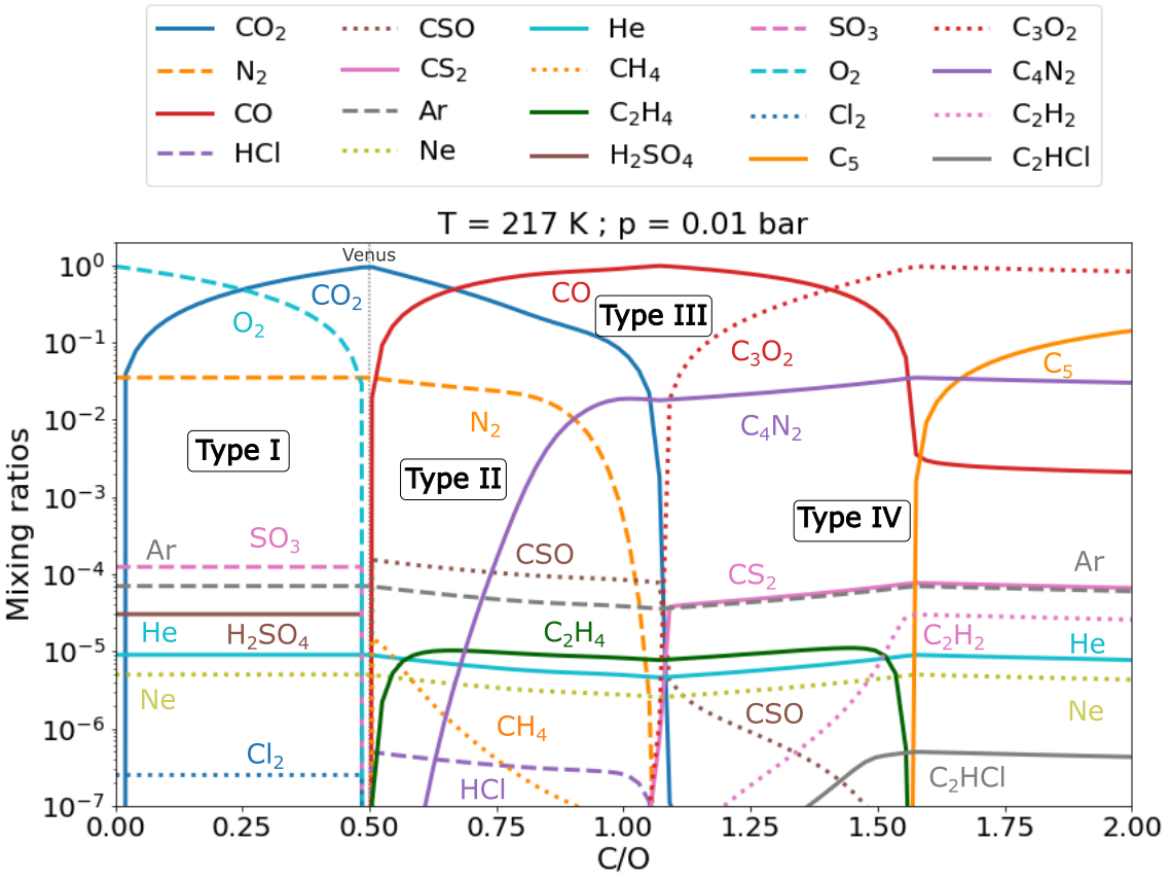

Figure 22: Mixing ratios under temperature and pressure conditions on the Venusian surface under different C/O ratios from 0 to 2. Please note that the boundaries of the Type III atmospheres are not as clear as in the cloud and surface layer. In particular, C_2H_4 is present at a nearly constant level for C/O ratios between 0.5 to 1.5, which is a much wider range than in the surface and cloud layer.

In Figure 23 the narrow region between C/O ratios 0.95 and 1.2 is shown again for the surface, cloud, and top layer, to better differentiate the species for atmospheres of Type III. Especially for Type III atmospheres, there is a noticeable variation in abundance for the different species between the surface, cloud, and top layer.

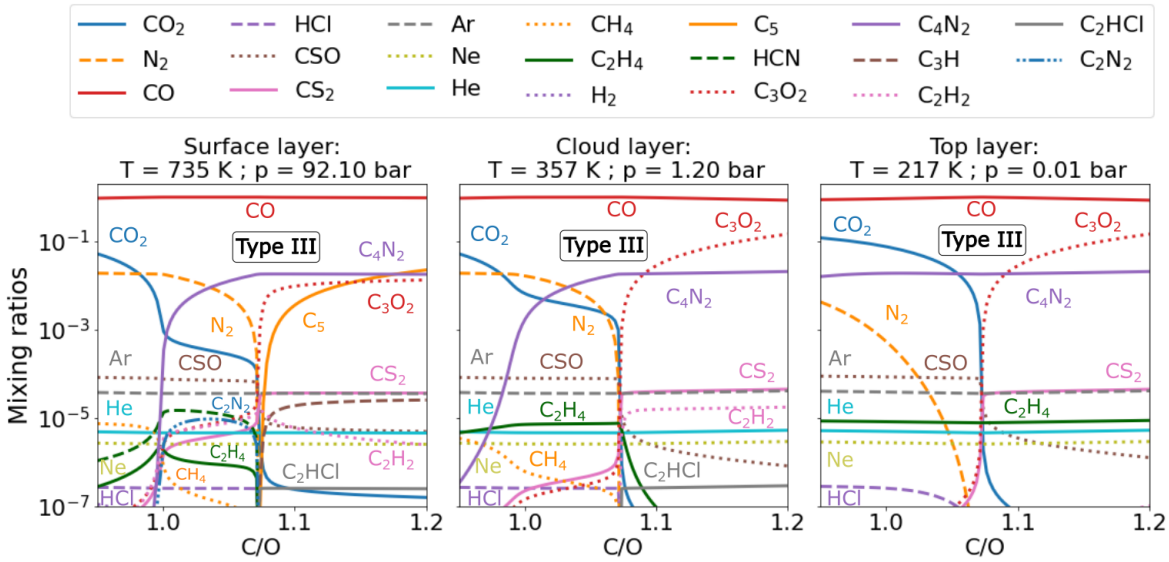

Figure 23: Mixing ratios at surface, cloud and top layer from 0.95 to 1.2 to zoom in at the behaviour of Type III atmospheres. Please note that the pressure of 0.01 of the top layer corresponds to an altitude of about 68 km, where the mesosphere is located.

3.3 C/N ratio variation

In Figure 24 the composition of the surface, cloud, and top layer is shown for C/N ratios between 0 and 40. One can still recognise the four atmosphere types, described in chapter 3.2.3 in detail. The similar behaviour of different species in Figure 24 to the one demonstrated for different C/O ratios in Figure 20, Figure 21, and Figure 22, can be attributed to the way the C-to-N ratio was calculated. Originally, all other species, including oxygen, where kept at constant abundance, while the carbon and nitrogen abundance was varied according to the C/N ratio, respectively. Therefore, the C/O ratio is not fixed and translates to the C/N ratio, since oxygen and carbon are much more abundant than nitrogen. The molecular abundance changes are analogous to variation in C/O.

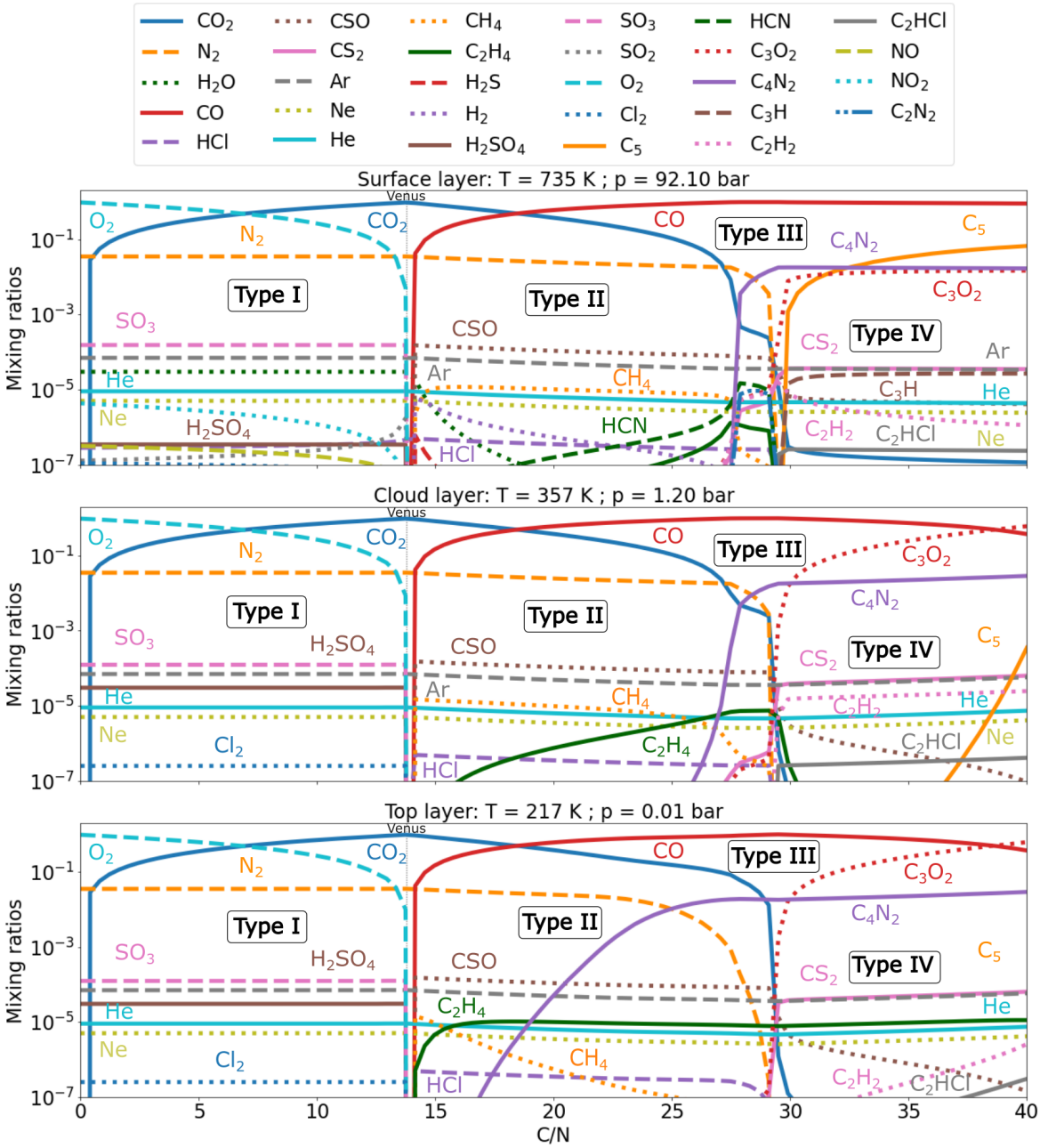

Figure 24: Mixing ratios under temperature and pressure conditions on the Venusian surface under different C/N ratios from 0 to 40. Please note that the C/O ratio varies here.

To get a better understanding how the C/N ratio influences Venus-like planets, the C/O ratio is kept constant at the Venus value of 0.499918, while the C/N ratio is varied. Furthermore,

to sustain the molecular abundances of noble gases, as input the sum of elemental C, O, and N is kept constant as the model input. In Figure 25 the results for different C/N ratios with constant C/O of 0.499918 and constant total elemental abundance of 99.99% oxygen, carbon and nitrogen, for the three discussed model layers. In this case, with a constant C/O ratio, only the amount of free oxygen, that is not bound in CO_2 changes with increasing C/N ratio. Therefore, for low C/N ratios, sulfur species containing less and/or no oxygen, such as S_2, H_2S, S_2O occur, while for C/N ratios above 3 the sulfur chemistry is dominated by SO_2 and CSO. The H_2O abundance is constant and independent from the C/N ratio. The differences between the observed layers are mainly found in the reduced species. For the surface layer, at high temperature and pressure, sulfur can be found as S_2, H_2S, and S_2O. For the top and cloud layer, however, octasulfur S_8 takes over and also appears at high C/N ratios, while S_6 and S_7 turn up in the cloud layer. Meanwhile, the CO abundance is under 10^{-7} in the cloud and top layer.

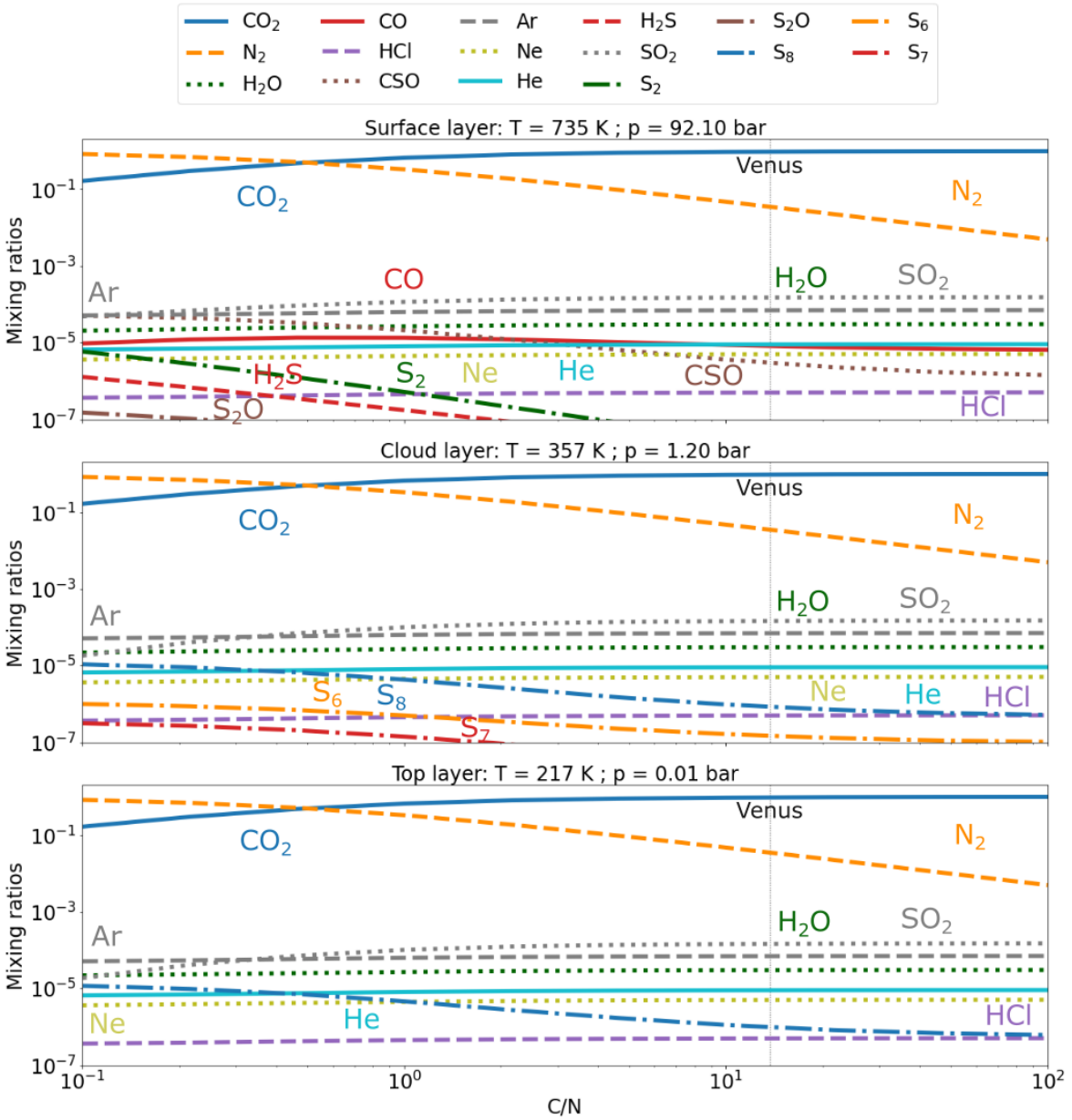

Figure 25: Mixing ratios under temperature and pressure conditions on the surface, cloud, and top layer of the Venus model calculated with `FastChem` under different C/N ratios from 0.1 to 100, with the conditions C+O+N = 99.99% and C/O = 0.499918.

3.4 Atmosphere-Surface Equilibration

Near the surface of an planet, the oxidation state of the atmosphere, that can be described using the oxygen fugacity (fO_2), which refers to the amount of available oxygen in a system, controls the gas abundance of minor species and the chemical weathering of surface minerals. For example, the relative concentrations of oxidised (e.g., CO_2, SO_2, H_2O) versus reduced (CO, CH_4, OCS, H_2S, S_2, and H_2) carbon, sulfur, and hydrogen species are dependent on the oxygen fugacity (Fegley Jr et al. 1997). This relation, that could also be seen at different carbon-to-oxygen ratios, can be described with the following equations:

$$2\ CO + O_2 \rightleftharpoons 2\ CO_2 \tag{18}$$

$$CH_4 + 2\ O_2 \rightleftharpoons CO_2 + 2\ H_2O \tag{19}$$

$$OCS + O_2 \rightleftharpoons SO_2 + CO \tag{20}$$

$$H_2O + {}^3\!/_2\ O_2 \rightleftharpoons SO_2 + H_2O \tag{21}$$

$$S_2 + 2\ O_2 \rightleftharpoons 2\ SO_2 \tag{22}$$

$$2\ H_2 + O_2 \rightleftharpoons 2\ H_2O \tag{23}$$

Furthermore, the stability of Fe^{2+}- (ferrous iron) and Fe^{3+}- (ferric iron) bearing minerals on the surface are influenced by the oxygen fugacity. Reducing conditions favour Fe^{2+}-bearing minerals, such as magnetite, ferrosilite, and fayalite, while oxidising conditions favour hematite (Fegley Jr et al. 1997). Therefore, the mineralogy of the surface can act as a chemical buffer which at a given temperature can set the oxygen fugacity of the system, that is a strong function of temperature (Kabbes et al. 2008). If the atmosphere is in chemical equilibrium with the surface then its fO_2 will also be the same. Therefore, the surface mineralogy can set the atmospheric C/O ratio. Mineral redox buffers consist of two to three minerals that transform among themselves to keep fO_2 constant, analogous to how a pH buffer behaves. The most common minerals that do this are those containing iron (Fe), that is encountered in three oxidation states (0, +2, or +3). At very low oxygen fugacity, as found in the Earth's core, iron is present as a metal (Fe^0). When the oxygen fugacity is higher, iron can mainly be found incorporated into silicates as the cation Fe^{2+}. This transition can be described by the quartz-iron-fayalite-iron buffer (QIF) in Eq. 24 (Frost & Lindsley 1991).

$$2\ Fe^0 + SiO_2 + O_2 \rightleftharpoons\ Fe_2SiO_4 \quad \text{(Iron + Quartz} \rightleftharpoons \text{Fayalite)} \quad \text{(QIF)} \tag{24}$$

The possible stable coexistence of pure iron and wüstite at higher oxygen fugacities, can be described by the iron-wustite (Eq. 25) buffer. At even higher fO_2, iron is present both in the ferrous (Fe^{2+}) and the ferric (Fe^{3+}) states and is mostly incorporated into magnetite, which can be described by the wüstite-magnetite (Eq. 26) and iron-magnetite (Eq. 27) buffers:

$$Fe + {}^1\!/_2\ O_2 \rightleftharpoons FeO \quad \text{(Iron} \rightleftharpoons \text{Wüstite)} \quad \text{(IW)} \tag{25}$$

$$3\ FeO + {}^1\!/_2\ O_2 \rightleftharpoons Fe_3O_4 \quad \text{(Wüstite} \rightleftharpoons \text{Magnetite)} \quad \text{(WM)} \tag{26}$$

$$3\ Fe\ + 2\ O_2 \rightleftharpoons Fe_3O_4 \quad \text{(Iron} \rightleftharpoons \text{Magnetite)} \quad \text{(IM)} \tag{27}$$

At very high oxygen fugacities iron occurs as ferric iron in the mineral hematite, which can be described by the magnetite-hematite (MH) buffer in Eq. 28. Furthermore, the fayalite-hematite-quartz (FHQ) in Eq. 29 and ferrosilite-hematite-quartz (FeHQ) in Eq. 30 buffer could be activated under oxidising conditions. Therefore, hematite (Fe_2O_3) surface minerals could play a key role for the stability in hot, CO_2 atmospheres (Grenfell et al. 2013).

$$4\ Fe_3O_4 + \ O_2 \rightleftharpoons 6\ Fe_2O_3 \quad \text{(Magnetite} \rightleftharpoons \text{Hematite)} \quad \text{(MH)} \tag{28}$$

$$2\ Fe_2SiO_4 + O_2 \rightleftharpoons 2\ Fe_2O_3 + 4\ SiO_2 \quad \text{(Fayalite} \rightleftharpoons \text{Hematite + Quartz)} \quad \text{(FHQ)} \tag{29}$$

$$4\ FeSiO_3 + \ O_2 \rightleftharpoons 2\ Fe_2O_3 + 2\ SiO_2 \quad \text{(Ferrosilite} \rightleftharpoons \text{Hematite + Quartz)} \quad \text{(FeHQ)} \tag{30}$$

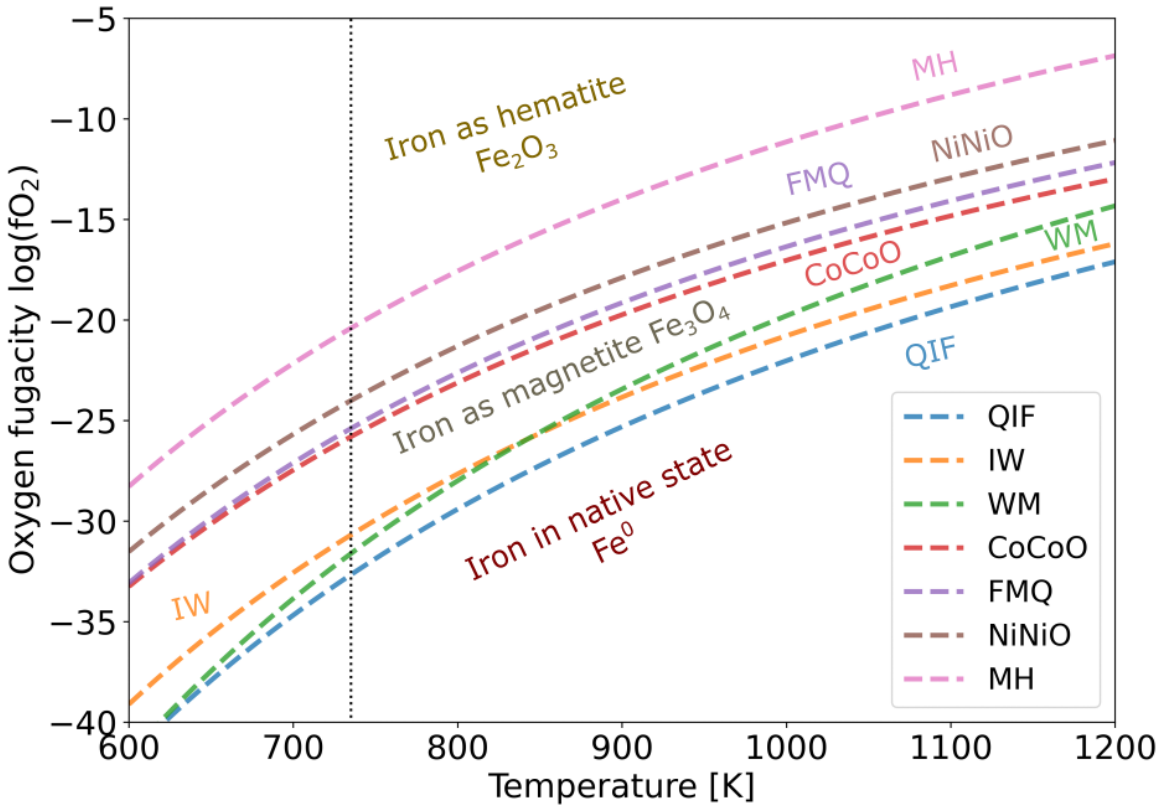

Figure 26: Logarithmic plot of the oxygen fugacity fO_2 versus temperature, showing the stability of different common buffers, calculated with Eq. 34, using coefficients from Frost & Lindsley (1991) from Table 11. Note that the oxygen fugacity of all considered buffers increases with the temperature, and that they have a similar slope. The Venusian temperature of 735 K is marked in the plot as a dotted line.

The temperature dependence of common buffers in fO_2 is shown in Figure 26 (calculated from Frost & Lindsley 1991). In the Figure, the fayalite-magnetite-quartz (FMQ) buffer (Eq. 31) is shown, along with the cobalt–cobalt oxide (CoCoO), and nickel-nickel oxide (NiNiO) buffers, describing the oxidation of metallic cobalt (Co) & nickel (Ni) toward the oxides CoO & NiO with gas phase O_2 according to Eq. 32 & Eq. 33.

$$3\ Fe_2SiO_4 + O_2 \rightleftharpoons 2\ Fe_3O_4 + 3\ SiO_2 \quad \text{(Fayalite} \rightleftharpoons \text{Magnetite + Quartz)} \quad \text{(FMQ)} \quad (31)$$

$$2\ Co + O_2 \rightleftharpoons 2\ CoO \quad \text{(Cobalt} \rightleftharpoons \text{Cobalt oxide)} \quad \text{(CoCoO)} \quad (32)$$

$$2\ Ni + O_2 \rightleftharpoons 2\ NiO \quad \text{(Nickel} \rightleftharpoons \text{Nickel oxide)} \quad \text{(NiNiO)} \quad (33)$$

The equilibria for the common redox buffers shown in Figure 26 have been calculated with Eq. 34 using the equilibrium expressions noted by Frost & Lindsley (1991). In Table 11 the corresponding coefficients for common redox buffers are shown.

$$\log(fO_2) = \frac{A}{T} + B + \frac{C(p-1)}{T} \qquad \text{(T in Kelvins)} \qquad (34)$$

As illustrated in Figure 26 the oxygen fugacity changes considerably for a given buffer over the shown temperature range. However, the range of oxygen fugacity between different buffers at given temperatures is comparatively small.

Table 11: Coefficients to calculate the logarithm of the oxygen fugacity fO_2 as a function of temperature and pressure (Frost & Lindsley 1991). The temperature range for which this extrapolations are applicable are indicated. Furthermore, the oxygen fugacity at the Venusian surface are calculated Eq. 34 for a temperature of 735 K (~460°C) and pressure of 92.1 bar.

Buffer	A	B	C	Temp. range [°C]	log fO_2 (T_{Venus})
QIF	-29435.7	7.3910	0.044	150-573	-32.65
IM	-28690.6	8.1300	0.056	300-565	-30.80
FMQ	-26455.3	10.344	0.092	400-573	-25.64
MH	-25497.5	14.330	0.019	300-573	-20.36
CoCoO	-24332.6	7.2950	0.052	600-1200	-25.80
NiNiO	-24530.0	9.3600	0.046	600-1200	-24.01

The atmospheric composition of the Venus-like planets could be related to the composition of the surface, as the temperature and pressure of these planets are high enough that some atmospheric species may react with surface minerals (Schaefer & Fegley 2011). Thus, the chemical equilibration with these minerals will affect the atmospheric composition, primarily the C/O ratio. To study this behaviour, the atmospheric composition of Venus-like planets near the surface of different C/O ratios are simulated with `FastChem`. The mixing ratio of O_2 (pO_2) is then matched with the oxygen fugacity fO_2 (same units) of different mineral redox buffers. Figure 27 shows the logarithmic oxygen fugacitiy as function of the carbon-to-oxygen ratio in a very narrow region between C/O = 0.49987 and C/O = 0.49995 around the calculated Venusian C/O ratio of 0.499918. In close proximity to the Venusian C/O ratio, at approximately 0.4999135 ($\Delta C/O \approx 4.5 \cdot 10^{-6}$), there is a significant change of the oxygen fugacity spanning over about 19 orders of magnitude in a extremely narrow C/O range.

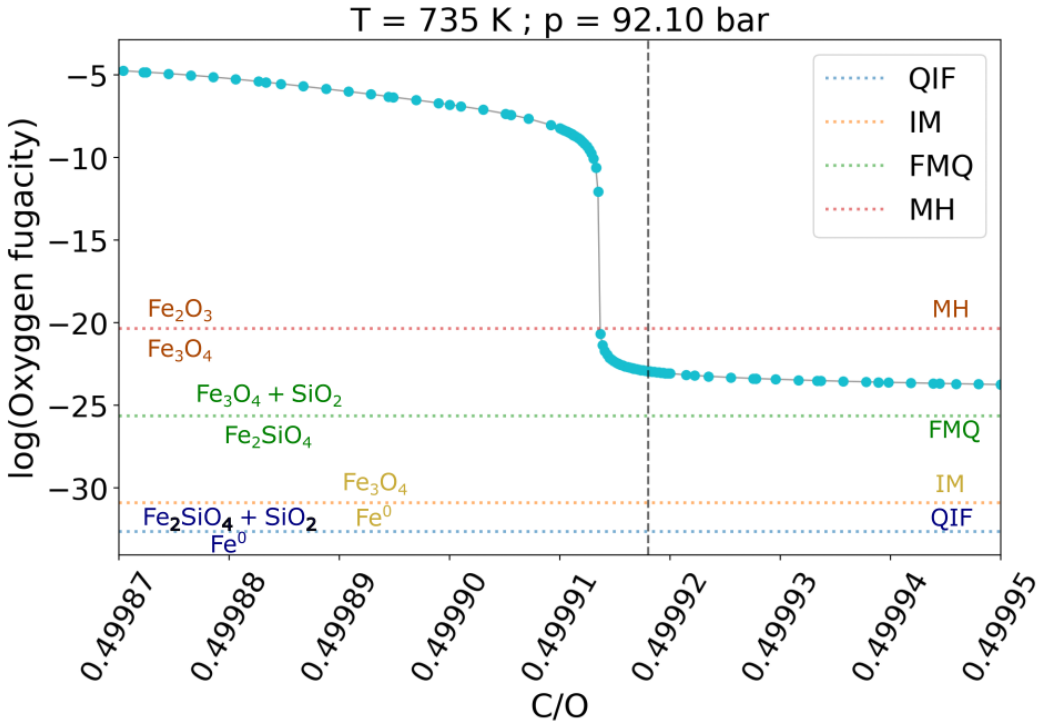

Figure 27: Logarithmic oxygen fugacity log fO_2 for temperature and pressure conditions of the Venusian surface, with C/O ratios between 0.49987 and 0.49994. Furthermore, the fO_2 values, where the quarz-iron-fayalite (QIF), iron-magnetite (IM), fayalite-magnetite-quarz (FMQ), and magnetite-hematite (MH) buffers are effective, are illustrated. The Venusian C/O ratio is marked in the plot as a dashed line.

In Figure 26 the calculated effective oxygen fugacity for different buffers at Venusian surface conditions (T = 735 K; p = 92.1) are shown. It seems that the Venusian atmosphere equilibrated at oxygen fugacities between those of the fayalite-magnetite-quarz (FMQ) and magnetite-hematite (MH) buffer. This result suggests that magnetite, and not hematite, is stable on the Venusian surface. The found oxygen fugacity of the Venusian surface of approximately $1.2 \cdot 10^{-23}$ ($\log_{10} fO_2 = -22.92$) correlates with results from Lewis (1970), who calculated $\log_{10} fO_2$ being −23.1 at 747 K on the surface of Venus, using the observed CO abundance at cloud level. Fegley Jr et al. (1997) also studied the redox state of the lower atmosphere and surface of Venus and found $\log_{10} fO_2$ values ranging from -21.31 to -21.35, with a dispersion of 0.08, which is slightly lower than our results. The most intriguing result seen in Figure 27 is that very minor changes in C/O ratio around the Venusian atmosphere could have an immense effect on the oxygen fugacity and further on the mineral composition of the surface. Therefore, the C/O ratio of Venus might be set by a combination of different mineral redox buffers to a value slightly below 0.5. The surface mineralogy also has implications on the atmospheric composition, since very oxidised minerals like hematite (Fe_2O_3) would produce a CO_2-rich atmosphere, while more reduced minerals like wüstite (FeO) would produce a CO-rich or even CH_4 atmosphere. Furthermore, the mineralogy of the surface assumably reflects the crust, which is vigorously exchanging with the atmosphere over the planetary timescales. Rimmer et al. (2021) used GGchem to investigate whether the surface and atmosphere of Venus are in chemical equilibrium, using oxide ratios measured by the *Vega 2* lander (see Table 4). Their results showed that the solid composition of the Venusian surface rock is a felsic mixture of enstatite ($MgSiO_3$) and quartz (SiO_2), while iron was found to be entirely bound in magnetite (Fe_3O_4), although the analysis of further surface minerals is needed to test these predictions.

The oxidation state of the Venusian atmosphere and surface has been investigated in several different studies. Lewis & Kreimendahl (1980) concluded from *Pioneer Venus* observations that the oxidation state of the Venusian surface was controlled by the pyrite–calcite–anhydrite-wüstite (PCAW) buffer according to Eq. 35. Furthermore, they found $\log_{10}(fO_2) = -22.6^{+0.1}_{-0.4}$ based on results from the *Pioneer Venus* mass spectrometer, which correlates well with the fO_2 value found in this study.

$$\begin{gathered} 2\ FeS_2 + 2\ CaCO_3 + 7\ O_2 \rightleftharpoons 2\ CaSO_4 + FeO + 2\ CO_2 \\ (\text{Pyrite} + \text{Calcite} \rightleftharpoons \text{Anhydrite} + \text{Wüstite}) \end{gathered} \tag{35}$$

Barsukov et al. (1982) suggested the pyrite–calcite–anhydrite–magnetite (PCAM) assemblage as the buffering system to control the redox state of Venus' surface and lower atmosphere, after calculating $\log_{10}(fO_2) \approx 22.1$ at 750 K using *Venera 11* & *12* and *Pioneer Venus* measurements:

$$\begin{gathered} 3\ FeS_2 + 6\ CaCO_3 + 11\ O_2 \rightleftharpoons 6\ CaSO_4 + Fe_3O_4 + 6\ CO_2 \\ (\text{Pyrite} + \text{Calcite} \rightleftharpoons \text{Anhydrite} + \text{Magnetite}) \end{gathered} \tag{36}$$

The temperature and pressure at the Venusian surface was found to match a point on the mineral decarbonation equilibrium of the calcite–quartz–wollastonite (CcQWo) reaction (Eq. 37), which has been suggested to buffer the CO_2 content of the Venusian atmosphere. However, Treiman & Bullock (2011) stated that this cannot be the case, since the CcQWo reaction would amplify perturbations in temperature and pressure, while a chemical buffer would act to diminish chemical perturbations in the atmosphere. It should be noted that chemical perturbations are not necessary the same as temperature and pressure changes, but they are linked through the climate.

$$\begin{gathered} CaCO_3 + SiO_2 \rightleftharpoons CaSiO_3 + CO_2 \\ (\text{Calcite} + \text{Quarz} \rightleftharpoons \text{Wollastonite} + CO_2) \end{gathered} \tag{37}$$

The abundance of minor gas species, such as sulfur dioxide (SO_2), could also be buffered or affected by reactions with surface minerals (Treiman & Bullock 2011). For example, reactions involving iron oxide (e.g., magnetite) and iron sulfide (e.g., pyrite) could buffer the SO_2 content of the Venusian atmosphere via the reaction in Eq. 38.

$$\begin{aligned} 3\,FeS_2 + 16\,CO_2 &\rightleftharpoons Fe_3O_4 + 6\,SO_2 + CO \\ (\text{Pyrite} + CO_2 &\rightleftharpoons \text{Magnetite} + SO_2 + CO) \end{aligned} \tag{38}$$

In Figure 28 the oxygen fugacity is shown for the C/O range of the different atmosphere types discussed in chapter 3.2.3 from 0 to 2. The four defined atmosphere types seem to incorporate distinct oxygen fugacity levels at the surface. For Type I atmospheres the average oxygen fugacity is -0.45 ± 0.44, Type II atmospheres vary a bit more around -33.35 ± 1.31, for Type III the average oxygen fugacity is about -40.16 ± 0.84, and Type IV atmospheres are nearly depleted of free oxygen with $fO_2 \approx -46.87 \pm 0.18$. The strongly varying oxygen fugacity for the different atmosphere types could also have implications on their surface composition. While for Type I atmospheres, oxidised minerals such as hematite (Fe_2O_3) are likely to occur, in Type II atmospheres the oxygen fugacity could suggest that wüstite (FeO) is present on the surface of these planets. The highly reducing conditions of Type III and Type IV atmospheres could lead to iron being present in its metallic form on the surface, rather than being incorporated in silica. Highly reduced iron-rich chondrites such as enstatite chondrites or the Bencubbin-like chondrites are examples for meteorites with very high proportion of metallic iron (Malavergne et al. 2010).

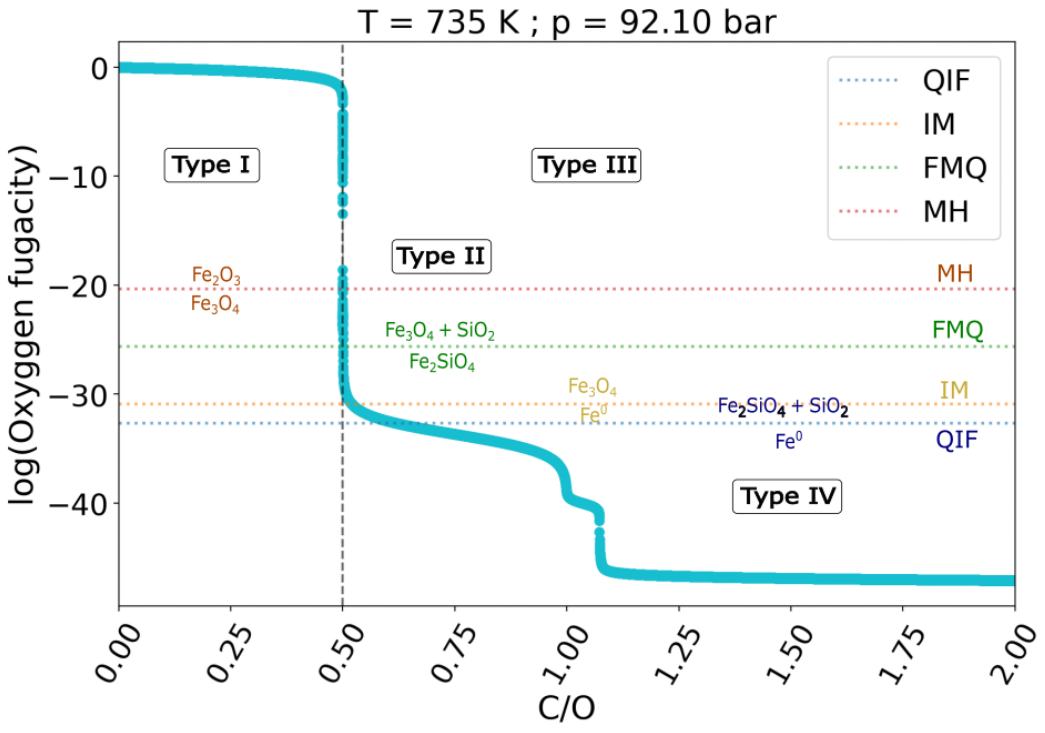

Figure 28: Logarithmic oxygen fugacity log fO_2 at Venusian surface temperature (735 K), and pressure (92.1 bar), with varying C/O ratios between 0 and 2. The fO_2 values, where the quarz-iron-fayalite (QIF), iron-magnetite (IM), fayalite-magnetite-quarz (FMQ), and magnetite-hematite (MH) buffers are effective, are illustrated. Furthermore, the four atmospheric types found in this study are indicated, while the Venusian C/O ratio is marked with a dashed line.

4 Discussion

4.1 Classes of Venus-like atmospheres

In this Master's thesis the composition of Venus-like planets with atmospheres in chemical equilibrium was investigated for different carbon-to-oxygen and carbon-to-nitrogen ratios. From this study four distinct atmosphere types seem to emerge for different C/O ratios at Venusian conditions. Therefore, gas phase equilibrium calculations were performed with the chemical equilibrium code `FastChem`. In Table 12 the occuring species are shown for the four atmospheric types described in chapter 3.2.3. Species not occurring over the whole C/O range in specific atmosphere types are shown in round brackets in Table 12.

Table 12: Most abundant species of the different atmosphere types: Type I ($0 < C/O < 0.5$), Type II ($0.5 < C/O < 0.95$), Type III ($0.95 < C/O < 1.075$), and Type IV ($1.075 < C/O$). Species that do not occur over the entire C/O range or in all layers of the atmosphere are indicated in round brackets.

	CO_2	O_2	CO	C_3O_2	C_5	N_2	C_4N_2	NO_2	H_2O
Type I	✓	✓	✗	✗	✗	✓	✗	✓	✓
Type II	✓	✗	✓	✗	✗	✓	(✓)	✗	(✓)
Type III	✓	✗	✓	✗	✗	✓	✓	✗	✗
Type IV	✗	✗	✓	✓	✓	✗	✓	✗	✗
	SO_3	H_2SO_4	CSO	CS_2	CH_4	HCN	H_2	C_2H_4	C_2H_2
Type I	✓	✓	✗	✗	✗	✗	✗	✗	✗
Type II	✗	✗	✓	✗	✓	(✓)	(✓)	(✓)	✗
Type III	✗	✗	✓	(✓)	(✓)	(✓)	✗	✓	(✓)
Type IV	✗	✗	(✓)	✓	✗	✗	✗	✓	✓

As one can see in Table 12, the four described atmosphere types harbour a combination of distinct species that could in theory be detected in atmospheres of Venus-like planets. The so-called Type I atmospheres mainly consist of the oxygenated species O_2, CO_2, N_2, NO_2, H_2O, SO_3, and H_2SO_4. Type II atmospheres mainly contain CO, CO_2, CH_4, CSO, and N_2. Krissansen-Totton et al. (2019) proposed the coexistence of CH_4 and CO_2 (without CO) in an atmosphere as a biosignature, arguing that only biological fluxes could be high enough to replenish CH_4 in the upper atmosphere, where it is rapidly destroyed by photochemical processes. The absence of CO as a secondary condition is due to the fact that it would be unlikely that non-biological processes, such as volcanic outgassing, would produce carbon in its most (CO_2) and least (CH_4) oxidised form simultaneously without producing CO. In the Type II atmospheres described in this study, CO is therefore present together with CH_4 and CO_2. The Type III atmospheres mostly contain CO, N_2, C_4N_2, and C_2H_4. For Type IV atmospheres, C_3O_2 and C_5 together with CO dominate the carbon species. Furthermore, nitrogen, hydrogen and sulfur appear in their most carbonated forms C_4N_2, CS_2, and C_2H_4. The main question for Type IV atmospheres is if graphite condensation would allow such high carbon concentrations in the gas phase. A more likely scenario could be the formation of graphite clouds in such carbon-rich atmospheres. Consequently, the cloud particles could maybe rain out through gravitational settling (Helling et al. 2017). Furthermore, organic hazes could form if there is hydrogen and/or sulfur available. Saturn's moon Titan is surrounded by a thick organic haze layer (Trainer et al. 2006), and maybe even Pluto has thin multilayered organic hazes (Rannou & Durry 2009). Organic hazes are also expected to have formed on Archean Earth. These hazes would not necessarily rain out, but could have spectral and climatic effects on the planet (Arney et al. 2017).

Woitke et al. (2021) proposed a classification scheme for atmospheres based on the carbon, oxygen, and hydrogen abundances. In Figure 29 the four atmosphere types are drawn into a diagram as a function of C/(H+O+C) and (O-H)/(O+H) for C/O ratios between 0 and 1.5, where C, H, and O represent the respective element abundance. The grey triangle in the center corresponds to the region where H_2O, CH_4, and CO_2 coexist in chemical equilibrium. Furthermore, the thin grey lines mark where H_2O & CO_2 (dashed), CO_2 & CH_4 (dash-dotted), and CH_4 & H_2O (dotted) occur in equal concentration. A detailed description on how these conditions were derived by solving a system of linear equations can be found in Woitke et al. (2021). In this Master's project, we investigate atmospheres that are dominated by oxygen and carbon. Therefore, in the diagram all atmosphere types can be found at (O-H)/(O+H) of approximately unity. The O_2, CO_2, and CO abundance of the different types can also be recognised in the diagram. When going to high C/(H+O+C) on the x-axis, more reduced carbon species would dominate.

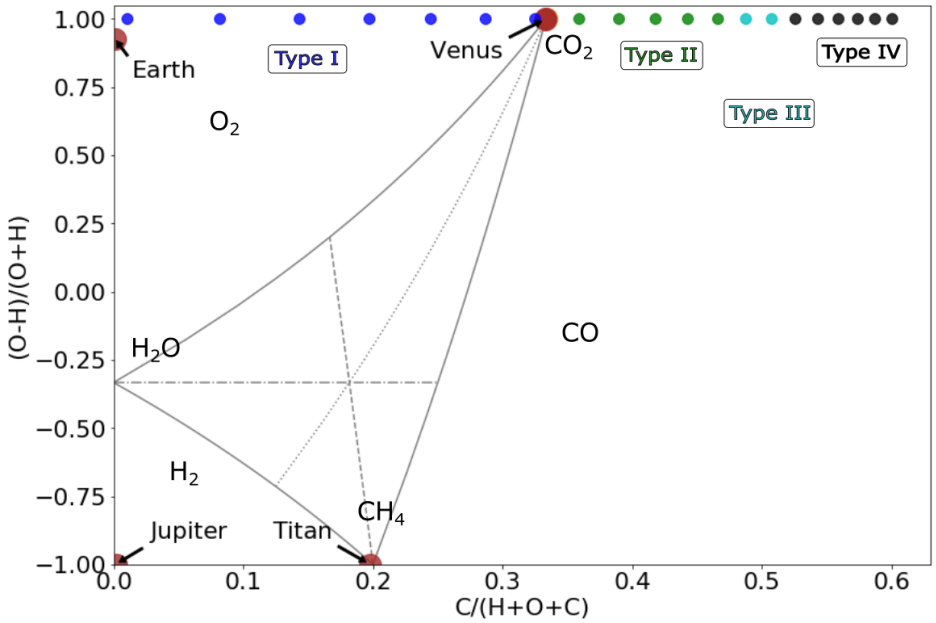

Figure 29: Atmosphere types in classification scheme of Woitke et al. (2021). The grey triangle marks the region in which H_2O, CO_2, and CH_4 coexist. Furthermore, grey lines inside the triangle indicate where the H_2O & CO_2 (dashed), CO_2 & CH_4 (dash-dotted), and CH_4 & H_2O (dotted) concentrations are equal. Besides the position of Type I, Type II, Type III, and Type IV atmospheres for C/O ratios between 0 and 1.5, the atmospheric compositions of Earth, Venus, Jupiter, and Titan are shown.

Woitke et al. (2021) introduced three distinctive atmospheric types for atmospheres consisting of of hydrogen, carbon, nitrogen, and oxygen: Type A (hydrogen-rich, mostly contain CH_4, H_2O, and NH_3), Type B (oxygen-rich, mostly contain O_2, N_2, CO_2, and H_2O), and Type C (mostly contain H_2O, CO_2, CH_4, and N_2). In this study, we included the reactive elements sulfur (S), chlorine (Cl), and fluorine (F) in the model. However, the Type I atmospheres defined in this work correspond well with the composition of their Type B atmospheres. Furthermore, Type II atmospheres are similar to their Type C, but they contain CO and only little H_2O, CH_4. At the moment there is a paper in preparation by Janssen et al. (2022), where the classification scheme of Woitke et al. (2021) is extended to include sulfur species, which will be interesting to compare with the results of this research project. The atmosphere types found in this study could be useful for the observational characterisation of Venus-like atmospheres based on their C/O ratio.

4.2 Drivers of C/O

The carbon-to-oxygen (C/O) ratio can vary between planets and over time. While the solar C/O ratio is about 0.54 (Asplund et al. 2009), other stars and planets have C/O ratios spanning sub-solar to super-solar values. Brewer & Fischer (2016) investigated the C/O ratio for 852 stars of spectral type F, G, and K in the solar neighborhood and found a median C/O ratio of 0.47, while the stars they studied had C/O ratios between 0.21 and 0.66, with uncertainties of ±10%. For one star in their survey, the spectroscopic binary HD 120064, they even report a C/O ratio of 0.04, which could also be due to an error, as they only report this value in a published catalog. Carbon-rich stars with C/O ratios above 1 have also been reported by several studies. For example, Delgado Mena et al. (2010) found a C/O ratio of 1.12 ± 0.19 for 55 Cancri and HD 195019 A. This even resulted in a discussion of the possibility of carbon-rich graphite or even diamond planets (Madhusudhan et al. 2012). However, other studies found that stars with C/O > 1 are probably very rare (Gaidos 2015; Teske et al. 2014). The difference in C/O ratios for different stars originates in slightly different stellar nucleosynthetic pathways for carbon and oxygen (Gaidos 2015). These C/O ratio variations are likely reflected in the composition of the atmospheres of exoplanets (Fleury et al. 2020).

A planet's composition depends on the composition of the material accreted from the proto-planetary disk during planet formation. The C/O ratio of the gas and solids in the disk varies strongly due to the freeze-out of certain volatile species, such as H_2O, CO, and CO_2, around their individual snowlines. Therefore, depending on the planet's formation location it can accrete material with a wide range of C/O ratios (Madhusudhan 2019). This has a strong influence on the composition of the planet, as for example in regions with high C/O carbonates are the main building blocks of the planets, while in regions of low C/O planets have magnesium silicate compositions (Brewer & Fischer 2016). The crust and interior composition of a planet can strongly influence the C/O ratio of the atmosphere.

Furthermore, the atmospheric C/O ratio can change over the lifetime of a planet. For example, the thermal and non-thermal escape of hydrogen to space has important implications for the water inventory of a planet (Kulikov et al. 2006). When hydrogen atoms escape hydrodynamically, they can drag heavier atoms, such as oxygen, with them (Lammer et al. 2020). If oxygen is lost faster than carbon, the C/O ratio can be affected. A selective escape of oxygen relative to carbon (or vice versa) can lead to changes in the C/O ratio in the course of atmospheric evolution. If carbon escape dominates against oxygen escape, the composition can maybe change from a more reducing to a more oxygenated atmosphere.

Another driver of the ratio between carbon and oxygen in the atmosphere can be clouds. In particular, condensate formation and settling can be responsible for different C/O ratios over a planet's lifetime. For example, the removal of carbon from graphite condensation can result in a lower C/O ratio, resulting in a more oxygenated atmosphere. In addition to carbon dust decreasing C/O, the formation and settling of silicate clouds could increase the C/O ratio, due to the consumption of oxygen by silicate formation, which depends on the initial composition and temperature of the atmosphere (Woitke et al. 2018). The composition of clouds in carbon-rich atmospheres differs from their oxygen-rich counterparts (Helling et al. 2017). This also has important implications on the observation and characterisation of the atmospheres, as clouds together with hazes can affect the exoplanetary spectra (Madhusudhan 2019). Outgassed atmospheres can also vary in C/O ratio. Mbarek & Kempton (2016) studied super-Earth atmospheres with cores made of material from of chondritic meteorites, finding a wide range of atmospheric composition, spanning from highly reducing to oxidising. An interplay of the described processes can be responsible for changes in the C/O ratio over the lifetime of a planet.

4.3 Observations of Venus-like exoplanets

The number of rocky exoplanets whose atmosphere have already been characterised is very small. However, with space missions, such as the James Webb Space Telescope (JWST) and the PLAnetary Transits and Oscillations of stars (PLATO) the number of exoplanet atmospheres in reach for detailed analysis will increase (Herbort et al. 2020). The atmospheric composition of exo-Venus analogs such as Trappist-1b, c and d, GJ 1132b, and LHS 3844b could be characterised via transmission spectroscopy with JWST (Krissansen-Totton et al. 2021). However, the possible absence of thick atmospheres for these planets, as reported by Kreidberg et al. (2019) for the hot terrestrial exoplanet LHS 3844b using 100 hours of Spitzer's InfraRed Array Camera (IRAC, Fazio et al. 2004), even though less exciting, would still yield an interesting result about the frequency of Venus-like atmospheres.

For exoplanet atmospheres the C/O ratio can be derived from the relative abundances of simple molecules, such as CO and H_2O, and possibly CO_2 and CH_4, that are observable in spectra of transiting exoplanets (Eistrup et al. 2018). The atmosphere types for Venus-like planets found in this study, that strongly depend on the C/O ratio, could therefore be derived. Recently, the first transmission spectra of the transiting exoplanet WASP-96b, recorded using the Near-Infrared Imager and Slitless Spectrograph (NIRISS), was released. The spectrum shows clear signature of water vapour and gives a foretaste of the quality of data that will be obtained with JWST in future. Most recently, the detection of carbon dioxide (CO_2) in the atmosphere of WASP-39b, a hot gas giant orbiting a G7-type star, was reported by Ahrer et al. (2022), obtained using JWST's Near-Infrared Spectrograph (NIRSpec).

In the mid-infrared (MIR) spectral range, some of the species listed in Table 12, which characterise the four different atmosphere types, are detectable. The Mid-Infrared Instrument (MIRI) onboard of the JWST will obtain spectroscopic data between 4.9 and 28.3 μm (Labiano et al. 2021). Furthermore, observations in the near-infrared (NIR) can be performed using NIRSpec, the Near Infrared Camera (NIRCam), sensitive from 1 to 5 μm , and NIRISS, covering the wavelength range from 0.6 to 5.3 μm (Birkmann et al. 2016). Krissansen-Totton et al. (2019) stated that molecules need to have a minimum concentration of about 10^{-4} (100 ppm) to be detectable with JWST. Therefore, in Table 13 the main spectral features are shown for the most abundant species of the four atmosphere types described in this study.

Table 13: Spectral feature in the NIR and MIR of species occuring at abundances above 10^{-4} for the different described atmosphere types (Catling et al. 2018). For O_2 and N_2 absorption features of the O_2-O_2 and N_2-N_2 dimers, that are more sensitive to pressure and density than that of monomers, are listed as well (Misra et al. 2014).

Species	Spectral feature [μm]
CO_2	15, 4.3, 4.8, 2.7, 2.0, 1.6, 1.4
O_2	6.4, 1.57, 1.27, 0.76, 0.69, 0.630, 0.175-0.19
	O_2-O_2: 1.27, 1.06, 0.57, 0.53, 0.475, 0.445
CO	4.67, 2.34, 1.58, 0.128-0.16
C_3O_2	(4.5 [ice])
N_2	0.1-0.15; N_2-N_2: 4.3, 2.15
C_4N_2	21.18, 93.46
H_2S	7, 3.8, 2.5, 0.2
CSO	4.8, 11.6, and 19.1
(SO_2)	20, 8.8, 7.4, 4, 0.22–0.34

For exoplanets, CO-rich atmospheres look very different from CO_2-rich atmospheres. CO_2 is an excellent coolant of the upper atmosphere (Roble & Dickinson 1989), but CO much less so. Absorption lines of carbon dioxide and carbon monoxide could already be detected in the atmospheres of Hot Jupiters (e.g., de Kok et al. 2013; Oppenheimer et al. 2013). CO_2 possesses numerous strong absorption bands in the mid- and near-IR, such as the ones at 15 μm, 4.3 μm, and 4.8 μm. Contrarily, molecular oxygen has a weak absorption band at 6.4 μm, that overlaps with a much stronger H_2O absorption feature. Stronger O_2 bands are located at 0.76 μm (A-band) and 0.69 μm (B-band). Furthermore, collisional absorption features of the O_2-O_2 dimer occur mainly at 1.06 μm, and 1.27 μm. Carbon suboxide (C_3O_2) is made up of two carbon monoxide groups linked to a carbon atom to form a linear structure: O=C=C=C=O. Spectral features of monomeric C_3O_2 are, therefore, unobservable in the gas phase, as the molecule is a linear and symmetric with no dipole moment and no rotational transitions, but as ice there is a feature at 4.5 μm (Gerakines & Moore 2001). Sulfur trioxide (SO_3) also does not possess a permanent dipole moment due to its symmetry (Jacquinet-Husson et al. 2016). Furthermore, molecular nitrogen (N_2) is challenging to detect, but collisional pairs of nitrogen (N_2-N_2) could produce detectable absorption signals (Schwieterman et al. 2018). The strongest observable bands of C_4N_2 are located in the mid- and far-infrared at 21.18 μm and 93.46 μm (Jolly et al. 2013) and carbonyl sulfide (OCS) has absorption bands at 4.8, 11.6, and 19.1 μm (Jordan et al. 2021). The main question for observing these species is still, how high the abundances of a species must be for a sufficient detection with JWST. For Venus-like exoplanets the temperature and pressure profile could vary from the Venusian temperature-pressure profile used in this study, leading to different abundances of some species in the upper atmosphere.

Lustig-Yaeger et al. (2019) investigated the potential of JWST to detect and characterise the atmospheres of the seven known planets in the TRAPPIST-1 system, orbiting a nearby ultracool dwarf star (Gillon et al. 2017). They found that many molecular absorption features may be detectable with JWST in between 2 and 15 transits, which can also be used to identify the presence of an atmosphere. For this purpose, they recommended the use of CO_2 absorption features to first detect the atmospheres. However, if Venus-like H_2SO_4 aerosols are present in the atmosphere, they stated that up to 12 times more transits could be required to detect an atmosphere. Furthermore, cloudy or hazy atmospheres could require significantly more observations. With the TRAPPIST-1 system being among the first targets to be observed with JWST, the first atmospheres of Venus-like exoplanets could soon be characterised. The C/O ratio in these exoplanet atmospheres could be directly calculated from the abundance of all carbon- and oxygen-bearing species present in the transmission and emission spectra. This very straightforward approach would of course neglect molecules that are not easily detectable spectroscopically and the carbon and oxygen in condensates. Nevertheless, it would provide a good estimate of the C/O ratio in the atmosphere (Greene et al. 2016). The atmosphere types found in this study could be useful to maybe constrain abundances of minor species from the C/O ratio.

Beyond JWST, future dedicated missions for atmospheric studies such as the Atmospheric Remote-sensing Infrared Exoplanet Large-survey (ARIEL) and the ground-based extremely large telescopes (ELTs) will contribute to surveying the atmospheres of exoplanets (Kempton et al. 2018). The characterisation of Venus-like exoplanets could lead to the clarification of the dichotomy of habitability that we see between Earth and Venus (Ostberg & Kane 2019; Kane et al. 2019).

4.4 Clouds and other complexities

Clouds in general could have important implications for the detectability of the different atmosphere types. Helling (2019) found that for cloud-forming exoplanets, the C/O ratio varies strongly with altitude due to the element depletion by cloud formation. Consequently, in these exoplanets there is no one C/O ratio that can characterise the atmosphere. Helling (2019) described that cloud formation could maybe even convert the gas-phase chemistry of an atmosphere from oxygen-rich to carbon-rich. This is relevant, since the atmospheres of exoplanets likely have substantial cloud coverage. The presence of clouds can also lead to changes in the observed spectrum, as they can block the view into underlying atmospheric layers, as is the case for Venus, and weaken spectral features.

Additionally, interactions of the atmosphere with the surface were investigated in this study. It was found that the oxygen fugacity of the Venusian atmosphere is in a range where small fluctuations in the C/O ratio can lead to extreme changes in the oxygen fugacity of several orders of magnitude. Therefore, the Venusian surface is likely stabilising the atmospheric composition in the form of mineral redox buffers. Furthermore, the oxygen fugacity varies strongly for the different atmosphere types described in chapter 3.2.3, which could have implications on their mineral surface composition. While in Type IV atmospheres iron is expected to be present as metal (Fe^0), in Type I atmospheres it is expected to be present in the ferrous state (Fe^{2+}) in the form of hematite. For present Venus we found magnetite, a combination of iron in its ferric and ferrous state, to be the expected Fe-bearing mineral, from the modelled oxygen fugacity. However, the validity of such simplified assumptions is limited. Even the composition of the Venusian surface is still largely unknown, as the planet is a very difficult target for in-situ exploration (Taylor et al. 2018). The dense atmosphere and high surface temperature and pressure turn even the simplest analyses into severe technical challenges (Treiman et al. 2021). Klingelhöfer & Fegley Jr (2000) investigated the iron mineralogies at the *Vega 2* and the *Venera 14* landing sites using synthetic spectra, finding that magnetite and hematite could be detected at the 1% level using Mössbauer spectroscopy. However, mineral redox buffers could potentially help to get a rough idea of the surface composition of exoplanets based on the composition of their atmosphere, when the temperature of the surface is known.

Furthermore, the strong temperature dependence of the oxygen fugacity (fO_2) for the different mineral redox buffers, seen in Figure 26, might affect the composition of the atmosphere. If the temperature of the atmosphere rises, the higher fO_2 would likely translate in higher abundances of CO_2 and possibly O_2, with the free oxygen likely combining with carbon monoxide CO in the atmosphere to form CO_2. This will affect the surface temperature, since CO_2 is a greenhouse gas, and thus provide a positive feedback, where the initial increase in atmospheric temperature would lead to an even greater rise in temperature. Therefore, some potential buffering reactions could be unstable for planetary atmospheres, as the positive feedback could lead to catastrophic greenhouse runaway (Treiman & Bullock 2011). Nevertheless, the atmospheric composition can be strongly influenced by chemical reactions with minerals on the surface.

5 Conclusions

Venus-like planets that were simulated in this Master's project with the chemical equilibrium codes `FastChem` and GGchem show distinct atmospheric features when varying atmospheric parameters such as the carbon-to-oxygen (C/O) or carbon-to-nitrogen (C/N) ratio. With a Venusian C/O ratio of approximately 0.5, we found that very small changes of this parameter can lead to severe changes in the planet's chemistry. It is even possible for a formerly oxygen-rich atmosphere to change into a more reduced atmosphere through very small fluctuations of the C/O ratio. In addition, four different atmosphere types with distinct atmospheric composition were found for planets with a similar temperature and pressure profile and initial elemental composition as planet Venus, but different C/O ratios. These atmosphere types could help characterising the atmospheres of Venus-like exoplanets. Future missions such as TESS, PLATO and ARIEL will increase the sample of exo-Venus candidates.

Another aspect that should be taken into account in modelling of planetary atmospheres is the potential presence of clouds and condensates. The characterisation of planetary atmospheres is mainly based on species in the gas phase, that were simulated in this study using the chemical equilibrium code `FastChem`. However, clouds and condensates can change the atmospheric composition by depleting the atmosphere of certain elements. In this project, the code GGchem was used to examine the possible influence of condensates. For the simulated Venusian atmosphere, the solid sulfur condensate S_2[s] became present at altitudes where the Venusian cloud layer is expected to be located, depleting the atmosphere of reduced sulfur species at higher altitudes. The Venusian clouds were measured to mainly consist of water vapour and sulfuric dioxide. However, here only gas phase species were considered as a model input, as the exact abundance of condensates in the cloud layer is unknown. As the atmosphere above the cloud layer is dominated by photochemistry and, therefore, is likely out of chemical equilibrium, we focused on the lower atmosphere in this study.

In the Venusian atmosphere the loss of significant amounts of hydrogen and water is indicated by a very high deuterium-to-hydrogen (D/H) ratio. However, Earth and Venus have similar amounts of carbon and nitrogen, when accounting for locked-up amounts in the solid Earth. It is therefore very important to study the causes of the different evolution of these two planets, which are similar in size and mass. At present, the evolution history of the Venusian atmosphere is still poorly understood and it is unclear if Venus was a potentially habitable planet at some time of its early evolution (Chassefière et al. 2012). Venus-like planets are, therefore, the ultimate control case for studying how Earth developed and maintained conditions suited for life, which will be important in the search for exoplanets that are potentially habitable.

Upcoming missions, such as *DAVINCI+*, *VERITAS* and *EnVision* by NASA and ESA will hopefully help to better constrain the history and evolution of Venus (Krissansen-Totton et al. 2021). Measurements of the elemental and isotopic abundances of noble gases on planet Venus will be crucial to improve atmospheric models of Venus-like planets. This will help to better understand the history of these planets and will, moreover, be beneficial to create better models for the evolution of the Venusian atmosphere. Therefore, atmosphere modelling efforts, as the ones performed in this study, will help to provide a better understanding of what species are expected to occur in the atmospheres of Venus-like exoplanets.

Appendix

Acknowledgements

I would like to gratefully acknowledge the supervision of Prof. Manuel Güdel and Prof. Eric Gaidos. Without their hints and ideas, this work had not been possible. Furthermore, I would like to thank Dr. Oliver Herbort for very fruitful discussions and for introducing me to the importance of condensates in chemical equilibrium calculations. I also would like to thank Prof. Bernard Foing for the opportunity to participate in different scientific campaigns and conferences during my Master's studies. Last but not least, I would like to express my sincere gratitude to my family and friends, who supported me during my studies.

Abstract (German)

In unserem Sonnensystem ist der Planet Venus der Erde sowohl bezüglich der Größe als auch der Masse am ähnlichsten. Trotzdem verfügt Venus über sehr lebensfeindliche Bedingungen, mit einer von Kohlenstoffdioxid (CO_2) dominierten Atmosphäre, sowie Oberflächentemperaturen von ungefähr 460°C und einem Druck von 92 bar. In dieser Masterarbeit werden Venus-ähnliche Planeten mit Atmosphären im chemischen Gleichgewicht mit dem Programm `FastChem` simuliert. Hierfür werden unterschiedliche Parameter wie das Verhältnis von Kohlenstoff zu Sauerstoff (C/O) oder zu Stickstoff (C/N) in der simulierten Atmosphäre der Planeten variiert und Veränderungen in der chemischen Zusammensetzung aufgezeichnet. Weiters werden die Einflüsse von unterschiedlichen Mineralien auf der Oberfläche mithilfe von sogenannten Redoxpuffern untersucht.

Abstract (English)

In our solar system, the planet Venus is the most similar to Earth in both size and mass. Nevertheless, Venus has very hostile conditions, with an atmosphere dominated by carbon dioxide (CO_2), as well as surface temperatures of about 460°C and a pressure of 92 bar. In this study, Venus-like planets with atmospheres in chemical equilibrium are simulated with the codes `FastChem` and GGchem. For this purpose, different parameters, such as the ratio of carbon to oxygen (C/O) or to nitrogen (C/N), are varied in the simulated atmosphere of the planets and changes in the chemical composition are recorded. Furthermore, the influences of different minerals on the surface are examined with the help of mineral redox buffers.

List of Figures

Ich habe mich bemüht, sämtliche Inhaber der Bildrechte ausfindig zu machen und ihre Zustimmung zur Verwendung der Bilder in dieser Arbeit eingeholt. Sollte dennoch eine Urheberrechtsverletzung bekannt werden, ersuche ich um Meldung bei mir.

List of Tables

References

Ahrer, E.-M., Alderson, L., Batalha, N. M., et al. 2022, arXiv e-prints, arXiv

Ando, H., Imamura, T., Tellmann, S., et al. 2020, Scientific reports, 10, 1

Arney, G., Meadows, V., Crisp, D., et al. 2014, Journal of Geophysical Research (Planets), 119, 1860

Arney, G. N., Meadows, V. S., Domagal-Goldman, S. D., et al. 2017, The Astrophysical Journal, 836, 49

Asplund, M., Grevesse, N., Sauval, A. J., & Scott, P. 2009, arXiv preprint arXiv:0909.0948

Avduevsky, V., Marov, M. Y., & Rozhdestvensky, M. 1970, Journal of Atmospheric Sciences, 27, 561

Bains, W., Petkowski, J. J., Seager, S., et al. 2021, Astrobiology, 21, 1277

Bains, W., Shorttle, O., Ranjan, S., et al. 2022, Universe, 8, 54

Barsukov, V., Volkov, V., & Khodakovsky, I. 1982, Journal of Geophysical Research: Solid Earth, 87, A3

Basilevsky, A. T. 1997, Journal of Geophysical Research: Planets, 102, 9257

Basilevsky, A. T. & Head, J. W. 2003, Reports on Progress in Physics, 66, 1699

Bertaux, J.-L., Vandaele, A.-C., Korablev, O., et al. 2007, Nature, 450, 646

Bertaux, J.-L., Widemann, T., Hauchecorne, A., Moroz, V., & Ekonomov, A. 1996, Journal of Geophysical Research: Planets, 101, 12709

Bézard, B. 1994, Communication at the 30th COSPAR Scientific Assembly (Session C3. 1), 11

Bezard, B., de Bergh, C., Crisp, D., & Maillard, J. P. 1990, Nature, 345, 508

Birkmann, S. M., Ferruit, P., Rawle, T., et al. 2016, in Space Telescopes and Instrumentation 2016: Optical, Infrared, and Millimeter Wave, Vol. 9904, SPIE, 92–102

Bond, J. C., O'Brien, D. P., & Lauretta, D. S. 2010, The Astrophysical Journal, 715, 1050

Brecht, A., Brecht, S., Luhmann, J., et al. 2021, Bulletin of the American Astronomical Society, 53, 100

Brewer, J. M. & Fischer, D. A. 2016, The Astrophysical Journal, 831, 20

Cami, J., Bernard-Salas, J., Peeters, E., & Malek, S. E. 2010, Science, 329, 1180

Campbell, B. A., Campbell, D. B., Carter, L. M., et al. 2019, Icarus, 332, 19

Catling, D. C. & Kasting, J. F. 2017, Atmospheric Evolution on Inhabited and Lifeless Worlds (Cambridge University Press)

Catling, D. C., Kiang, N., Robinson, T., et al. 2018, Astrobiology

Catling, D. C. & Zahnle, K. J. 2009, Scientific American, 300, 36

Chase, M. W. 1998, J. Phys. Chem. Ref. Data, Monograph, 9, 1

Chassefière, E., Wieler, R., Marty, B., & Leblanc, F. 2012, Planetary and Space Science, 63, 15

Colin, L. 1980, Journal of Geophysical Research: Space Physics, 85, 7575

Colin, L. & Hall, C. F. 1977, Space Science Reviews, 20, 283

Damiani, S., Garcia, J. M., Guilanyà, R., Muñoz, P., & Muller, M. 2015, in 25th International Symposium on Space Flight Dynamics ISSFD

De Bergh, C., Bezard, B., Crisp, D., et al. 1995, Advances in Space Research, 15, 79

de Kok, R. J., Brogi, M., Snellen, I. A., et al. 2013, Astronomy & Astrophysics, 554, A82

Delgado Mena, E., Israelian, G., Hernández, J. G., et al. 2010, The Astrophysical Journal, 725, 2349

Dobrovolskis, A. R. & Ingersoll, A. P. 1980, Icarus, 41, 1

Drake, M. J. 2005, Meteoritics & Planetary Science, 40, 519

Drossart, P., Piccioni, G., Adriani, A., et al. 2007, Planetary and Space Science, 55, 1653

D'Incecco, P., Filiberto, J., López, I., et al. 2021, Solar System Research, 55, 315

Eistrup, C., Walsh, C., & van Dishoeck, E. F. 2018, Astronomy & Astrophysics, 613, A14

Elston, J., Bullock, M. A., Stachura, M. Z., et al. 2021, Bulletin of the American Astronomical Society, 53, 373

Encrenaz, T., Greathouse, T. K., Marcq, E., et al. 2020, Astronomy & Astrophysics, 643, L5

Esposito, L., Knollenberg, R., Marov, M. I., Toon, O., & Turco, R. 1983, Venus, 484

Fazio, G., Hora, J., Allen, L., et al. 2004, The Astrophysical Journal Supplement Series, 154, 10

Fegley Jr, B. & Treiman, A. H. 1992, Washington DC American Geophysical Union Geophysical Monograph Series, 66, 7

Fegley Jr, B., Zolotov, M. Y., & Lodders, K. 1997, Icarus, 125, 416

Fleury, B., Gudipati, M. S., Henderson, B. L., & Swain, M. 2020, The Astrophysical Journal, 899, 147

Florensky, C., Basilevsky, A., Kryuchkov, V., et al. 1983, Science, 221, 57

French, R., Mandy, C., Hunter, R., et al. 2022, Aerospace, 9

Frost, B. & Lindsley, D. 1991, Reviews in Mineralogy"/BR Frost//Mineralogical Society of America, 25, 1

Gaidos, E. 2015, The Astrophysical Journal, 804, 40

Gail, H.-P. & Sedlmayr, E. 2014, Physics and chemistry of circumstellar dust shells, Cambridge Astrophysics No. 52 (Cambridge University Press)

Garvin, J. B., Getty, S., Arney, G. N., et al. 2020, in AGU Fall Meeting Abstracts, Vol. 2020, P026–0001

Gelman, B. G., Zolotukhin, V. G., Lamonov, N. I., et al. 1979, An analysis of the chemical composition of the atmosphere of Venus on an AMS of the Venera-12 using a gas chromatograph

Gerakines, P. & Moore, M. 2001, Icarus, 154, 372

Ghail, R. C., Hall, D., Mason, P. J., et al. 2018, International journal of applied earth observation and geoinformation, 64, 365

Gillon, M., Triaud, A. H., Demory, B.-O., et al. 2017, Nature, 542, 456

Gilmore, M., Treiman, A., Helbert, J., & Smrekar, S. 2017, Space Science Reviews, 212, 1511

Greaves, J. S., Richards, A. M. S., Bains, W., et al. 2021, Nature Astronomy, 5, 655

Greene, T. P., Line, M. R., Montero, C., et al. 2016, The Astrophysical Journal, 817, 17

Grenfell, J. L., Stock, J. W., & Patzer, A. B. C. 2013, Planetary and Space Science, 84, 14

Grevesse, N., Asplund, M., & Sauval, A. 2007, Space Science Reviews, 130, 105

Grinspoon, D. H. & Lewis, J. S. 1988, Icarus, 74, 21

Hansen, J. E. & Hovenier, J. 1974, Journal of Atmospheric Sciences, 31, 1137

Head, J. W., Campbell, D. B., Peterfreund, A. R., & Zisk, S. A. 1984, Geology of Maxwell Montes, Venus., In NASA. Washington Repts. of Planetary Geol. Program p 79-80 (SEE N84-23431 13-91)

Head, J. W., Crumpler, L., Aubele, J. C., Guest, J. E., & Saunders, R. S. 1992, Journal of Geophysical Research: Planets, 97, 13153

Helbert, J., Säuberlich, T., Dyar, M. D., et al. 2020, in Infrared Remote Sensing and Instrumentation XXVIII, Vol. 11502, SPIE, 36–59

Helbert, J., Vandaele, A. C., Marcq, E., et al. 2019, in Infrared Remote Sensing and Instrumentation XXVII, Vol. 11128, SPIE, 18–32

Helling, C. 2019, Annual Review of Earth and Planetary Sciences, 47, 583

Helling, C., Tootill, D., Woitke, P., & Lee, E. 2017, Astronomy & Astrophysics, 603, A123

Herbort, O., Woitke, P., Helling, C., & Zerkle, A. 2020, Astronomy & Astrophysics, 636, A71

Herbort, O., Woitke, P., Helling, C., & Zerkle, A. L. 2022, Astronomy & Astrophysics, 658, A180

Hoffman, J., Hodges, R., Donahue, T., & McElroy, M. 1980, Journal of Geophysical Research: Space Physics, 85, 7882

Holm, N. G. & Andersson, E. 2005, Astrobiology, 5, 444

Horinouchi, T., Hayashi, Y.-Y., Watanabe, S., et al. 2020, Science, 368, 405

Horinouchi, T., Kouyama, T., Lee, Y. J., et al. 2018, Earth, Planets and Space, 70, 1

Jacquinet-Husson, N., Armante, R., Scott, N. A., et al. 2016, Journal of Molecular Spectroscopy, 327, 31

Janssen, L., Woitke, P., Herbort, O., et al. 2022, submitted to A&A

Jenkins, J. M., Kolodner, M. A., Butler, B. J., Suleiman, S. H., & Steffes, P. G. 2002, Icarus, 158, 312

Johnson, N. M. & de Oliveira, M. R. R. 2019, Earth and Space Science, 6, 1299

Jolly, A., Benilan, Y., Fayt, A., et al. 2013, in European Planetary Science Congress, EPSC2013–106

Jordan, S., Rimmer, P. B., Shorttle, O., & Constantinou, T. 2021, The Astrophysical Journal, 922, 44

Kabbes, J. E., Reaman, D. M., Whitaker, S., Campbell, A. J., & Panero, W. R. 2008, in AGU Fall Meeting Abstracts, Vol. 2008, MR42A–05

Kane, S. R., Arney, G., Crisp, D., et al. 2019, Journal of Geophysical Research: Planets, 124, 2015

Kane, S. R., Kopparapu, R. K., & Domagal-Goldman, S. D. 2014, The Astrophysical Journal Letters, 794, L5

Kasting, J. F., Whitmire, D. P., & Reynolds, R. T. 1993, Icarus, 101, 108

Keldysh, M. 1977, Icarus, 30, 605

Kempton, E. M. R., Bean, J. L., Louie, D. R., et al. 2018, Publications of the Astronomical Society of the Pacific, 130, 114401

Klingelhöfer, G. & Fegley Jr, B. 2000, Icarus, 147, 1

Kopparapu, R. K., Ramirez, R., Kasting, J. F., et al. 2013, The Astrophysical Journal, 765, 131

Kopparapu, R. K., Ramirez, R. M., SchottelKotte, J., et al. 2014, The Astrophysical Journal Letters, 787, L29

Kovalenko, I. D., Eismont, N. A., Limaye, S. S., et al. 2020, Advances in Space Research, 66, 21

Krasnopolsky, V. A. 1989, Icarus, 80, 202

Krasnopolsky, V. A. 2006, Planetary and Space Science, 54, 1352

Krasnopolsky, V. A. 2017, Icarus, 286, 134

Krasnopolsky, V. A. & Gladstone, G. R. 2005, Icarus, 176, 395

Kreidberg, L., Koll, D. D., Morley, C., et al. 2019, Nature, 573, 87

Kreslavsky, M. A., Ivanov, M. A., & Head, J. W. 2015, Icarus, 250, 438

Krissansen-Totton, J., Arney, G. N., Catling, D. C., et al. 2019, Bulletin of the American Astronomical Society, 51, 158

Krissansen-Totton, J., Bergsman, D. S., & Catling, D. C. 2016, Astrobiology, 16, 39, pMID: 26789355

Krissansen-Totton, J., Fortney, J. J., & Nimmo, F. 2021, The Planetary Science Journal, 2, 216

Kulikov, Y. N., Lammer, H., Lichtenegger, H., et al. 2006, Planetary and Space Science, 54, 1425

Kunde, V., Aikin, A., Hanel, R., et al. 1981, Nature, 292, 686

Labiano, A., Argyriou, I., Álvarez-Márquez, J., et al. 2021, Astronomy & Astrophysics, 656, A57

Lammer, H., Scherf, M., Kurokawa, H., et al. 2020, Space Science Reviews, 216, 1

Lammer, H., Zerkle, A. L., Gebauer, S., et al. 2018, The Astronomy and Astrophysics Review, 26, 1

Landis, G., Dyson, R., Oleson, S., et al. 2011, in AIAA SPACE 2011 Conference & Exposition, 7268

Lebonnois, S., Millour, E., Martinez, A., et al. 2021, in European Planetary Science Congress, EPSC2021–234

Lécuyer, C., Simon, L., & Guyot, F. 2000, Earth and Planetary Science Letters, 181, 33

Lee, Y., Yamazaki, A., Imamura, T., et al. 2017, The Astronomical Journal, 154, 44

Lewis, J. S. 1970, Earth and Planetary Science Letters, 10, 73

Lewis, J. S. & Fegley Jr, B. 1982, Science, 216, 1223

Lewis, J. S. & Kreimendahl, F. A. 1980, Icarus, 42, 330

Lewis, J. S. & Prinn, R. 1980, The Astrophysical Journal, 238, 357

Li, W., Cheng, Y., & Yang, Z. 2019, Geochemistry, Geophysics, Geosystems, 20, 2542

Liggins, P., Jordan, S., Rimmer, P. B., & Shorttle, O. 2021, arXiv preprint arXiv:2111.05161

Lincowski, A. P., Meadows, V. S., Crisp, D., et al. 2021, The Astrophysical Journal Letters, 908, L44

Lustig-Yaeger, J., Meadows, V. S., & Lincowski, A. P. 2019, The Astronomical Journal, 158, 27

Madhusudhan, N. 2012, The Astrophysical Journal, 758, 36

Madhusudhan, N. 2019, arXiv preprint arXiv:1904.03190

Madhusudhan, N., Harrington, J., Stevenson, K. B., et al. 2011, Nature, 469, 64

Madhusudhan, N., Lee, K. K., & Mousis, O. 2012, The Astrophysical Journal Letters, 759, L40

Malavergne, V., Toplis, M. J., Berthet, S., & Jones, J. 2010, Icarus, 206, 199

Marcq, E., Bézard, B., Drossart, P., et al. 2008, Journal of Geophysical Research: Planets, 113

Markiewicz, W., Titov, D., Limaye, S., et al. 2007, Nature, 450, 633

Mayer, C., McCullough, T., & Sloanaker, R. 1958, The Astrophysical Journal, 127, 1

Mayor, M. & Queloz, D. 1995, Nature, 378, 355

Mbarek, R. & Kempton, E. M.-R. 2016, The Astrophysical Journal, 827, 121

Misra, A., Meadows, V., Claire, M., & Crisp, D. 2014, Astrobiology, 14, 67

Moroz, V. & Zasova, L. 1997, Advances in Space Research, 19, 1191

Moses, J. I., Line, M. R., Visscher, C., et al. 2013, The Astrophysical Journal, 777, 34

Nakamura, M., Imamura, T., Ishii, N., et al. 2016, Earth, Planets and Space, 68, 1

Nakamura, M., Imamura, T., Ishii, N., et al. 2011, Earth, Planets and Space, 63, 443

Oppenheimer, B., Baranec, C., Beichman, C., et al. 2013, The Astrophysical Journal, 768, 24

Ostberg, C. & Kane, S. R. 2019, The Astronomical Journal, 158, 195

Oyama, V. I., Carle, G. C., Woeller, F., et al. 1980, Journal of Geophysical Research: Space Physics, 85, 7891

O'Brien, D. P., Izidoro, A., Jacobson, S. A., Raymond, S. N., & Rubie, D. C. 2018, Space Science Reviews, 214, 1

Patel, M., Zarnecki, J., & Catling, D. 2002, Planetary and Space Science, 50, 915

Perryman, M. 2018, The exoplanet handbook (Cambridge university press)

Pollack, J. B., Dalton, J. B., Grinspoon, D., et al. 1993, Icarus, 103, 1

Pollack, J. B. & Sagan, C. 1967, The Astrophysical Journal, 150, 327

Rannou, P. & Durry, G. 2009, Journal of Geophysical Research: Planets, 114

Rimmer, P. B., Jordan, S., Constantinou, T., et al. 2021, The Planetary Science Journal, 2, 133

Roble, R. & Dickinson, R. 1989, Geophysical Research Letters, 16, 1441

Russell, C., Elphic, R., & Slavin, J. 1979a, Science, 203, 745

Russell, C., Elphic, R., & Slavin, J. 1979b, Science, 205, 114

Sagdeev, R., Linkin, V., Blamont, J., & Preston, R. 1986, Science, 231, 1407

Samuelson, R., Mayo, L., Knuckles, M., & Khanna, R. 1997, Planetary and Space Science, 45, 941

Schaber, G., Strom, R., Moore, H., et al. 1992, Journal of Geophysical Research: Planets, 97, 13257

Schaefer, L. & Fegley, B. 2011, The Astrophysical Journal, 729, 6

Schlarmann, L., Foing, B., Cami, J., & Fan, H. 2021, A&A, 656, L17

Schubert, G., Bougher, S. W., Covey, C. C., et al. 2007, Washington DC American Geophysical Union Geophysical Monograph Series, 176, 101

Schulze-Makuch, D. 2021, Life, 11, 255

Schwieterman, E. W., Kiang, N. Y., Parenteau, M. N., et al. 2018, Astrobiology, 18, 663

Seager, S. & Bains, W. 2015, Science Advances, 1, e1500047

Smrekar, S. E., Hensley, S., Dyar, M., et al. 2020, in 51st Annual Lunar and Planetary Science Conference, Lunar and Planetary Science Conference, 1449

Snellen, I. A. G., de Kok, R. J., de Mooij, E. J. W., & Albrecht, S. 2010, Nature, 465, 1049

Snellen, I. A. G., Guzman-Ramirez, L., Hogerheijde, M. R., Hygate, A. P. S., & van der Tak, F. F. S. 2020, Astronomy & Astrophysics, 644, L2

Sossi, P. A., Burnham, A. D., Badro, J., et al. 2020, Science Advances, 6, eabd1387

Stenberg, G., Persson, M., Yamauchi, M., Pätzold, M., & Laufer, R. 2022, 44th COSPAR scientific assembly, 44, B4

Stock, J. W., Kitzmann, D., & Patzer, A. B. C. 2022, arXiv preprint arXiv:2206.08247

Stock, J. W., Kitzmann, D., Patzer, A. B. C., & Sedlmayr, E. 2018, Monthly Notices of the Royal Astronomical Society, 479, 865

Strom, R. G., Schaber, G. G., & Dawson, D. D. 1994, Journal of Geophysical Research: Planets, 99, 10899

Surkov, Y. A., Moskalyeva, L., Shcheglov, O., et al. 1983, Journal of Geophysical Research: Solid Earth, 88, A481

Surkov, Y. A., Moskalyova, L., Kharyukova, V., et al. 1986, Journal of Geophysical Research: Solid Earth, 91, E215

Surkov, Y. A., Shcheglov, O., Moskalyeva, L., et al. 1982, Analytical Chemistry, 54, 957A

Svedhem, H., Titov, D., McCoy, D., et al. 2007, Planetary and Space Science, 55, 1636

Taylor, F. W., Crisp, D., & Bézard, B. 1997, in Venus II: Geology, Geophysics, Atmosphere, and Solar Wind Environment, ed. S. W. Bougher, D. M. Hunten, & R. J. Phillips, 325

Taylor, F. W., Svedhem, H., & Head, J. W. 2018, Space Science Reviews, 214, 35

Teske, J. K., Cunha, K., Smith, V. V., Schuler, S. C., & Griffith, C. A. 2014, The Astrophysical Journal, 788, 39

Thompson, M. A. 2021, Monthly Notices of the Royal Astronomical Society, 501, L18

Trainer, M. G., Pavlov, A. A., DeWitt, H. L., et al. 2006, Proceedings of the National Academy of Sciences, 103, 18035

Treiman, A. H. 2007, Geophysical Monograph-American Geophysical Union, 176, 7

Treiman, A. H. & Bullock, M. A. 2011, in 42nd Annual Lunar and Planetary Science Conference, Lunar and Planetary Science Conference, 2146

Treiman, A. H., McCanta, M., & Filiberto, J. 2021, Bulletin of the AAS, 53, https://baas.aas.org/pub/2021n4i077

Trompet, L., Robert, S., Mahieux, A., et al. 2021, Astronomy & Astrophysics, 645, L4

Truong, N. & Lunine, J. 2021, Proceedings of the National Academy of Sciences, 118, e2021689118

Tsai, S.-M., Kitzmann, D., Lyons, J. R., et al. 2018, The Astrophysical Journal, 862, 31

Turbet, M., Bolmont, E., Chaverot, G., et al. 2021, Nature, 598, 276

Villanueva, G., Cordiner, M., Irwin, P., et al. 2021, Nature Astronomy, 5, 631

Von Zahn, U., Kumar, S., Niemann, H., & Prinn, R. 1983, Venus, 299

Way, M. J., Del Genio, A. D., Kiang, N. Y., et al. 2016, Geophysical research letters, 43, 8376

Woitke, P., Helling, C., Hunter, G., et al. 2018, Astronomy & Astrophysics, 614, A1

Woitke, P., Herbort, O., Helling, C., et al. 2021, Astronomy & Astrophysics, 646, A43

Wolszczan, A. & Frail, D. A. 1992, Nature, 355, 145

Yung, Y. L. & DeMore, W. B. 1998, Photochemistry of planetary atmospheres (Oxford University Press), 292

Zhang, T., Delva, M., Baumjohann, W., et al. 2008, Journal of Geophysical Research: Planets, 113

Zimmer, K., Zhang, Y., Lu, P., et al. 2016, Computers & geosciences, 90, 97

Table of Acronyms

ALMA	Atacama Large Millimeter/submillimeter Array
ARIEL	Atmospheric Remote-sensing Infrared Exoplanet Large-survey
AU	Astronomical units
DAVINCI+	Deep Atmosphere Venus Investigation of Noble gases, Chemistry, and Imaging, Plus
ELT	Extremely Large Telescope
ESA	European Space Agency
GCM	Global climate model
Gya	Billion years ago
IRAC	InfraRed Array Camera (Spitzer)
ISM	Interstellar medium
ISRO	Indian Space Research Organisation
JCMT	James Clerk Maxwell Telescope
JWST	James Webb Space Telescope
LUVOIR	Large Ultraviolet Optical Infrared Surveyor
MIR	Mid-infrared
MIRI	Mid-Infrared Instrument (JWST)
NASA	National Aeronautics and Space Administration
NIR	Near-infrared
NIRISS	Near-Infrared Imager and Slitless Spectrograph (JWST)
NIRSpec	Near-Infrared Spectrograph (JWST)
NIST	National Institute of Standards and Technology
PACMAN	Planetary Atmosphere, Crust, and MANtle
PLATO	PLAnetary Transits and Oscillations of stars
ppb / ppm	parts per billion / parts per million
ROCKE-3D	Resolving Orbital and Climate Keys of Earth and Extraterrestrial Environments with Dynamics
SOIR	Solar Occultation Infrared Spectrometer (*Venus Express*)
TESS	Transiting Exoplanet Survey Satellite
VCD	The Venus Climate Database
VERITAS	Venus Emissivity, Radio Science, InSAR, Topography, and Spectroscopy
VIRTIS	Visible and Infrared Thermal Imaging Spectrometer (*Venus Express*)
VOICE	Venus Volcano Imaging and Climate Explorer

Table of Molecules

- Carbon dioxide (CO_2)
- Nitrogen (N_2)
- Water (H_2O)
- Carbon monoxide (CO)
- Hydrogen chloride (HCl)
- Carbonylsulfid (CSO)
- Carbon disulfide (CS_2)
- Argon (Ar)
- Neon (Ne)
- Helium (He)
- Hydrogen fluoride (HF)
- Methane (CH_4)
- Ethylene (C_2H_4)
- Hydrogen sulfide (H_2S)
- Hydrogen (H_2)
- Sulfuric acid (H_2SO_4)
- Sulfur trioxide (SO_3)
- Sulfur dioxide (SO_2)
- Fluorosulfuric acid (HSO_3F)
- Oxygen (O_2)
- Chlorine (Cl_2)
- Carbon (C_5)
- Hydrogen cyanide (HCN)
- Carbon suboxide (C_3O_2)
- Dicyanoacetylene (C_4N_2)
- Propynylidyne (C_3H)
- Acetylene (C_2H_2)
- Chloroethyne (C_2HCl)
- Nitrogen monoxide (NO)
- Nitrogen dioxide (NO_2)

Table of Minerals

FeO	Wüstite	Fe_3O_4	Magnetite	$CaCO_3$	Calcite
FeS_2	Pyrite	Fe_2O_3	Hematite	$CaSO_4$	Anhydrite
$FeSiO_3$	Ferrosilite	Fe_2SiO_4	Fayalite	SiO_2	Quartz
$CaSiO_3$	Wollastonite	CoO	Cobalt oxide	NiO	Nickel oxide